CANADIAN THESES

THÈSES CANADIENNES

NOTICE

The quality of this microfiche is heavily dependent upon the quality of the original thesis submitted for microfilming. Every effort has been made to ensure the highest quality of reproduction possible.

If pages are missing, contact the university which granted the degree.

Some pages may have indistinct print especially if the original pages were typed with a poor typewriter ribbon or if the university sent us an inferior photocopy.

Previously copyrighted materials (journal articles, published tests, etc.) are not filmed.

Reproduction in full or in part of this film is governed by the Canadian Copyright Act, R.S.C. 1970, c. C-30

AVIS

La qualité de cette microfiche dépend grandement de la qualité de la thèse soumise au microfilmage. Nous avons tout fait pour assurer une qualité supérieure de reproduction.

S'il manque des pages, veuillez communiquer avec l'université qui a conféré le grade

La qualité d'impression de certaines pages peut laisser à désirer, surtout si les pages originales ont été dactylographiées à l'aide d'un ruban usé ou si l'université nous a fait parvenir une photocopie de qualité inférieure

Les documents qui font déjà l'objet d'un droit d'auteur (articles de revue, examens publiés, etc.) ne sont pas microfilmés

La reproduction, même partielle, de ce microfilm est soumise à la Loi canadienne sur le droit d'auteur, SRC 1970, c. C-30

THIS DISSERTATION
HAS BEEN MICROFILMED
EXACTLY AS RECEIVED

LA THÈSE A ÉTÉ
MICROFILMÉE TELLE QUE
NOUS L'AVONS REÇUE

Canada

FLOW AND HEAT TRANSFER IN A DROP TUBE FURNACE

by

ROBERT J. FLAXMAN

A thesis
presented to the University of Ottawa
in fulfillment of the
thesis requirement for the degree of
Master of Applied Science
in
Mechanical Engineering

ISBN 0-315-33316-2

UNIVERSITÉ D'OTTAWA
UNIVERSITY OF OTTAWA

The University of Ottawa requires the signatures of all persons using or photocopying this thesis. Please sign below, and give address and date.

ACKNOWLEDGEMENTS

I would like to thank my supervisor Dr. William Hallett for approaching me with the research topic and for his encouragement, guidance and aid throughout the past two years. I would like to thank Mr. Pat Hughes of CANMET Research Laboratories for proposing the research subject and for all his assistance. I would like to thank my wife, Carol-lynne Pettit, for her patience and understanding during all the late nights and weekends spent in Colonel By B203-F. I would also like to thank all my fellow students for their invaluable suggestions and for making my stay most gratifying. Financial assistance provided by Energy, Mines and Resources has been greatly appreciated.

ABSTRACT

A finite difference model has been developed to predict velocity and temperature fields within a drop tube furnace. The input variables were the inlet air mass flow, the air preheat temperature and the temperature of the furnace heating elements. Inert coal particles with diameters of 10, 30, 100, 300 μm were introduced into the furnace flow field and the velocities, temperatures and heating rates of the particles were calculated under different flow conditions.

NOMENCLATURE

A	constant in equation (4.3)
A	constant in equation (4.5)
B	constant in Sutherland equation
B	constant in equation (4.5)
C_D	drag coefficient of sphere
F_{PE}	view factor from particle to exit
F_{PP}	view factor from particle to primary inlet
F_{PS}	view factor from particle to secondary inlet
F_{PW}	view factor from particle to furnace wall
ID	inside diameter (m)
L	length (m)
OD	outside diameter (m)
P	pressure (kPa)
P'	pressure head
P	node point inside control volume
Pr	Prandtl number
Q	heat transfer to furnace (W)
R	dimensionless radius
R	inside furnace tube radius (m)
R	gas constant (0.287 kJ/kg K)
Re	Reynolds number

R_g	resistance of air (K m**2/W)
R_g^*	radial position of node closest to wall (m)
R_o	outside furnace radius (m)
R_r	radiation resistance (K m**2/W)
R_w	furnace wall resistance (K m**2/W)
S	constant in Sutherland equation
Sp^ϕ	source term in numerical formulation
Su^ϕ	source term in numerical formulation
T	temperature of air (K)
T_a	temperature of gas on axis [16] (K)
T_g	temperature of gas surrounding particle (K)
T_g^*	temperature at node closest to the wall (K)
T_{gb}	glow bar temperature (K)
T_o	inlet temperature (K) [16]
T_P	temperature of particle (K)
T_{P0}	temperature of particle at beginning of time increment (K)
T_w	inside furnace wall temperature (K)
T_{wo}	outside furnace wall temperature (K)
U	dimensionless velocity [15]
Z	dimensionless distance [15]
Z	dimensionless distance [16]

a^ϕ	coefficient in numerical formulation
c_P	specific heat of air (kJ/kg K)
c_{PP}	specific heat of coal (kJ/kg K)
d	tube diameter (m)

d_P	particle diameter (m)
g	gravitational constant (9.806 m/s**2)
g_z	same as above in axial direction
h	convective heat transfer coefficient(W/m**2 K)
h_{PE}	radiant heat transfer coefficient (W/m**2 K) from particle to exit
h_{PP}	radiant heat transfer coefficient from particle to primary inlet (W/m**2 K)
h_{PS}	radiant heat transfer coefficient from particle to secondary inlet (W/m**2 K)
h_{PW}	radiant heat transfer coefficient from particle to furnace wall (W/m**2 K)
k_g	thermal conductivity of gas (W/m K)
k_w	thermal conductivity of furnace wall (W/m K)
m	particle mass (kg)
$\dot{q}_w$	heat flux (W/m**2) [16]
r	radial position (m)
r_0	radius of tube (m) [15]
t	time (s)
u	axial gas velocity (m/s)
u_P	particle velocity (m/s)
u_{P0}	particle velocity at beginning of time increment (m/s)
v	radial gas velocity (m/s)
x	axial position (m)
y	radial postion (m)

Δt	time increment (s)
ΔT_{max}	maximum temperature increment (K)
Γ_ϕ	variable in equation (4.1)
Θ	dimensionless temperature [16]
ϵ	emissivity
μ	dynamic viscosity (kg m/s)
ϕ	dependent variable
ρ	density of air (kg/m**3)
ρ_{axis}	density of air on axis (kg/m**3)
ρ_o	reference density of air (kg/m**3)
ρ_P	density of coal particle (kg/m**3)
σ	Stefan-Boltzmann constant (W/m**2T**4)
∞	infinity

CONTENTS

LIST OF TABLES

LIST OF FIGURES

Chapter I

INTRODUCTION

The mechanism of coal combustion is extremely complex and is not fully understood, since different types of coal exhibit different combustion characteristics. Large coal-fired boilers burn coal in pulverized form in a turbulent, swirling jet; however, it is very difficult to study the combustion behaviour of coal particles in an actual furnace. In order to better understand coal combustion, it is desirable to isolate the processes undergone by the individual coal particles from the furnace flow by subjecting the particles to heating and reaction under controlled conditions. In this fashion the number of test variables can be reduced and parametric studies performed.

Energy, Mines, and Resources Canada has developed a coal testing facility that will be used to examine the combustion histories of different types of coal in pulverized form. The facility is an entrained flow reactor, also called a controlled mixing combustion history (CMCH) or 'drop tube' furnace, and consists of a long, electrically heated, vertical mullite refractory tube (Figure 1) through which a downward laminar flow of air is passed. Two streams of air are introduced into the top of the furnace through a burner; the first is a water-cooled primary flow used as a carrier gas to introduce the particles into the furnace, and the other a much larger secondary flow which constitutes the bulk of flow through the furnace. The burner is designed such that the primary flow enters the furnace through a central injector tube and the secondary flow enters the furnace through an annulus which surrounds the primary tube. The

furnace is heated by 64 – 500 W glow bars, 32 spaced evenly along each side, and is divided into four heating zones; the power into each zone can be independently regulated to control the temperature. At the furnace exit, a water–cooled sampling probe collects the combustion products, gases, and unburned coal particles and carries them away to be analyzed. The sampling probe can be axially traversed inside the furnace, which allows the coal particles to have variable residence times.

Coal is described as being composed of four components: moisture, volatiles, 'char' or fixed carbon, and ash. Volatiles are hydrocarbon components which range from light gases (eg methane, propane, etc.) to heavy oils and tars and other gases such as CO and CO_2. The volatiles escape from the surface of the particle and mix with the surrounding air. Volatiles burn rapidly in the gas phase, while the char (largely carbon) remaining after devolatilization undergoes surface reaction and burns much more slowly. The rate at which devolatilization occurs and the quantity of volatiles are very important in determining the ignition and the stabilization behaviour of a pulverized coal flame.

The CMCH furnace is intended to subject coal particles to a wide range of temperatures and heating histories, depending on the heater temperature and the preheat temperature of the incoming air stream. The furnace simulates the heating undergone by a particle approaching a flame front in a furnace. In order to interpret the results of devolatilization experiments in this furnace, it is essential to know the particle heating histories and residence times. The velocities and temperatures within the furnace can not be measured however, owing to the fact that access to the furnace is nearly impossible, and hence the particle heating rates cannot be found experimentally. In the present work,

therefore, a finite difference scheme was developed to predict the gas velocity and temperature within the furnace under different operating conditions. Particle heating rates were also calculated, based on the furnace gas velocities and temperature. This thesis presents the development of the model and representative results; it also examines the flow within an isothermal model of the furnace, using flow visualization.

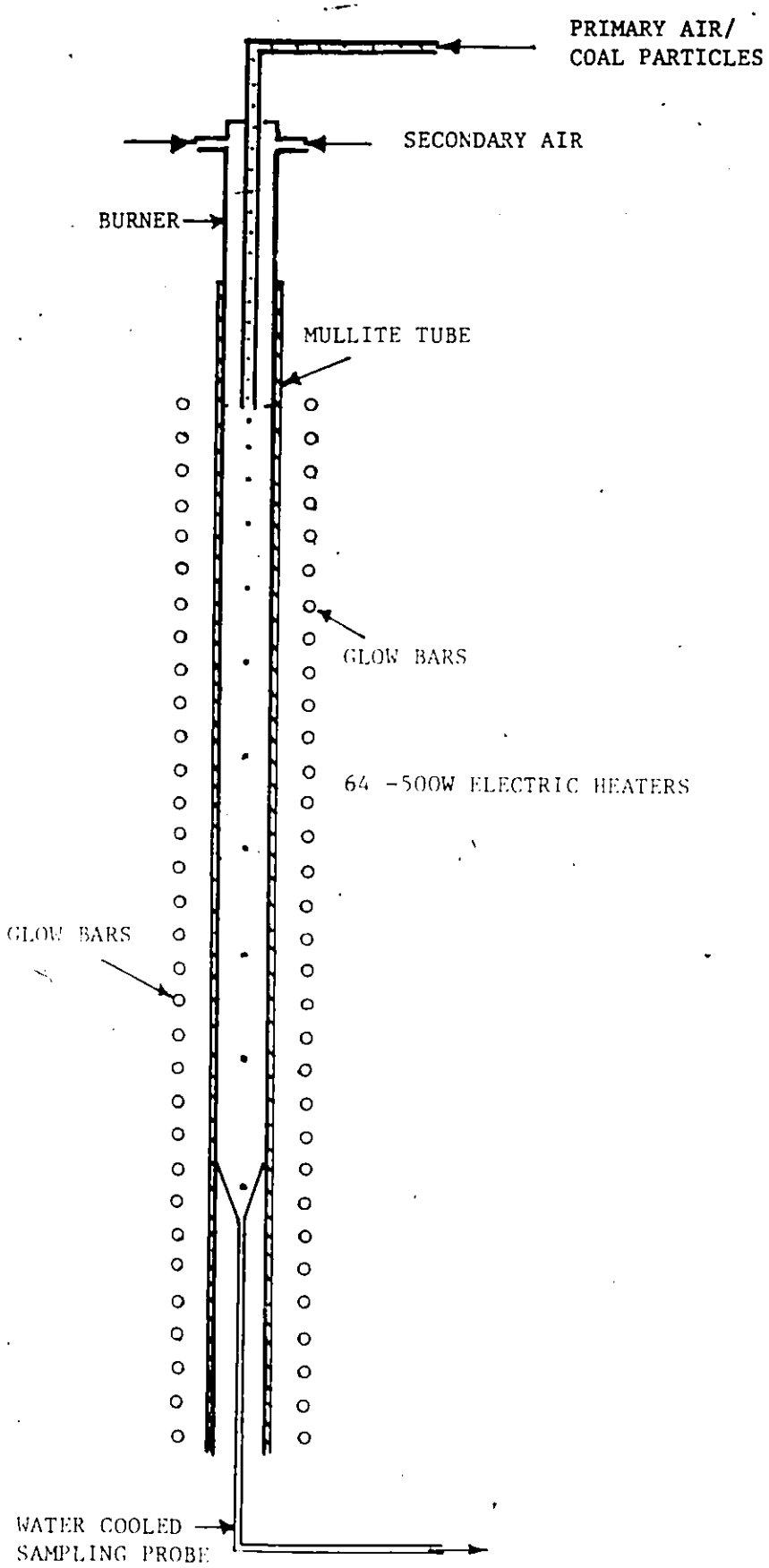

Figure 1: Cross-section of the CCRL Drop Tube Furnace

Chapter II

LITERATURE SURVEY

2.1 INTRODUCTION

The objective of this study was to develop a numerical model to predict the temperature and heating histories of coal particles when passed through the EMR 'drop tube' furnace. The physical problem is that of a downward, developing flow of gas in an externally heated circular tube, with possible buoyant effects at the hot wall. Cold particles are introduced on the axis of the flow, and are heated by convection and radiation.

A number of test cases were examined in the development of the model. The numerical model was first used to solve isothermal developing laminar pipe flow with constant properties. Subsequently, the effects of temperature, buoyancy, and variable properties were included. Once the final form of the flow regime model had been developed, the particles were introduced into the model. For the present study the particles were assumed to be inert and of low concentration; therefore, the particles were considered to have a negligible effect on the furnace flow field.

A literature review of heated laminar flow in tubes was performed to obtain solutions to which a comparison could be made in developing the model. Existing entrained flow reactors were also reviewed in order to examine their operating conditions.

2.2 LAMINAR FLOW THROUGH TUBES

2.2.1 Developing Velocity - Isothermal Flow

Laminar pipe flow has had considerable attention in the past, the main focus of which has been to determine the magnitude of the pressure drop and the length necessary to obtain fully developed flow, chiefly in connection with piping and heat exchangers. The equations to be solved are the Navier-Stokes equations of motion. Analytical difficulties arise from the non-linearity of these equations, and four methods have been used to obtain solutions: linearization , integral techniques, patched solutions (matching of boundary layer and fully developed flow solutions) [13, 33, 38] and finite element or finite difference techniques [1, 15, 18, 41]. The numerical solutions of the problem were of particular interest for the present work.

A solution of the problem using a finite difference scheme was presented by Friedman et al [15], who obtained velocity field distributions in laminar pipe flow in the range of Reynolds numbers from 0 to 500. McDonald et al [27] used finite difference methods to solve tube flow with a Reynolds number of 200 and obtained results that were in good agreement with Friedman et al. Hasan et al [18] used finite element analysis to solve for flow development in the entrance region of a tube with Reynolds numbers ranging from 0 to 40. Different inlet velocity profiles were examined and were observed to have a marked effect on the flow field in the entry region of the tube. Wagner [41] studied developing flow ahead of a piston moving at constant speed through a tube using a finite difference method for Reynolds numbers 0 to 800. In each of the numerical solutions it was discovered that if the initial velocity profile was flat, the subsequent profiles developed two maxima positioned

symmetrically on either side of the axis near the wall and a local minimum positioned on the axis of symmetry. Abarbanel et al [1] showed that these 'bulges' were part of the exact solution and were not a numerical effect arising from truncation errors or from singularity at the tube wall. Friedman et al [15] found that the magnitude of the bulges decreased with increasing Reynolds numbers.

2.2.2 Laminar Forced Convection in Tubes

Most past interest in laminar forced convection has been in connection with the design of heat exchangers. The working fluids have usually been water or oil, and solutions have been presented to determine the heat transfer coefficients under various laminar flow conditions [24]. Temperature fields within the tubes were not of practical interest in these studies.

Kays [24] presented a finite difference solution for developing temperature profiles based on a Langhaar velocity distribution and a constant wall temperature. Grigull and Tratz [16] presented finite difference solutions for developing temperature profiles in fully developed laminar flow with constant properties. Three heating conditions were studied: constant wall temperature, constant heat flux, and constant temperature difference.

2.2.3 Laminar Combined Convection in Tubes

Buoyancy effects were thought to be significant in the CMCH furnace, owing to the large temperature difference between the wall and incoming flow

and moderate Reynolds numbers. Free convection effects will distort the developing velocity profiles. The forced convection through the furnace is downward, while buoyancy forces act upward, producing combined convection in opposing flow. The heated tube wall causes the flow velocity near the wall to decrease, resulting in an acceleration of the flow on the tube axis.

A number of researchers [5, 9, 10, 17, 19, 30, 31] examined the effects of laminar combined convection in opposing flow with a view to determining the effect of buoyancy on the heat transfer coefficient. Scheele and Hanratty [31] studied combined convection using water in tubes and observed a sudden transition from laminar steady to laminar unsteady flow while measuring tube wall temperatures. Hanratty et al [17] experimented with combined convection in water with Reynolds numbers ranging from 100 to 2100 and observed flow instabilities on the axis by the disturbance of an axially injected dye filament. Brown and Gauvin [9] examined the effects of buoyancy on the heat transfer coefficient in air for Reynolds numbers ranging from 380 to 6900. Collins [10] incorporated buoyancy into a finite difference marching scheme and illustrated the effect of variable properties; however, for strong buoyancy effects, instability occurred in the computer treatment.

2.3 ENTRAINED FLOW REACTORS

Entrained flow reactors have been used at least since 1966 for the study of coal combustion. Many different designs exist, and each furnace has its own geometry, gas flow, and particle feed rate. Usually, a specific type of coal was tested and a combustion model was developed from the experimental results. By examining the operating conditions and heating rates obtained in past research, an insight into the present furnace can be obtained.

Field [14] examined the reaction rates of char particles in the diameter range 20 to 100 μm in a laminar flow furnace. The main flow consisted of 80 l/min of an oxygen–nitrogen–argon mixture which was preheated to 1527 C with a plasma torch. The char particles entered through an alumina feeder tube which entered through the side of the furnace. The char feed rate was 0.125 g/min, entrained in 0.2 l/min of nitrogen. Two diametrically opposed slit-windows were used to observe the burning stream of particles, and to measure wall temperatures with optical pyrometers. The transit time of the particles was 27 ms over 120 mm.

A laminar flow furnace was used by Badzioch and Hawksley [3] to study 20 μm coal particles (also 40, 60, 62 μm) with nitrogen as the primary and secondary gas. The coal particles and nitrogen carrier gas were fed into a secondary stream of hot nitrogen preheated to the furnace wall temperature. Preheating could be varied from 400 C to 1000 C. The secondary gas flow rate was 40 l/min and a zirconia flow straightener was used; the primary flow rate was varied from 1.0 to 2.1 l/min such that it matched the secondary flow velocity entering the furnace. The mixing of the cold carrier nitrogen and the hot gas stream was said to be complete 5 cm from the top. The flow was approximately parabolic henceforth, and flow velocities ranging from 1.6 m/s at 400 C to 2.9 m/s at 1000 C were obtained. A water-cooled collector was used to quench and remove particles and devolatilization products. The coal feed rate was 0.25 to 0.5 g/min, and the particles were assumed to travel at the gas velocity. The residence times were varied from 30 to 110 msec by vertical movement of the collector. The heating rates were said to be approximately 25000 to 50000 C/s, and the final temperature of the particles was equal to the gas stream and the furnace wall.

Pulverized coal particles were burned by Baum and Street [4] in a laminar flow furnace using air as the primary and secondary flow. The secondary air flow rate was 30 l/min, preheated to approximately 917 C, while the furnace wall temperature ranged from 930 to 970 C. The coal feed rate of 2.6 to 2.7 g/min was entrained by a primary flow rate of 1 to 1.38 l/min. Visual observations were made through a slot which ran the length of the furnace, and local gas samples were withdrawn using a water-cooled sampling probe. Exit gas samples were extracted using a water-cooled collector which could be axially traversed from the bottom. Helium tracer techniques showed that less than 1 % of the flow was recirculated.

Kobayashi et al [25] studied devolatilization of coal particles at high temperatures. Size graded particles (400-325 Tyler Mesh - 37-44 μm) were injected into a hot argon stream using a cool argon carrier gas. The secondary (main) flow was heated to the furnace wall temperature using a plasma gun, and passed through a graphite honeycomb flow straightener before entering the furnace tube. Sight holes in the furnace wall enabled the particles to be observed, showing that they travelled down the centre of the furnace. The coal feed rate was varied from 0.12 to 0.18 g/min and the cool argon carrier gas flow rate ranged from 0.015 to 0.616 l/min. The main gas flow ranged from 29.4 to 150 l/min, giving average velocities from 0.81 m/s at 1000 K to 8.65 m/s at 2100 K. The particles were quenched at the furnace exit by means of twelve small water jets in the tip of the collector. A simplified flow model based on an approximate integral method was used to predict the temperature and velocity of the coal particles.

Rapid pyrolysis of lignite in nitrogen was studied by Scaroni et al [32] in an entrained flow , isothermal furnace. A dilute stream of coal and nitrogen was

injected into a preheated nitrogen stream and forced downward through a heated vertical tube. A flow straightener and careful injector design were used to limit the spreading of the coal jet. The main gas flow was preheated to the isothermal wall temperature. A variation of residence times was achieved by raising and lowering an isokinetic water-cooled collector. The mean diameter of the coal particles varied from 41 to 201 μm. The coal feed rate for all tests was 1.0 g/min and the mean gas velocity was 1.12 m/s. Preheated gas and wall temperatures varied from 700 to 1000 C, and the ratio of secondary to primary flow ranged from 16.7 to 12.5. The primary flow rate was the minimum necessary for efficient entrainment of the particles. The coal particle heating rate was estimated to be of the order of 10000 C/s. A cold flow (isothermal) experimental model indicated that particle velocities were size dependent, and that the assumption that gas and particles have the same velocity is not always valid. Particle residence times are affected by the size and the density of the particles during devolatilization. Exact gas velocities and flow patterns were not known, and therefore an average velocity was used.

An entrained flow furnace was used by Solomon et al [36] to study high temperature rapid pyrolysis of coal. Helium or nitrogen was used for the secondary gas flow, which was preheated to the furnace temperature, and for the entrainment gas. The furnace was designed to operate at 1923 K. The particles were 325-200 graded mesh size (44-74 μm) and the coal feed rate was 2 to 3 g/min. The secondary flow was varied from 25 to 40 l/min (depending on the temperature) in order to obtain a 1 m/s velocity through the furnace. The water-cooled carrier gas flow rate was 1 l/min. The coal particles were assumed to travel at the average gas velocity and their residence times were varied from 0 to 700 ms by movement of the

water-cooled injector. A water- cooled collector quenched the exiting stream. An optical port allowed Fourier Transform Infrared Spectrometer analysis of gas species and temperature.

Timothy et al [40] conducted experiments on pulverized coal using a laminar flow furnace consisting of an alumina muffle tube heated by a surrounding graphite element. The secondary flow consisted of a mixture of oxygen and argon or helium which was independently preheated to the furnace temperature; its oxygen volume fraction was varied from 15 to 100 % . The coal was entrained by a flow of helium and injected into the hot stream such that the velocities were matched. The particle sizes were 38-45 and 90-105 um in diameter. The furnace was operated at temperatures of 1250 and 1700 K and heating rates were estimated to be of the order 100000 K/s.

A transparent entrained flow reactor was used by Mitchell and McLean [28] to study the combustion of 90 um coal particles employing a methane-hydrogen-oxygen-nitrogen mixture as the primary and secondary gases. The oxygen mole fraction was varied from 0 to 30 % and furnace temperatures of 1000 to 1800 K were achieved. Particles were assumed to move at the local gas velocity. A two-colour pyrometer technique was used to measure the temperature of the burning coal particles.

Jorgensen and Zuiderwyk [23] studied the combustion of single particles of sulphide minerals in a laminar flow furnace. The secondary gas flow was an air and oxygen-nitrogen mixture which was preheated 773 to 1273 K. The particles were injected into the hot stream by means of a water-cooled injector which could be raised and lowered to vary the residence time. Observation of the exiting flow showed that a majority of the particles remained on the tube axis. The furnace had two sets of viewing ports which enabled two-colour pyrometer measurements.

Typical details of the entrained flow furnaces studied can now be summarized. The particle sizes used in these laminar flow reactors have been in the range 20 to 200 um with feed rates ranging from 0.015 to 3.0 g coal/min. The types of gas used included air, nitrogen, argon, helium, methane and mixtures of these. The secondary gas flow rate ranged from 25 to 150 l/min, yielding velocities of 0.81 to 8.65 m/s (depending on the furnace temperature). The secondary gas flow was always preheated, and typical inlet temperatures varied from 400 to 1823 C. Particle heating rates were claimed to range from 10000 to 100000 C/s. The present EMR furnace falls into the range of designs studied with a coal feed rate of 1.0 g coal/min, inlet velocities of 0.42 to 1.67 m/s, preheat temperatures of 300 to 1200 K, and inlet Reynolds numbers of 120 to 1350. The entrained flow reactors discussed have all been laminar; however, turbulent flow reactors have also been studied [22].

Chapter III

FLOW VISUALIZATION

3.1 INTRODUCTION

The CMCH furnace is a laminar flow test furnace designed to examine the heating histories of coal particles. Ideally, particles traversing the furnace should all be subjected to the same heating conditions and residence time. This can be achieved if the particles travel down the axis of the furnace with a minimum of spreading. A random dispersion of the coal particles would lead to variable particle heating rates and transit times and is therefore highly undesirable.

The furnace entrance geometry as originally designed included a thick water-cooled jacket between the primary and secondary streams. It was felt likely that a recirculating wake could form behind this jacket, which in turn could lead to flow instabilities such as vortex shedding and to particle dispersion within the furnace. In order to determine if the desired flow pattern could actually be obtained with the original geometry, a cold flow (isothermal) experimental model was constructed to match the geometry of the actual furnace (see Figure 2). Flow visualization experiments were carried out using smoke in the primary flow as a tracer to study the effects of primary and secondary flow rates on the flow characteristics.

3.2 THE EXPERIMENTAL APPARATUS

3.2.1 The Furnace Tube

The flow visualization model was a full-size, exact scale replica of the actual CMCH furnace. The model furnace tube consisted of a 1.83 m long cast acrylic tube (76.2mm OD, 63.5mm ID). A flange was attached to the top of the furnace tube to enable the furnace to be fastened to a steel support frame. A centering ring at the bottom of the furnace allowed it to be accurately adjusted vertically. The burner slid into the top of the furnace tube and was held in place by three nylon bolts which passed through the flange. A flexible exhaust hose was attached to the bottom of the furnace tube to direct the exiting smoke into an exhaust system.

3.2.2 The Burner – Original Design

The model of the original burner consisted of three straight concentric tubes (Figure 3a). The primary air and smoke entered through the top into the central tube (6.4mm DIA), while the secondary air entered into the burner from the sides through two horizontally opposed tubes near the top of the outer annulus (57.1mm OD, 38.1mm ID). The lengths of the inlet sections were the same as those in the actual furnace, so that the exit velocity profiles would be the same. A jacket occupied the inside annulus (38.1mm OD, 6.4mm ID) which separated the two streams. This in the actual furnace is a water-cooled jacket to keep the coal particles cold and prevent reaction before the particles enter the furnace.

3.2.3 The Gas Supply and Flow Measurement

Air was used as the primary and secondary fluid. The air supplied to the experimental system was delivered at 100 psig to a pressure regulator, which reduced the pressure down to 60 psig. The flow was then split into two streams, a primary flow and a secondary flow; each passed through a needle valve and a rotameter which measured the volumetric flow rate of each stream. The flow rates were chosen such that the Reynolds number of the flow through the furnace model would be 2000 or less (ie laminar region). The secondary flow rotameter had a range of 12 to 120 l/min and the primary rotameter 0.2 to 4.8 l/min. Rotameter readings were corrected for temperature and barometric pressure variations. The secondary air was directed into the model, while the primary air flowed first into a smoke generator.

3.2.4 The Smoke Generator

Smoke was generated by the combustion of pipe tobacco with the primary air. The primary air was fed into an Erlenmeyer flask through a glass nipple molded onto its side. Pipe tobacco was placed inside a large glass tube (22 mm OD, 150mm L) and ignited. A one hole stopper with a glass tube was placed onto the end of the large glass tube and this combustion tube was placd inside the flask. The primary air and smoke exited through the glass tube into a similar but smaller Erlenmeyer flask filled with crushed charcoal and fiber matting. This filtering flask was placed in an ice bath in order to cool the mixture. The cool filtered smoke then entered the furnace model through the primary inlet.

A bypass tube and a stop cock was used to control the quantity of smoke that mixed with the primary air entering the furnace model. The flow of smoke was reduced to the minimum amount necessary for visual observation.

3.3 EXPERIMENTS AND OBSERVATIONS – ORIGINAL BURNER

The original design called for identical burner exit velocities for the primary and secondary flows. The two flows were to merge together and continue down the furnace tube as a laminar steady stream.

A series of flow rates were chosen with Reynolds numbers in the laminar region and with identical secondary and primary burner exit velocities. Recirculation and flow instabilities were observed for all flow rates of practical interest. The flow became stable only at flow rates too low for practical operation of the furnace (Reynolds number less than 100). The recirculation occurred behind the jacket and the flow rapidly dispersed following the recirculation zone. The flow instabilities were observed to lead to turbulence and dispersion of the central jet for all flows of practical interest. This is highly undesirable for the function of the furnace, as it would cause the coal particles to disperse randomly.

A series of primary/secondary flow ratios were also examined and similar instabilities were observed (see Table 1). Figures 4 to 6 show the recirculation and instabilities that were observed at the top of the furnace; the flow remained unstable until the exit.

3.4 EXPERIMENTS AND OBSERVATIONS – MODIFIED BURNER

3.4.1 Modifications

The tests showed that the original burner design could not achieve the desired flow pattern through the furnace, and it was necessary to modify the burner to obtain a laminar steady flow. To eliminate the recirculation as much as possible, the 'cooling jacket' was removed (Figure 3b) and a honey-comb flow straightener and a foam screen were fitted snugly between the primary air tube and the furnace wall. The flow straightener is intended to produce a uniform velocity at the secondary flow outlet.

3.4.2 Experiments with Modified Burner

The addition of a flow straightener and elimination of the cooling jacket enabled the desired flow pattern to be obtained in the furnace. The smoke mixture entered the furnace and continued in a laminar steady stream until the exit; however, the flow was found to be stable only up to certain Reynolds numbers. A series of primary/secondary flow ratios were examined to determine the limit of this stability region. A primary/secondary flow ratio was chosen and was kept fixed through out the test; the resulting flow patterns were observed while both flows were reduced to the lowest possible values. A number of ratios were chosen and the procedure was repeated thereafter (see Table 2).

The flow stability curve that was obtained is shown in Figure 7. There is an apparent upper limit of stability for the furnace, marked by a transition from steady laminar flow with no noticable dispersion of the primary stream through increasingly unsteady laminar flow to fully turbulent conditions with

increasing Reynolds number. The turbulent region had no discernible regular pattern and was entirely characteristic of turbulent flow (see Figure 8). The unsteady laminar region exhibited distinguishable laminar filaments which oscillated in a regular 'wiggly' pattern; the magnitude of the oscillations decreased with decreasing Reynolds number (see Figure 9). The steady laminar region was characterized by smooth, undisturbed laminar flow with negligible dispersion of the central ('coal') jet (see Figure 10). At very low Reynolds numbers the flow was observed to break down at some point in the furnace tube. Since the flow in general can be expected to become more stable as the Reynolds number decreases, the breakdown observed here is evidently caused by an external disturbance, and is not an intrinsic feature of the flow. The point of break down was found to roughly correspond to the position of the lamp used to illuminate the smoke particles; it is probable that radiation from the hot lamp was absorbed by the smoke particles inducing a buoyancy effect which resulted in a breakdown of the flow. These points are noted in the lower left of Figure 7.

3.5 CONCLUSIONS FROM THE FLOW VISUALIZATION RESULTS

Past designs of actual entrained flow reactors have had success in obtaining a laminar flow through the furnace tube; observation ports in the sides of these furnaces have verified this claim [4, 25, 28, 36]. The stream of coal particles was observed to travel down the centre of the furnace tube while the furnace was running at its operating temperature.

However, the present cold flow experimental model showed that flow in the EMR furnace with the original burner design was unstable for almost all flow rates and was therefore unsatisfactory for the purpose of controlled mixing and controlled heating.

The results of the flow visualization tests using the experimental model yielded two conclusions to be drawn about the EMR furnace.

1. The EMR burner as originally designed must be modified in order to achieve the desired flow pattern in the furnace. A flow straightener should be used to obtain a uniform secondary velocity profile at the inlet to the furnace.
2. The primary and secondary flow rates must be adjusted such that the inlet velocity ratio and secondary Reynolds number fall within the range of stability in Figure 7.

These conclusions can strictly speaking only be applied to the real furnace under isothermal conditions; temperature differences and buoyancy effects in the furnace under non-isothermal conditions would change the limits shown in Figure 7. Owing to the inaccessibility of the interior of the EMR furnace, conclusions about dispersion in it could only be made from residence time distribution measurements.

TABLE 1

Original Burner Design – Test Flow Rates

Sec. Flow	US	Prim. Flow	UP	UP/US	Re-sec	Remarks
l/min	m/s	l/min	m/s			
120.0	1.399	2.70	1.397	1.00	1700	-turbulent after 8 cm
60.0	0.700	1.35	0.700	1.00	851	-turbulent
30.0	0.350	0.66	0.342	0.98	425	-unsteady laminar
105.0	1.224	4.80	2.487	2.03	1487	-turbulent dispersion
53.4	0.623	2.40	1.243	2.00	757	-unsteady laminar
26.7	0.311	1.20	0.622	2.00	378	-unsteady laminar
13.4	0.156	0.60	0.311	1.99	190	-unsteady laminar
53.4	0.623	4.80	2.487	3.99	757	-rapid dispersion
26.7	0.311	2.40	1.243	4.00	378	-turbulent
20.0	0.233	1.80	0.933	4.00	283	-unsteady laminar
13.4	0.156	1.20	0.622	3.99	190	-unsteady/turbulent
26.7	0.311	4.80	2.487	8.00	378	-turbulent
13.4	0.156	2.40	1.243	7.97	190	-turbulent after 30 cm
10.0	0.117	1.80	0.933	7.97	142	-unsteady laminar

TABLE 2

Modified Burner Design - Test Flow Rates

Sec. Flow	Vs	Prim. Flow	Vp	Vp/Vs	Re-sec	Remarks
l/min	m/s	l/min	m/s			
96.0	0.525	1.00	0.518	0.99	1700	-laminar
20.0	0.109	0.20	0.104	0.95	354	-first disturbance
10.0	0.055	0.10	0.052	0.95	177	-breakdown at tube bottom
119.0	0.651	1.50	0.777	1.19	2107	-unsteady laminar
110.0	0.602	1.38	0.715	1.19	1948	-unsteady laminar
100.0	0.547	1.25	0.648	1.18	1771	-unsteady laminar
90.0	0.492	1.13	0.585	1.19	1594	-nearly steady
80.0	0.438	1.00	0.518	1.18	1417	-steady laminar
119.0	0.651	1.87	0.969	1.49	2107	-fully turbulent
96.0	0.525	1.50	0.777	1.48	1700	-turbulent, more regular
83.0	0.454	1.30	0.674	1.48	1470	-turbulent, regular
70.0	0.383	1.09	0.565	1.48	1240	-nearly steady
60.0	0.328	0.94	0.487	1.48	1063	-steady laminar
96.0	0.525	2.00	1.036	1.97	1700	-turbulent
72.0	0.394	1.40	0.725	1.84	1275	-unsteady laminar
63.0	0.345	1.20	0.622	1.80	1116	-unsteady laminar
48.0	0.262	1.00	0.518	1.98	850	-steady laminar
5.0	0.027	0.10	0.052	1.93	89	-breakdown at bottom
70.4	0.385	2.20	1.140	2.96	1247	-fully turbulent
64.0	0.350	2.00	1.036	2.96	1133	-turbulent-regular
60.0	0.328	1.88	0.974	2.97	1063	-unsteady laminar
50.0	0.274	1.56	0.808	2.96	885	-nearly steady
53.0	0.290	2.20	1.140	3.93	940	-fully turbulent
52.8	0.289	2.20	1.140	3.94	936	-turbulent
51.0	0.279	2.10	1.088	3.90	904	-periodic laminar
48.0	0.262	2.00	1.036	3.95	849	-unsteady laminar
46.0	0.252	1.90	0.984	3.90	817	-nearly laminar
9.0	0.049	1.40	0.207	4.22	159	-remained laminar
42.2	0.231	2.20	1.140	4.94	749	-unsteady laminar
38.0	0.208	2.00	1.036	4.98	674	-nearly laminar
34.6	0.189	1.80	0.933	4.94	612	-steady laminar
35.2	0.192	2.20	1.140	5.94	622	-laminar/turbulent bursts
32.0	0.175	2.00	1.036	5.92	567	-laminar/unsteady bursts
26.5	0.145	2.20	1.140	7.86	470	-laminar

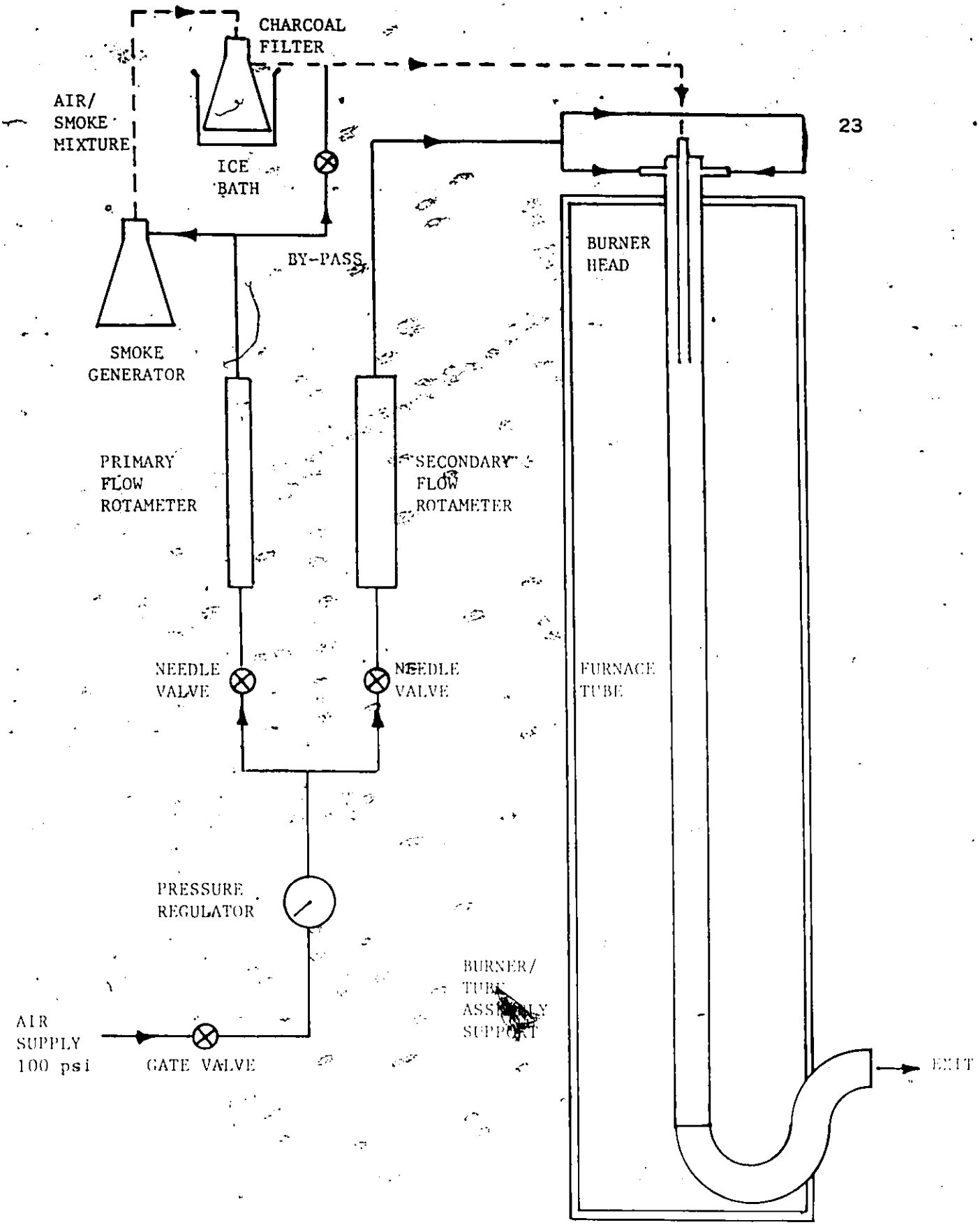

Figure 2: Schematic Drawing of Experimental Apparatus

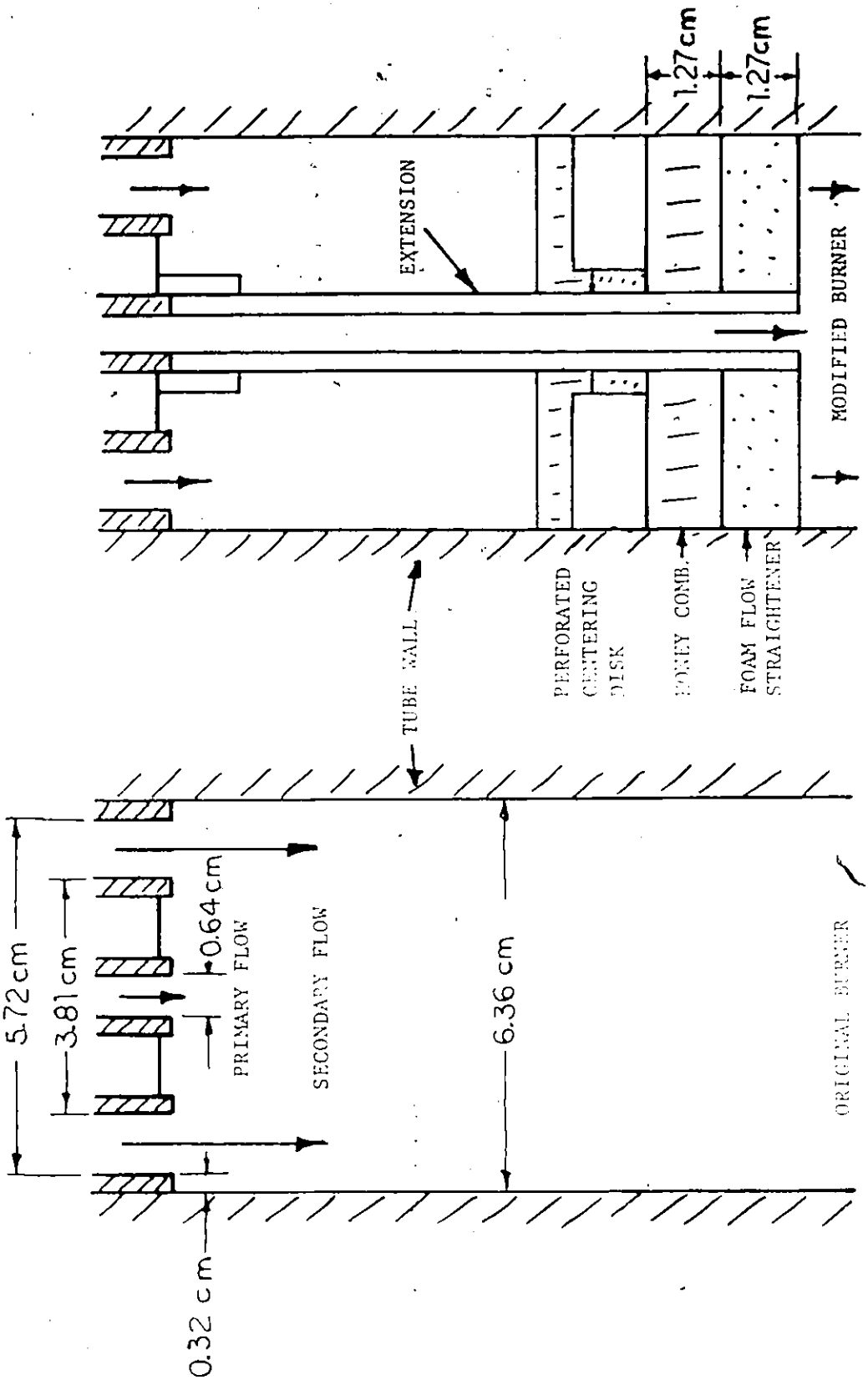

Figure 3: Detail of Burner Head – Original and Modified

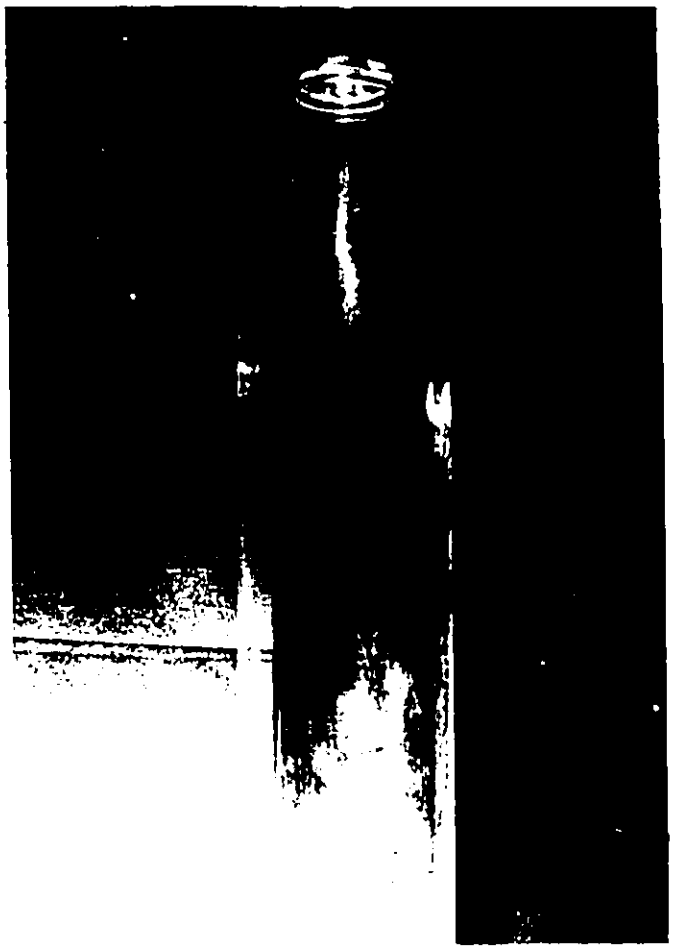

Primary Inlet Reynolds number 234
Secondary Inlet Reynolds number 850
Furnace Tube Reynolds number 1310

Figure 4: Original Burner – UP/US = 1:1 – turbulent flow

Primary Inlet Reynolds number	142
Secondary Inlet Reynolds number	427
Furnace Tube Reynolds number	656

Figure 5: Original Burner – UP/US – 1:1 – unsteady laminar flow

Primary Inlet Reynolds number 947
Secondary Inlet Reynolds number 1447
Furnace Tube Reynolds number 2257

Figure 6: Original Burner – UP/US – 2:1 – turbulent flow

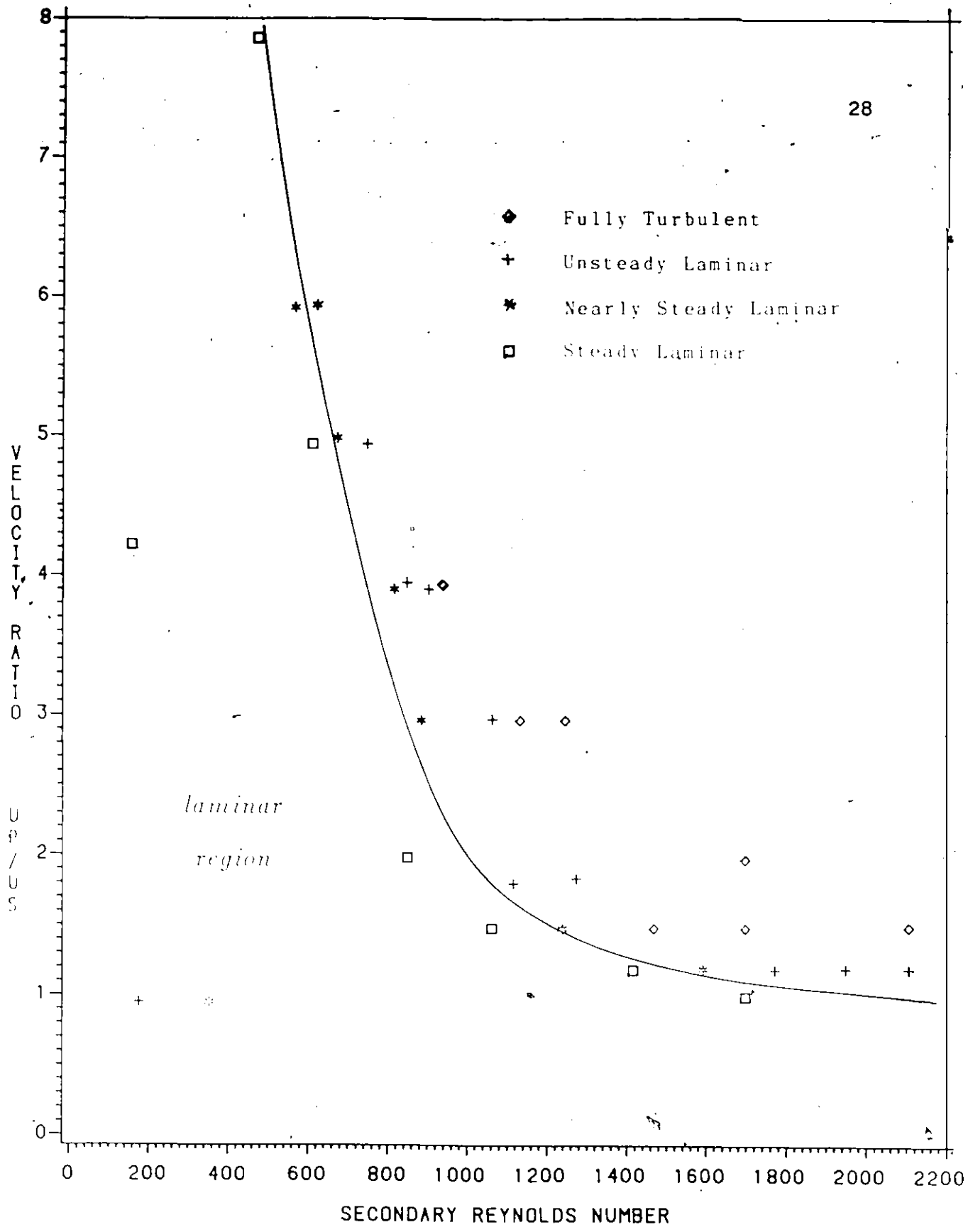

Figure 7: Stability Curve for Isothermal Flow – Modified Burner

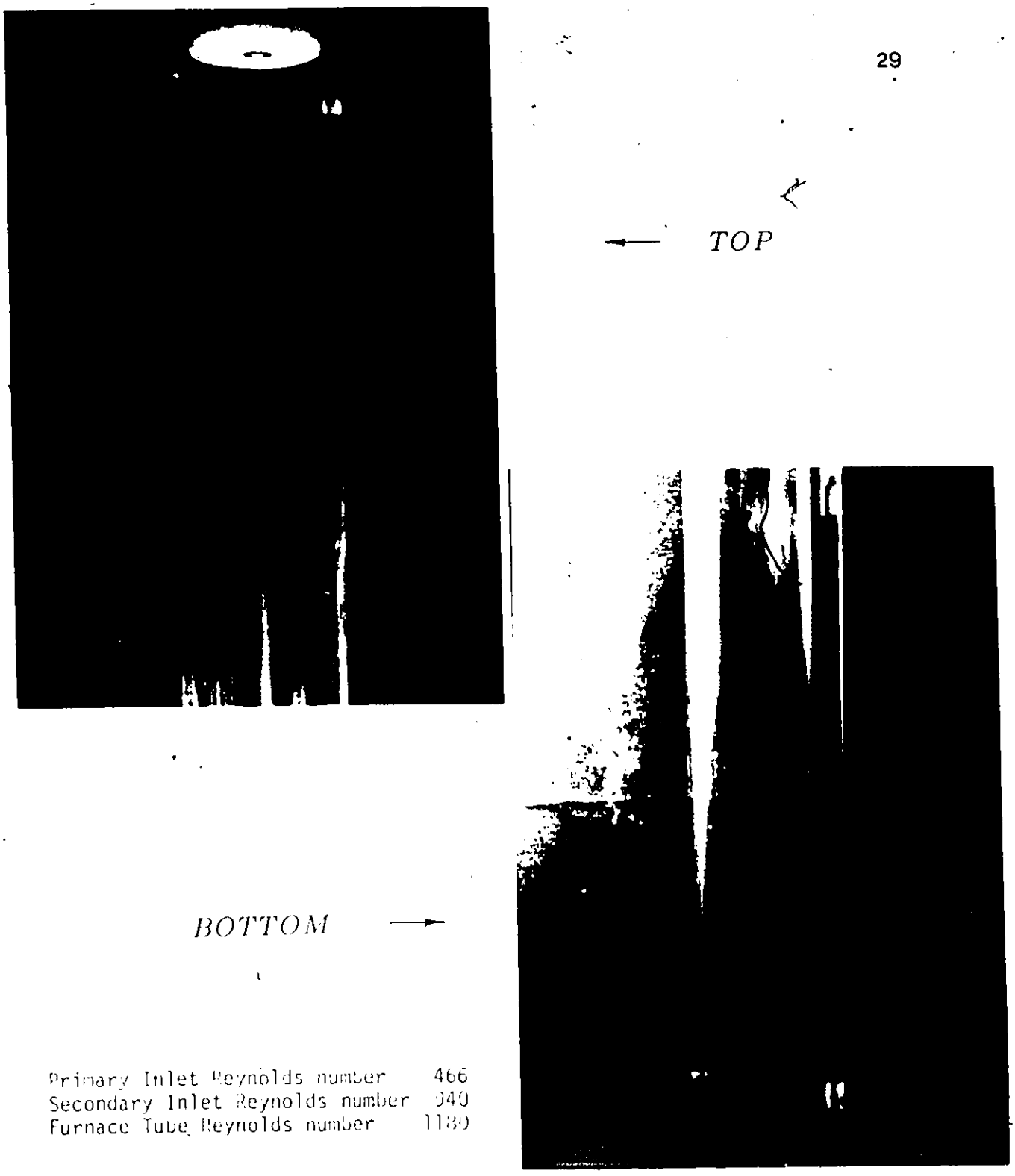

Figure 8: Modified Burner – GP/GS = 4:1 – turbulent flow

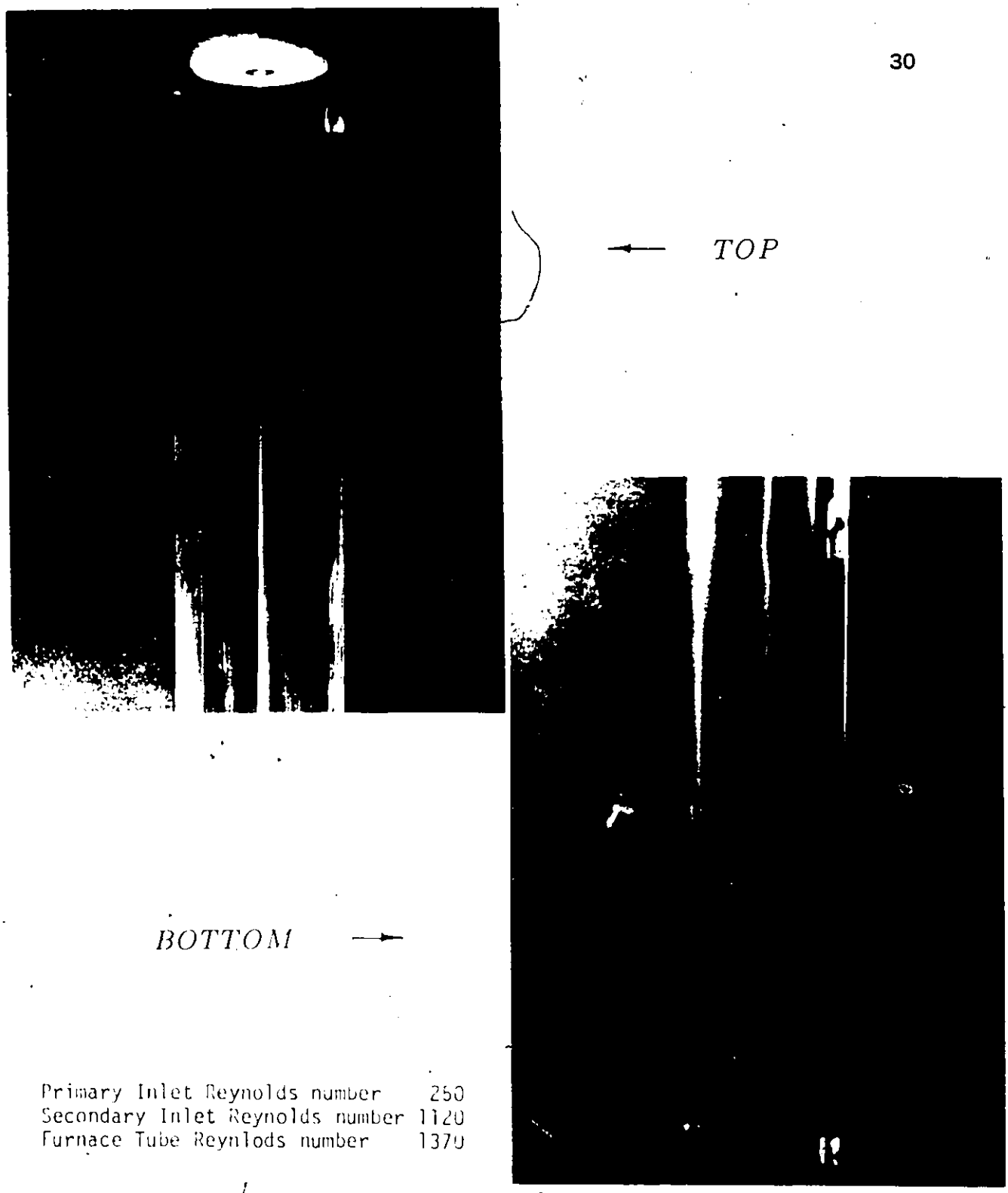

Primary Inlet Reynolds number 250
Secondary Inlet Reynolds number 1120
Furnace Tube Reynlods number 1370

Figure 9: Modified Burner – UP/US = 2:1 – unsteady laminar flow

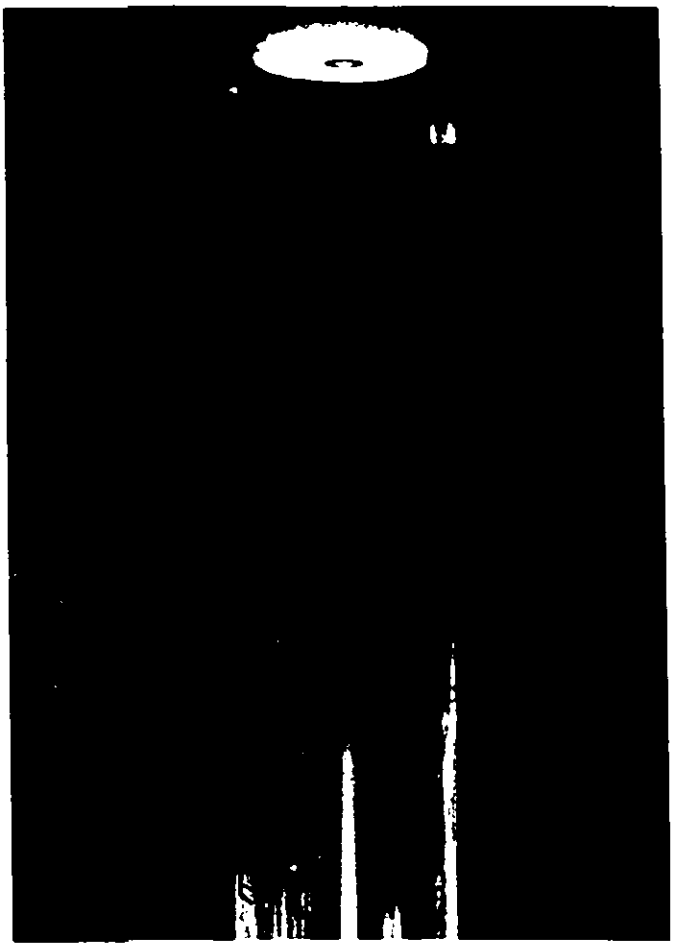

TOP ←

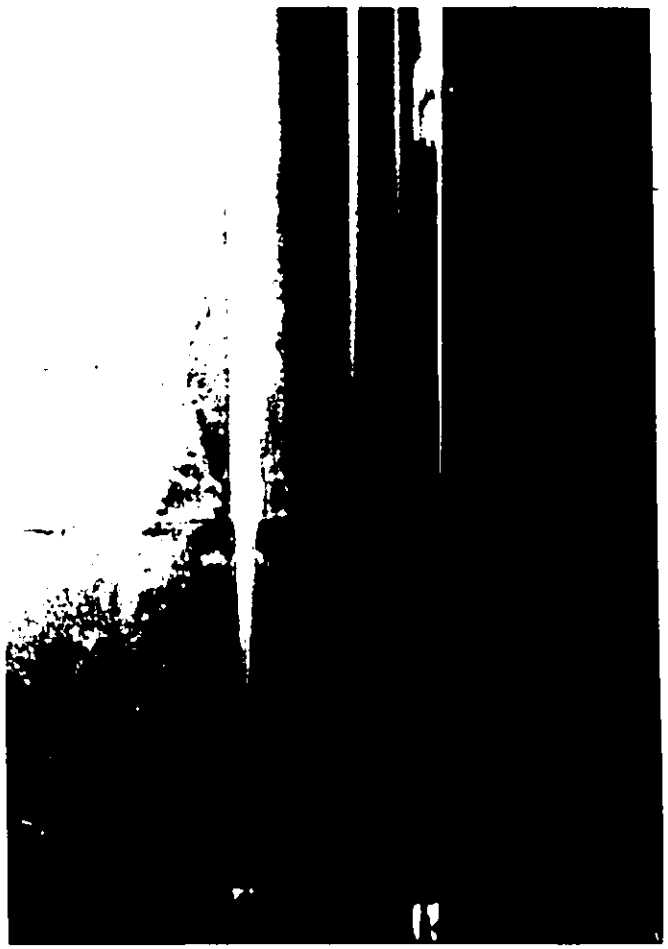

BOTTOM →

Primary Inlet Reynolds number 210
Secondary Inlet Reynolds number 425
Furnace Tube Reynolds number 535

Figure 10: Modified Burner – UP/US – 4:1 – steady laminar flow

Chapter IV

THE NUMERICAL MODEL

4.1 INTRODUCTION

A numerical model which gives flow field patterns and particle heating rates was developed for the CMCH coal testing facility; it is to be used in a parametric study to determine the various particle heating rates that could be achieved with the furnace. Input data are the inlet flow velocities and temperatures and the heating element temperatures of each of the four heating zones. The model incorporates variable properties and the buoyancy effects which result from the large temperature difference between the downward flow and the furnace wall. The coal particles are treated as inert (ie no chemical reaction) for this study; a combustion model is to be the subject of future research. The small concentration of particles was considered to contribute very little to the overall energy and momentum balances; the effects of the particles on the gas flow were therefore ignored, allowing the gas flow and particle heating problems to be decoupled (see Appendix A). The numerical scheme was required to resolve a laminar flow downwards through a vertical tube furnace with four independent heating zones and subsequently solve particle heating and transit times through the same furnace.

4.2 THE FURNACE FLOW FIELD

4.2.1 The Mathematical Problem

The problem to be solved is a parabolic, 2-D axisymmetric, non-isothermal, steady laminar flow. The equations involved are those of momentum, energy and continuity. The reduced forms of the differential equations necessary to solve this problem are shown in Table 3. It was assumed that viscous dissipation and compressibility effects were negligible in the energy equation, and specific heats and Prandtl number were assumed constant over the temperature range of interest. The differential equations are all interlinked with each other and with the inlet and boundary conditions. These interactions add to the complexity of the problem, and a successful numerical scheme must be able to conform to all these interactions.

4.2.2 The TEACH Program

The numerical scheme that was chosen for the solution was the 1974 Imperial College TEACH (Teaching Elliptic Axisymmetric Characteristics Heuristically) finite difference program. The TEACH computer code is based on a primitive pressure - velocity approach, solving for pressure and velocity as primary variables. TEACH is a widely used, standard computer code that has been used for a number of fluid dynamic and heat transfer problems [2, 26, 29]. TEACH puts the governing differential equations into finite difference form by integration over a control volume. The solution combines each of the equations of energy, momentum and continuity with the boundary and inlet conditions and solves them simultaneously using an iterative procedure. The program consists of a main routine which calls a series of subroutines to solve for the dependent variables. A TDMA (Tri-Diagonal Matrix Algorithm) is used to

solve the flow field equations and the equations are solved iteratively until a convergence criterion is met.

4.2.3 The Formulation of the Problem

The equations of momentum, energy and continuity are similar and contain terms for both convection and diffusion of momentum, energy and mass as well as source terms. The governing differential equations in Table 3 can all be put into the following convenient form:

$$\frac{1}{r}\left[\frac{\partial}{\partial x}(\rho u r\phi) + \frac{\partial}{\partial r}(\rho v r\phi) - \frac{\partial}{\partial x}(r\Gamma_\phi \frac{\partial \phi}{\partial x}) - \frac{\partial}{\partial r}(r\Gamma_\phi \frac{\partial \phi}{\partial r})\right] = Su^\phi + Sp^\phi \phi \quad (4.1)$$

The values for ϕ, Su^ϕ and Sp^ϕ for each equation are shown in Table 4. These are the equations necessary to solve the furnace flow field. The unknown variables are the axial and radial velocities, the pressure and the temperature.

The flow field area is divided into small control volumes which form a grid pattern. The control volumes need not be uniform, and can have varying sizes. Figure 11 shows a typical control volume, through which momentum, energy and mass are transported by convection and diffusion, while generation and dissipation of momentum within the cell also takes place. Conservation of these quantities is necessary for each cell. Values of variables are stored at the node points within the cell, except for the axial and radial velocity, which are stored at points on the control volume boundaries. The nodes are placed such that the control volume boundaries lie exactly halfway between adjacent nodes. This type of formulation results in a staggered grid, as discussed by Patankar [29].

As a result of the staggered grid, two further control volumes arise for the axial and radial velocities ('U' and 'V' cells – the cell first shown in Figure 11 is referred to as a 'C' cell). These are shown in Figure 12. For each control volume there is a centre point and its four neighbouring points N,S,W,and E, as illustrated in Figure 11. By integrating over the appropriate control volume, a quantity at the centre of the control volume can be expressed in terms of the neighbouring grid point values. Details of the integration can be found in [2, 26, 29]. The result is an equation of the form:

$$a_P^{\phi}\phi_P = \sum_j a_j^{\phi}\phi j + Su^{\phi}$$

where $$a_P^{\phi} = \sum_j a_j^{\phi} - Sp^{\phi}$$

for each cell, where ϕ can represent any variable, and the coefficients 'a^{ϕ}' represent the influence of each neighbour cell on P.

This formulation is applied to each cell control volume in the grid domain. The cells in the grid are adjacent to each other; therefore, the east face of one cell is the west face of the cell immediately to the right, and so forth. Similarly, the south face of one cell is the north face of the cell beneath it. Expressions for each cell are obtained in this fashion.

For each control volume there will be a diffusive and a convective flux into and out of the cell. A 'hybrid' scheme is used to calculate these, which employs different expressions for the total flux, depending on whether one flux dominates or the two are of the same order of magnitude. Defining the Peclet number as the ratio of convective to diffusive transport of the variable ϕ, the hybrid scheme uses as a criterion a Peclet number equal to 2 to determine the dominating flux. If the Peclet number is greater than 2, the upstream

convective flux dominates (ie the flux through the west cell face), and an upwind difference formulation is used, in which the value of ϕ at point W is assumed convected into cell P, and diffusion is neglected. If the Peclet number is less than -2, the downstream convective flux dominates (ie flux through east cell face), leading to a similar formulation involving point E. If the Peclet number lies between -2 and 2 (convection and diffusion of the same order of magnitude), diffusion is included, and a central difference formulation is used for convection, in which the value of ϕ at the cell boundary (determined by linear interpolation) is convected into the cell. All the cells in the grid domain are treated in the same manner. The hybrid scheme is said to be a good approximation to an exact one-dimensional solution. The exact solution is not recommended because it contains exponentials, which are expensive to compute, and because it is not exact for two or three dimensions (Patankar [29]).

The U and V cells (representing the axial and radial equations of motion) contain pressure gradient terms not present in the C cell. In order to solve the U and V equations, the pressure field must be known. An estimate of the pressure field P^* is used as a trial, and subsequent estimates of velocity fields U^* and V^* are made based on this pressure field. A pressure correction is then made, which forces the velocity field to obey the continuity equation by applying the correction to U^* and V^* to give U and V. The corrected pressures are then used as the new trial values, and so on till convergence is achieved.

The finite difference equations are coupled with the inlet and boundary conditions, all of which must be solved simultaneously. The coefficients and source terms are functions of the variables, and the velocities are strongly dependent on the pressure. The equations are solved by a cyclic repetition of the following steps:

1. Estimate all of the dependent variables
2. Solve the axial and radial momentum equations and obtain estimates for the U and V velocity fields
3. Solve for the pressure correction field P'
4. Calculate the true pressure field and correct the U and V velocity fields
5. Calculate the temperature field T
6. Calculate the density and viscosity
7. Treat the values obtained as better estimates of each field. Return to 2. and repeat the procedure until convergence

A flow chart of the procedure is shown in Figure 13. A listing of the computer program is included at the end of this paper.

4.2.4 The Grid Pattern

The grid pattern for a particular problem is determined from the geometry, the type of flow and the boundary and inlet conditions. The number of grid points and the spacing between them is important in obtaining an accurate solution. The CMCH furnace was considered to be a heated pipe with developing temperature and velocity profiles, and four wall heating zones whose temperatures could be varied independently.

The furnace can be represented by a series of annular segments, which are the control volumes over which the differential equations are integrated. Since the furnace is axisymmetric, only one half of the furnace need be examined. Developing velocity and temperature profiles in a tube approach their final form asymptotically. The profiles change quite rapidly in the initial region of the tube, and the changes become less as the flow approaches its final fully

developed state. To correspond to this, a grid spacing was chosen such that there were many points in the region of large gradients and fewer points as the gradients became smaller; the resulting scheme gave a grid spacing which increased approximately exponentially with distance along the furnace. Similarly, the grid lines were spaced more closely in the radial direction at the tube wall and the burner inlet because of the large gradients expected there.

A series of tests were performed to determine the number and spacing of points that were necessary for accuracy, taking into account the points discussed above and the requirement that the boundaries of the four heating zones correspond with the cell boundaries. To aid in this decision, the program was used to solve a number of simple test cases for which solutions were available from the literature. The test cases were as follows:

1. Iso-thermal developing pipe flow
2. Fully developed pipe flow subject to heating at constant wall temperature
3. As in 2. but heating with constant heat flux

These are discussed in detail in Section 5.1. The number of points and their spacing in the furnace tube was consequently modified so that they would conform to published results.

The grid pattern that was chosen for this problem consisted of 28 nodal points in the axial direction and 20 nodal points in the radial direction. The grid is shown in Figure 14.

4.2.5 Inlet Conditions

The flow was introduced into the furnace through the burner mouth. It consisted of a primary and secondary stream of air. The primary flow was assumed to have had sufficient length to attain a fully developed parabolic profile before entering the furnace, while the secondary flow velocity was assumed uniform. The results of the flow visualization experiments showed that a modification to the burner was necessary in order to obtain a stable flow; hence, the modified burner geometry was used for all calculations.

The primary flow was assumed kept at a constant temperature by means of the water-cooled jacket, while the secondary flow was assumed preheated to a specified inlet temperature.

4.2.6 Boundary Conditions

The physical boundaries for this problem were the furnace wall, the burner and the water-cooled injector. The grid cells which lie along these boundaries have to be modified to incorporate the known boundary values. Each cell is a small control volume over which the differential equations are integrated. If a cell face falls on a boundary, the known boundary value is used for that face, and any fluxes (heat) associated with the boundary are introduced via a source term (Equation 4.1). The boundary value incorporated into the source term remains fixed throughout each iteration. The remaining faces of the boundary cell and subsequently all cells throughout the flow field adjust with each iteration to incorporate the boundary value.

4.2.6.1 Velocity Boundary Conditions

The boundary conditions for the axial and radial velocity fields are shown in Figure 15. The boundaries specified are the furnace wall, the tube axis and the water–cooled section of the burner. The outlet represents no physical boundary, therefore no boundary conditions are imposed. The only requirement at the outlet boundary is the overall conservation of mass. At each iteration, the total mass leaving the furnace is subtracted from the total mass entering the furnace. The difference is evenly divided and added to the control volumes on the outlet boundary, therefore continuity is satisfied.

4.2.6.2 Temperature Boundary Condition

There are two wall surfaces which need to have a temperature boundary condition specified: the face of the water–cooled jacket of the burner, and the furnace tube wall. The temperature of the water–cooled jacket is considered to remain constant at the cooling water temperature, while the temperature of the furnace wall is unknown and must be solved for.

The furnace tube is heated by 64 – 500 W glow bars. These are spaced evenly down the length of the tube, 32 on each side. The furnace tube is completely surrounded by refractory material in which the glow bars are embedded . The furnace is separated into four independent heating zones and the temperature of each zone is measured using a thermocouple. Since the furnace is well enclosed and well insulated, the refractory surface surrounding the tube was considered as a uniformly radiating surface at the measured zone temperature with an emissivity equal to one. Figure 16 shows a cross section through the furnace tube. The radiation from the refractory brick to the outside wall of the furnace tube is given by:

$$\dot{Q} = 2\pi R_o L \sigma \epsilon (T_{gb}^4 - T_{wo}^4)$$

or $$\dot{Q} = 2\pi R_o L \sigma \epsilon (T_{gb} - T_{wo})(T_{gb} + T_{wo})(T_{gb}^2 + T_{wo}^2)$$

where ϵ = 0.90 furnace tube (Bolz and Tuve [8])

Heat conduction through the mullite furnace tube is given by:

$$\frac{Q}{2\pi R\ L} = \frac{k_w (T_{wo} - T_w)}{R \ln (R_o / R)}$$

where, k_w = 2.076 W/m K (Bolz and Tuve [8])

Heat conduction from the inner tube wall to the flowing gas is given by:

$$\frac{\dot{Q}}{2\pi R L} = k_g \left(\frac{\partial T}{\partial r} \right)_w \qquad \text{where} \qquad \left(\frac{\partial T}{\partial r} \right)_w \quad \begin{matrix} T_w & T_g \\ R & R_g \end{matrix}$$

The overall expression for the heat transfer from the glow bars to the gas inside the tube is then:

$$\frac{\dot{Q}}{2\pi R L} \quad \begin{matrix} T_{gb} & T_g \\ R_w + R_g + R_r \end{matrix}$$

where

$$R_g \quad \begin{matrix} R & R_g \\ k_g \end{matrix}$$

$$R_w \quad \begin{matrix} R \ln (R_o / R) \\ k_w \end{matrix}$$

$$R_r \quad \begin{matrix} R & 1 \\ R_o \sigma \epsilon (T_{gb} + T_{wo})(T_{gb}^2 + T_{wo}^2) \end{matrix}$$

This expression is used as the boundary condition for the furnace wall temperature. The four zone temperatures can be changed independently.

4.2.7 Buoyancy

Buoyancy forces become significant in this problem because of the large temperature differences between the furnace wall and the incoming fluid, leading to large density differences within the furnace.

Consider the following terms in the U momentum equation:

$$\ldots = -\frac{\partial P}{\partial x} + \rho g_x$$

This will appear as a source term in the axial momentum equation. In order to avoid instability in a numerical solution, it is desirable to make sources as small as possible. In this case, this can be done by choosing a arbitrary reference density ρ_0 ,leading to:

$$\ldots = -\frac{\partial P'}{\partial x} + g_x(\rho - \rho_0)$$

where $$P' \quad P \quad \int \rho_0 g_x dx$$

Since this integral is only a function of x and not of y:

$$\frac{\partial P}{\partial y} \quad \frac{\partial P'}{\partial y}$$

the radial velocity field is not affected. The reference density was chosen as ρ_{axis} since:

$$\frac{\partial}{\partial y}(\rho_{axis}) = 0$$

The pressure calculated now becomes the 'pressure head' at the centre of the flow. By using this formulation for the reference density, the number of iterations necessary for convergence is reduced because of less round-off error and less instability. The disadvantage is that the pressure now is calculated as P' rather than the actual pressure P; however, P is not required for any further purpose (Spalding [37]).

4.2.8 Fluid Properties

4.2.8.1 Density

Air is considered to be an ideal gas, therefore the density is calculated using the ideal gas law:

$$\rho = P/RT$$

where P = pressure

R = gas constant

T = temperature

The temperature is calculated from the solution of the energy equation; hence,the density must be updated with each iteration.

4.2.8.2 Viscosity

The variation of viscosity with temperature was accounted for by using the Sutherland equation:

$$\mu = \frac{BT^{\frac{3}{2}}}{(T + S)}$$

where B = 1.5 E-6

S = 130.0

T = temperature

The constants B and S were determined by fitting the equation to values in tables (Holman [20]). Figure 17 compares actual air viscosities to those predicted by the Sutherland equation. As with the density, the local viscosity must be updated each iteration.

4.2.9 Convergence Criterion

The respective differential equations (Equation 4.1) are integrated over each corresponding control volume (ie C, U, or V cell) in the grid domain. If these equations are not satisfied, there will be a remaining or residual momentum, mass or energy source in the control volume, which can be either positive or negative. There will be axial momentum residuals for the U cells, radial momentum residuals for the V cells, and mass and energy residuals for the C cells. The absolute values of the residuals for each control volume are totalled over the grid domain for each of the four residual quantities and made non–dimensional by means of the corresponding inlet values (ie inlet momentum, mass and energy fluxes).

Inlet momentum flux $= 2\pi \int_0^{r_o} \rho u^2 r\, dr$

Inlet mass flux $= 2\pi \int_0^{r_o} \rho u r\, dr$

Inlet energy flux / c_P $= 2\pi \int_0^{r_o} u T r\, dr$

where u = inlet velocity

r = radial postion

T = temperature

ρ = density

c_P = specific heat

With each iteration and subsequent adjustments of the flow field, each of the four residuals will be reduced (or increased). If the solution is converging, then the residual terms will tend to zero (conversely, if the solution is diverging, then the terms will tend to infinity). If the residual terms are small enough that further adjustments of the flow field are negligible then the solution can be said to be converged. In this case, the criterion used for convergence was that all four dimensionless residuals be less than 2%. Tests showed that a more stringent criterion did not significantly change the solution. It should be noted that, since there are 560 points in the grid, this represents a residual source of less than 0.004% for each cell on the average. The criterion is made more stringent by the fact that the residuals are calculated before the pressure correction is applied to obtain the final, correct velocity field. The execution of the program will stop if any of the following criteria are met:

1. The solution has converged.
2. The solution has diverged.
3. The maximum number of iterations has been reached.

To aid in the convergence and avoid oscillations, the solution uses an under-relaxation factor (URF) which reduces the magnitude of the flow field changes after each iteration. The formulation for under-relaxation is as follows:

$$\phi_P^{n+1} = (URF)\tilde{\phi}_P^{n+1} + (1 - URF)\phi_P^n$$

where $\tilde{\phi}_P^{n+1}$ represents the newly calculated value of ϕ_P at the (n+1)th iteration. A fraction (URF) of the new calculated value of ϕ_P at the (n+1)th iteration is taken and the remaining fraction is taken as the previously calculated value at the (n)th iteration. This is done for each value in the domain thus reducing the magnitude of the changes of ϕ_P between sucessive

iterations; the resulting field is used for calculations in the other subroutines. The effect of the under-relaxation factor is substantial, and oscillating or diverging solutions can result if URF is not chosen correctly. The URF must be chosen to suit each problem. Four URF are used in this problem:

axial velocity URFU = 0.5

radial velocity URFV = 0.5

pressure URFP = 0.2

temperature URFT = 0.8

4.3 PARTICLE MOTION AND HEATING

4.3.1 Introduction

Once the flow and temperature field has been solved for, the flow and heating of the particles can be introduced. In order to simplify the problem, a number of assumptions were made in the development of this model:

1. The volumetric concentration of particles is small enough such that individual particles are not affected by neighbouring ones (see Appendix A).
2. The addition of particles to the furnace does not affect the momentum, energy or continuity balances in the gas significantly.
3. The particles are treated as grey spheres exchanging heat by radiation and convection with the gas and the furnace wall and are considered small enough and of sufficiently low concentration not to cause any effect on the radiant exchange between surfaces. By the same token, scattering of radiation by particles ('cloud effects') is neglected.
4. The particles do not react chemically

5. The particles follow a straight line down the centre line and are not dispersed radially.
6. The temperature is assumed uniform within each particle, ie internal temperature gradients due to heating are neglected.

4.3.2 Particle Motion

The coal particles were considered spherical in shape; therefore, the forces experienced by the particle are those of gravity and drag. The acceleration of the particle is given by:

$$\frac{\partial u_P}{\partial t} = g - \frac{3}{4}\frac{C_D \rho}{\rho_P d_P}(u_P - u)|u_P - u|$$

where $$C_D = \frac{24}{Re}(1 + 0.15Re^{0.687}) \qquad (4.2)$$

(Smoot[35])

$$Re = \frac{\rho|u_P - u|d_P}{\mu}$$

For small Re, the expression inside the brackets on the right of Equation (4.2) will be small; therefore, it can be linearized as:

$$\frac{du_P}{dt} = g - A(u_P - u) \qquad (4.3)$$

where $$A = \frac{18\mu}{\rho d_P^2}(1 + 0.15Re_0^{0.687})$$

The solution uses an explicit marching scheme, following the particle along the axis of the tube in discrete time steps Δt and calculating each new velocity based on the local air velocities and previous particle velocities. Equation (4.3) is an exact differential equation and could be solved directly if A were constant; however, the gas velocity and the Reynolds number are constantly changing. If a small enough time step is chosen, then u and Re_0 can be assumed constant throughout the time step Δt (Smoot [35]), and Equation (4.3) integrated to give:

$$u_P = u - \frac{1}{A}\left[\left(g - A(u_{P0} - u)\right)e^{-A\Delta t} - g\right]$$

where u_P = the velocity at the end of the time step

u_{P0} = the velocity from the previous time step

Properties of the gas are evaluated at the film temperature, which is the arithmetic mean of the particle temperature and the surrounding gas temperature.

4.3.3 Particle Heating

The heating of a particle is based on the net energy received by the particle as it travels through the furnace. The particle receives or loses energy by radiation from/to the surrounding surfaces and loses or gains energy by convection to/from the surrounding gas. The furnace was separated into four radiating surfaces: the furnace wall, the primary inlet and water-cooled jacket, the secondary inlet, and the water-cooled collector. The temperature of the furnace wall is not constant, but varies along the furnace length. To simplify

the problem, the model uses a 'long furnace' approximation, which assumes that the effective radiating temperature of the wall is the temperature of the wall section radially opposite the particle (Hottel and Sarofim [21]). The temperature of the other radiating surfaces was assumed constant, and the appropriate view factor was used in determining the radiant balance. Since the particle is small, the radiant exchange between it and the other particles was considered negligible.

The expression for particle heat transfer is given as follows:

$$mc_{PP}\frac{dT}{dt} = A_P q_{net} \qquad (4.4)$$

where $$m = \rho_P \frac{\pi}{6} d_P^3$$

$$A_P = \pi d_P^2$$

$$q_{net} = |q_{rad} - q_{conv}|$$

c_{PP} coal = 1.3 kJ/kg K (Bolz and Tuve [8])

therefore, rearranging;

$$\frac{dT}{dt} = \frac{6}{\rho_P c_{PP} d_P}|q_{rad} - q_{conv}|$$

where $$q_{conv} = h(T_P - T_g)$$

$$h = 2.0 + (0.4Re^{1/2} + 0.06Re^{2/3})(Pr^{0.4})\left(\frac{\mu}{\mu_P}\right)^{1/4}\frac{\mu c_P}{Pr d_P} \quad \text{(Holman[20])}$$

and

$$q_{rad} = h_{PP}(T_1 - T_P) + h_{PS}(T_S - T_P) + h_{PE}(T_E - T_P) + h_{PW}(T_W - T_P)$$

$$h_{PP} = \sigma\epsilon F_{PP}(T_1 + T_P)(T_1^2 + T_P^2)$$

$$h_{PS} = \sigma\epsilon F_{PS}(T_S + T_P)(T_S^2 + T_P^2)$$

$$h_{PE} = \sigma\epsilon F_{PE}(T_E + T_P)(T_E^2 + T_P^2)$$

$$h_{PW} = \sigma\epsilon F_{PW}(T_W + T_P)(T_E^2 + T_P^2)$$

$\epsilon_{coal} = 0.8$ (Hottel and Sarofim [21])

F_{PP}, F_{PW}, F_{PE}, F_{PS} are the view factors and can be found in Appendix (B).

The expression for particle heating can be written as:

$$\frac{dT_P}{dt} = -AT_P + B \qquad (4.5)$$

where $$A = \frac{6}{\rho_P c_{PP} d_P}\left[h_{PP} + h_{PS} + h_{PE} + h_{PW} + h\right]$$

$$B = \frac{6}{\rho_P c_{PP} d_P}\left[h_{PP}T_1 + h_{PS}T_S + h_{PE}T_E + h_{PW}T_W + hT_g\right]$$

As with the particle velocity, the wall temperature and the gas temperature are changing axially along the furnace tube. To be able to integrate this equation, these values are assumed constant over the time step Δt. By integrating Equation (4.5) over Δt the expression becomes:

$$T_P = \frac{1}{A}\left[B + AT_{P0}e^{-A\Delta t}\right] \qquad (4.6)$$

The value of Δt must be selected such that the assumptions of constant u, T, Re are valid. By choosing a time step such that $T_{P0} - T_P$ is less than ΔT_{max}, where ΔT_{max} is an arbitrarily chosen constant which would give a fixed increase in temperature between points, (chosen as 5 K). Equation (4.4) becomes:

$$\Delta t \approx \frac{\rho_P c_{PP} d_P \Delta T_{max}}{6(q_{rad0} - q_{conv0})}$$

where q_{rad0} , q_{conv0} are from the previous time step

By selecting Δt in this manner, Δt would be small initially where the heating was very rapid, and would become progressively larger downstream where the temperature increase becomes less. An upper limit for the time step was chosen (5 ms) in order to ensure the validity of the assumption that the gas velocity was constant over the time step.

The particle velocity and temperature model was added onto the main furnace flow program as a subroutine. Once the furnace flow field had been calculated, the particle model subroutine was called to calculate particle velocities and temperatures.

TABLE 3

Governing Differential Equations

EQUATION OF CONTINUITY

$$\frac{1}{r}\left[\frac{\partial}{\partial x}(\rho u r) + \frac{\partial}{\partial r}(\rho v r)\right] = 0$$

EQUATION OF MOTION

axial direction

$$\frac{1}{r}\left[\frac{\partial}{\partial x}(\rho u^2 r) + \frac{\partial}{\partial r}(\rho u v r) - \frac{\partial}{\partial x}(r\mu\frac{\partial u}{\partial x}) \quad \frac{\partial}{\partial r}(r\mu\frac{\partial u}{\partial r})\right]$$
$$= -\frac{\partial P}{\partial x} + \frac{\partial}{\partial x}(\mu\frac{\partial u}{\partial x}) + \frac{1}{r}\frac{\partial}{\partial r}(r\mu\frac{\partial v}{\partial x}) - \frac{2}{3}\frac{\partial}{\partial x}(\frac{\mu}{r}\frac{\partial}{\partial r}(rv) + \mu\frac{\partial u}{\partial x}) + \rho g_x$$

radial direction

$$\frac{1}{r}\left[\frac{\partial}{\partial x}(\rho u v r) + \frac{\partial}{\partial r}(\rho v^2 r) - \frac{\partial}{\partial x}(r\mu\frac{\partial v}{\partial x}) - \frac{\partial}{\partial r}(r\mu\frac{\partial v}{\partial r})\right]$$
$$= -\frac{\partial P}{\partial r} - \frac{2\mu v}{r^2} + \frac{\partial}{\partial x}(\mu\frac{\partial u}{\partial r}) + \frac{1}{r}\frac{\partial}{\partial r}(r\mu\frac{\partial v}{\partial r}) \quad \frac{2}{3}\frac{\partial}{\partial r}(\frac{\mu}{r}\frac{\partial}{\partial r}(rv) + \mu\frac{\partial u}{\partial x})$$

EQUATION OF ENERGY

$$\frac{1}{r}\left[\frac{\partial}{\partial x}(\rho u T r) + \frac{\partial}{\partial r}(\rho v T r) \quad \frac{\partial}{\partial x}(r\frac{k}{c_p}\frac{\partial T}{\partial x}) \quad \frac{\partial}{\partial r}(r\frac{k}{c_p}\frac{\partial T}{\partial r})\right] = 0$$

TABLE 4

Expressions for the Variables of the Generalized Equation

ϕ	Γ_ϕ	Sp^ϕ	Su^ϕ
1	0	0	0
u	μ	0	$\frac{\partial}{\partial x}\left(\mu \frac{\partial u}{\partial x}\right) + \frac{1}{r}\frac{\partial}{\partial r}\left(r\mu \frac{\partial v}{\partial x}\right) - \frac{\partial P}{\partial x} + \rho g_x$
v	μ	$-\frac{2\mu}{r^2}$	$\frac{\partial}{\partial x}\left(\mu \frac{\partial u}{\partial r}\right) + \frac{1}{r}\frac{\partial}{\partial r}\left(r\mu \frac{\partial v}{\partial r}\right) - \frac{\partial P}{\partial r}$
T	$\frac{k}{c_P}$	0	0

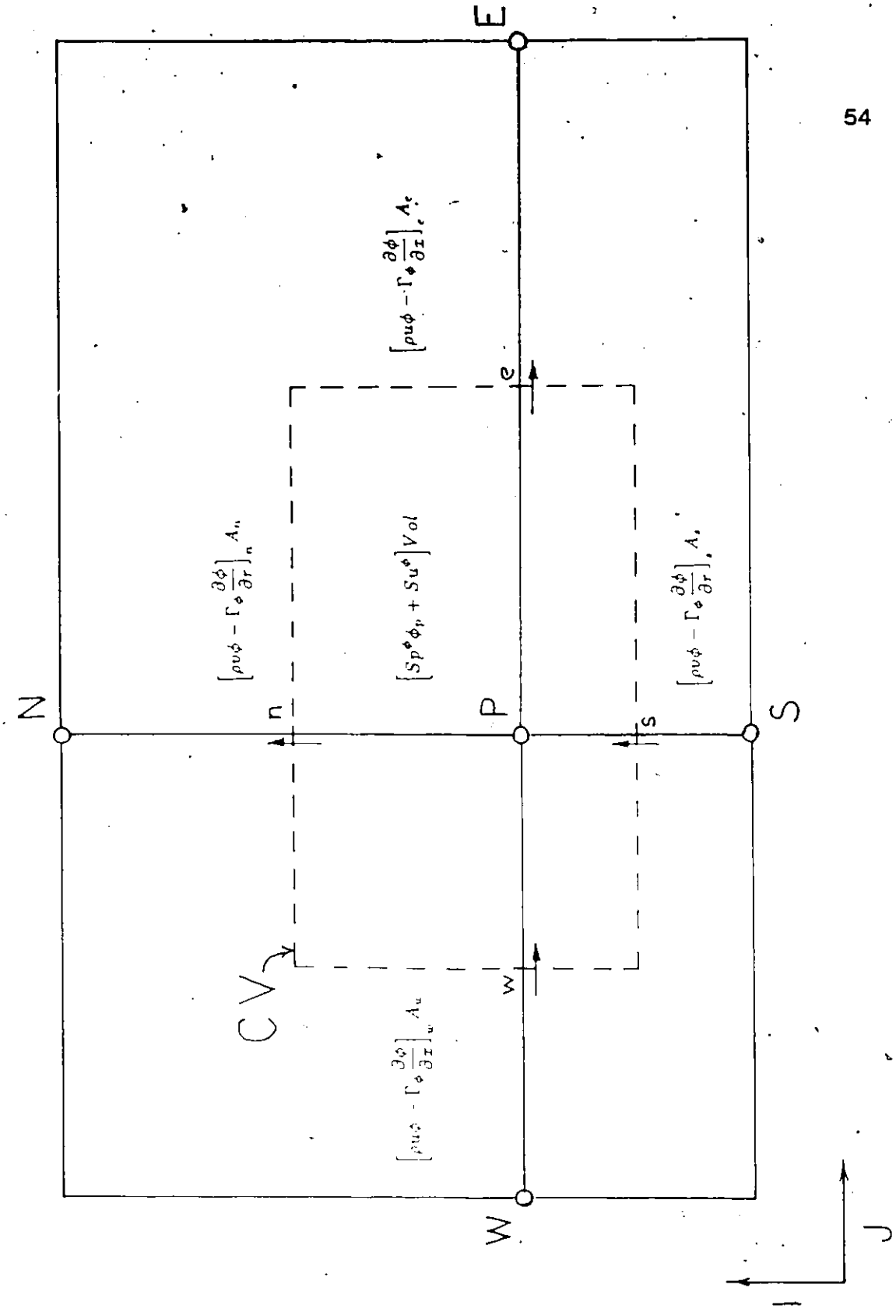

Figure 11: Typical Control Volume for Numerical Model of Furnace

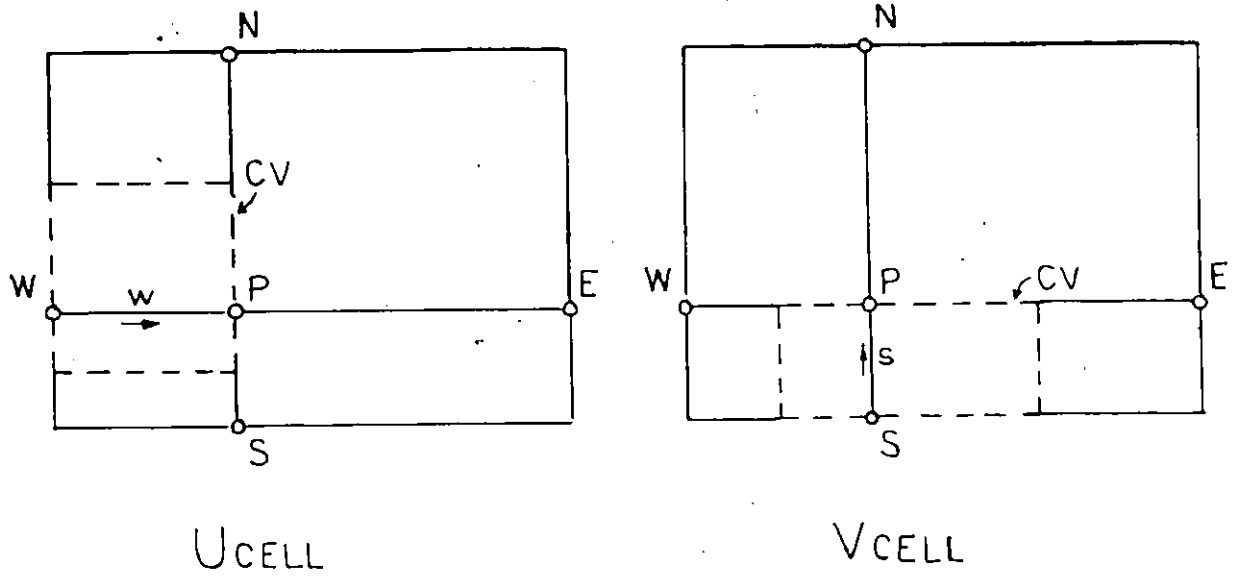

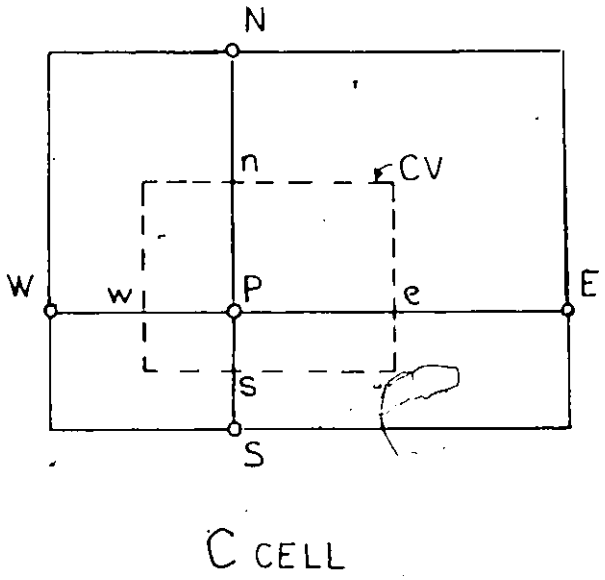

Figure 12: U, V and C Cells for Numerical Model

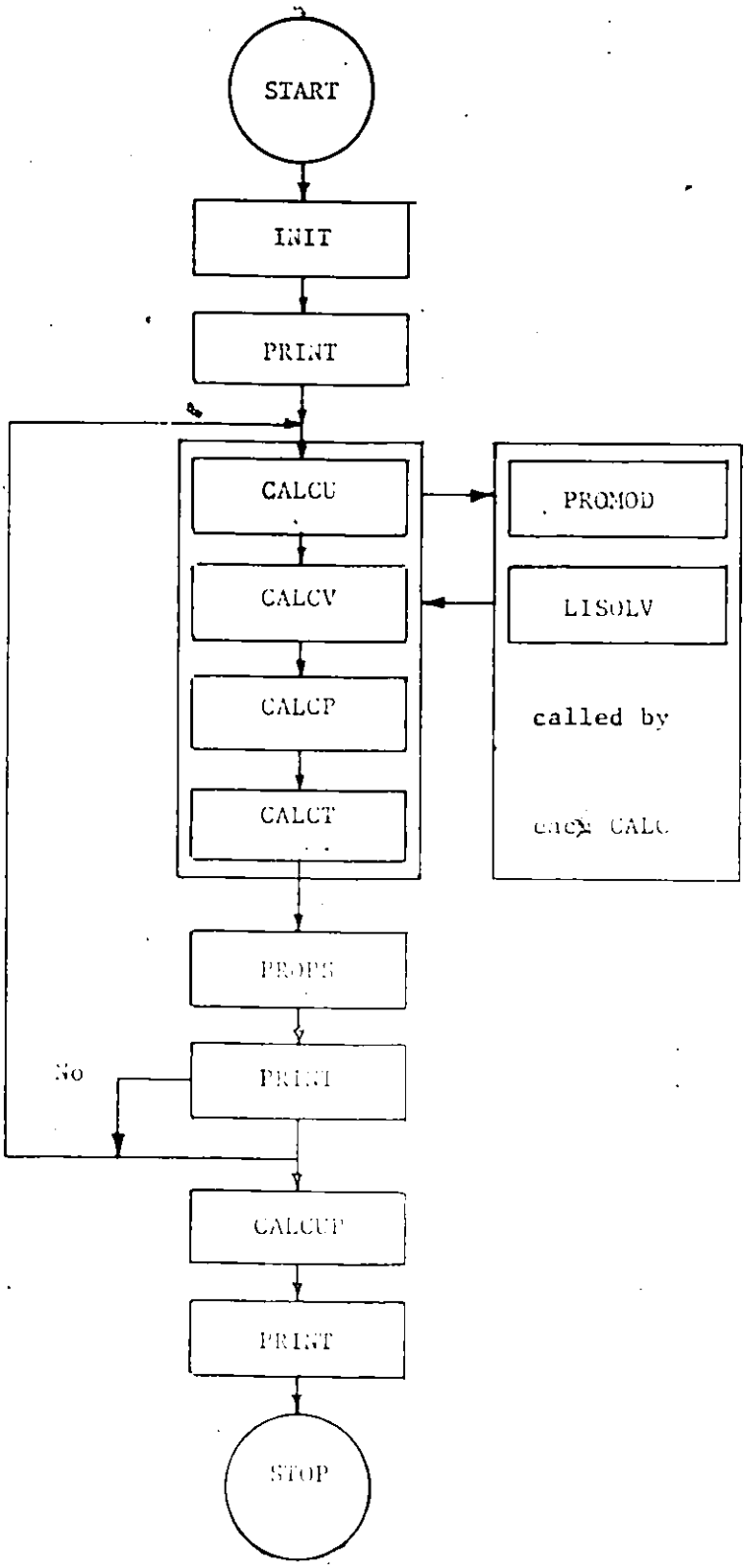

Figure 13: Flowchart of the Numerical Model

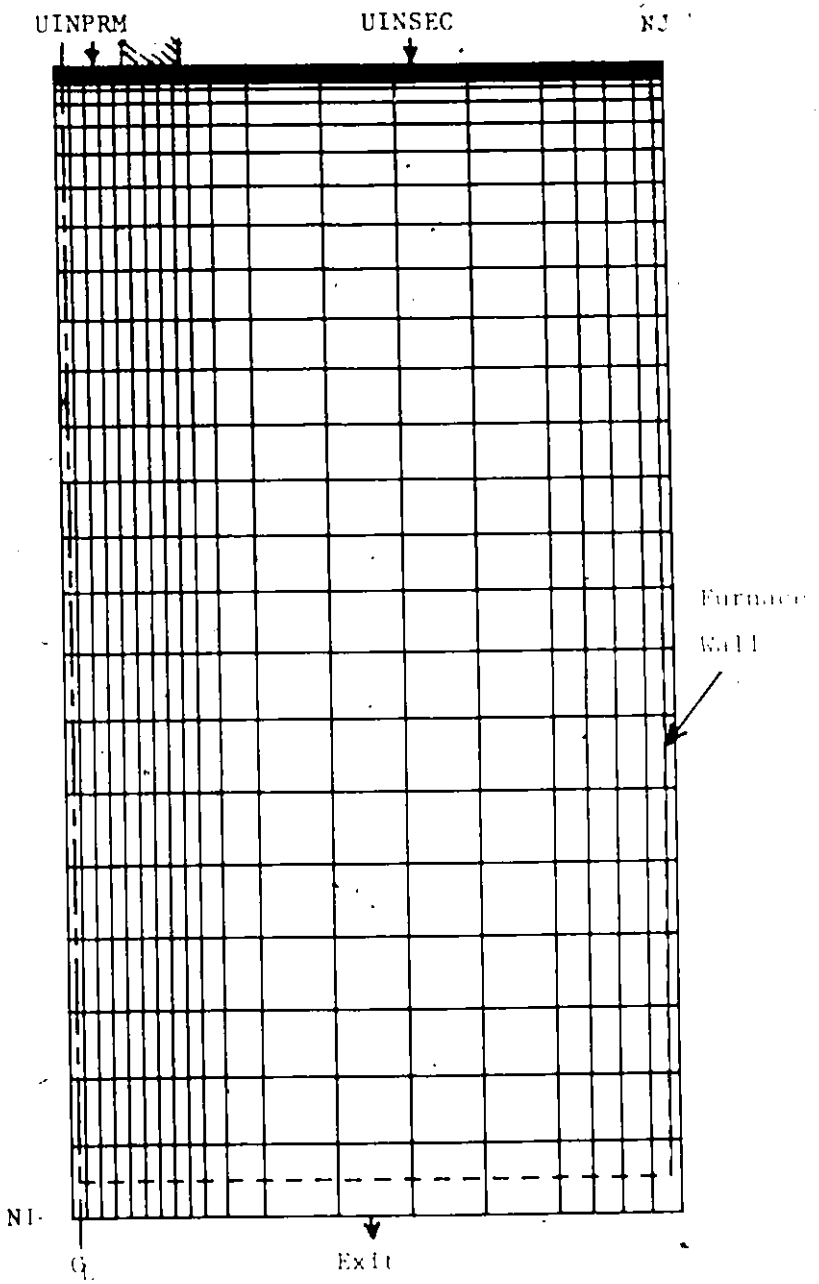

Figure 14: Grid Pattern Used to Divide the Furnace into Segments

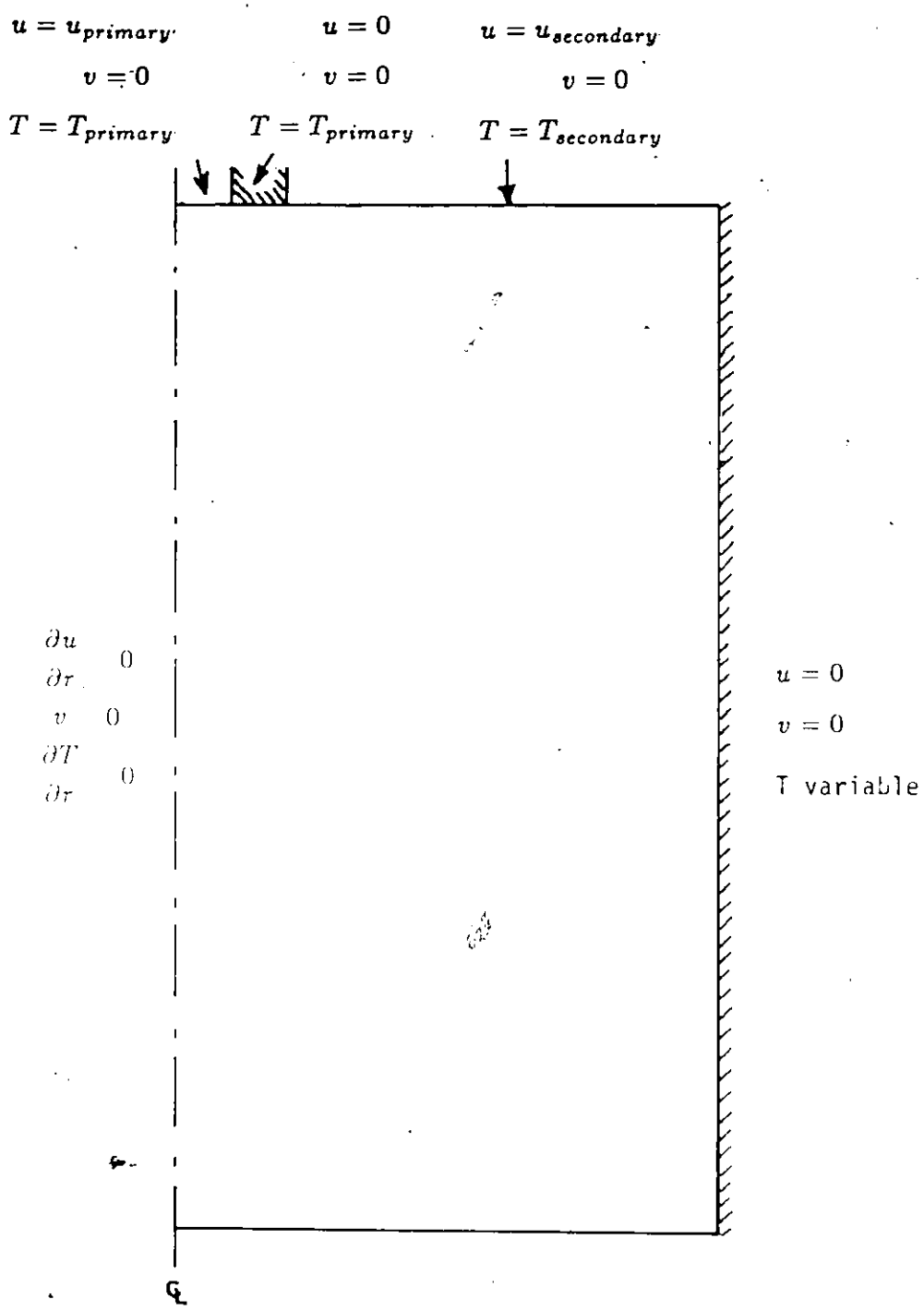

Figure 15: Boundary Conditions for Furnace

GLOW BARS TO OUTSIDE WALL

$$\dot{q} = \frac{\sigma(Tgb - Two)(Tgb + Two)(Tgb^2 + Two^2)}{R/Ro}$$

OUTSIDE WALL TO INSIDE WALL

$$\dot{q} = \frac{kw(Two - Tw)}{R\ln(Ro/R)}$$

INSIDE WALL TO GAS

$$\dot{q} = kg\left(\frac{\partial T}{\partial r}\right)_w \qquad \text{where} \quad \left(\frac{\partial T}{\partial r}\right)_w = \frac{Tw - Tg^*}{R - Rg^*}$$

HEAT FLUX FROM GLOW BARS TO GAS

$$\dot{q} = \frac{Tgb - Tg^*}{Rr + Rw + Rg}$$

where $Rr = R/(Ro\sigma\varepsilon(Tgb + Two)(Tgb^2 + Two^2))$

$Rw = R\ln(Ro/R)/kw$

$Rg = (R - Rg^*)/kg$

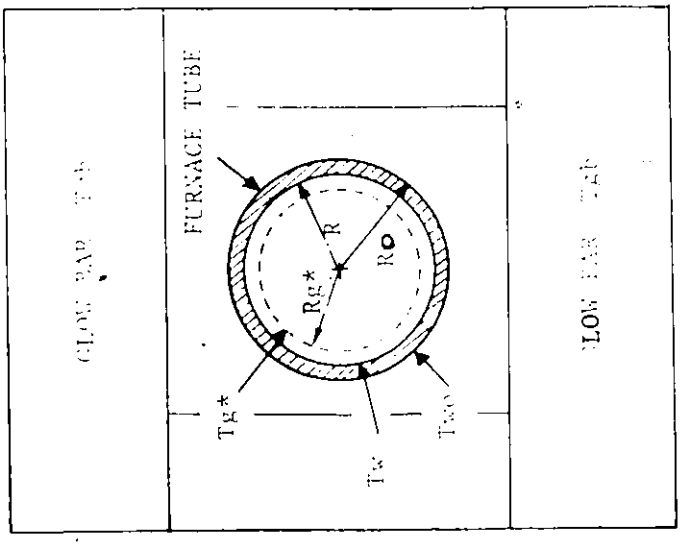

Figure 16: Cross-section through the Drop Tube Furnace

(Showing Temperature Boundary Condition)

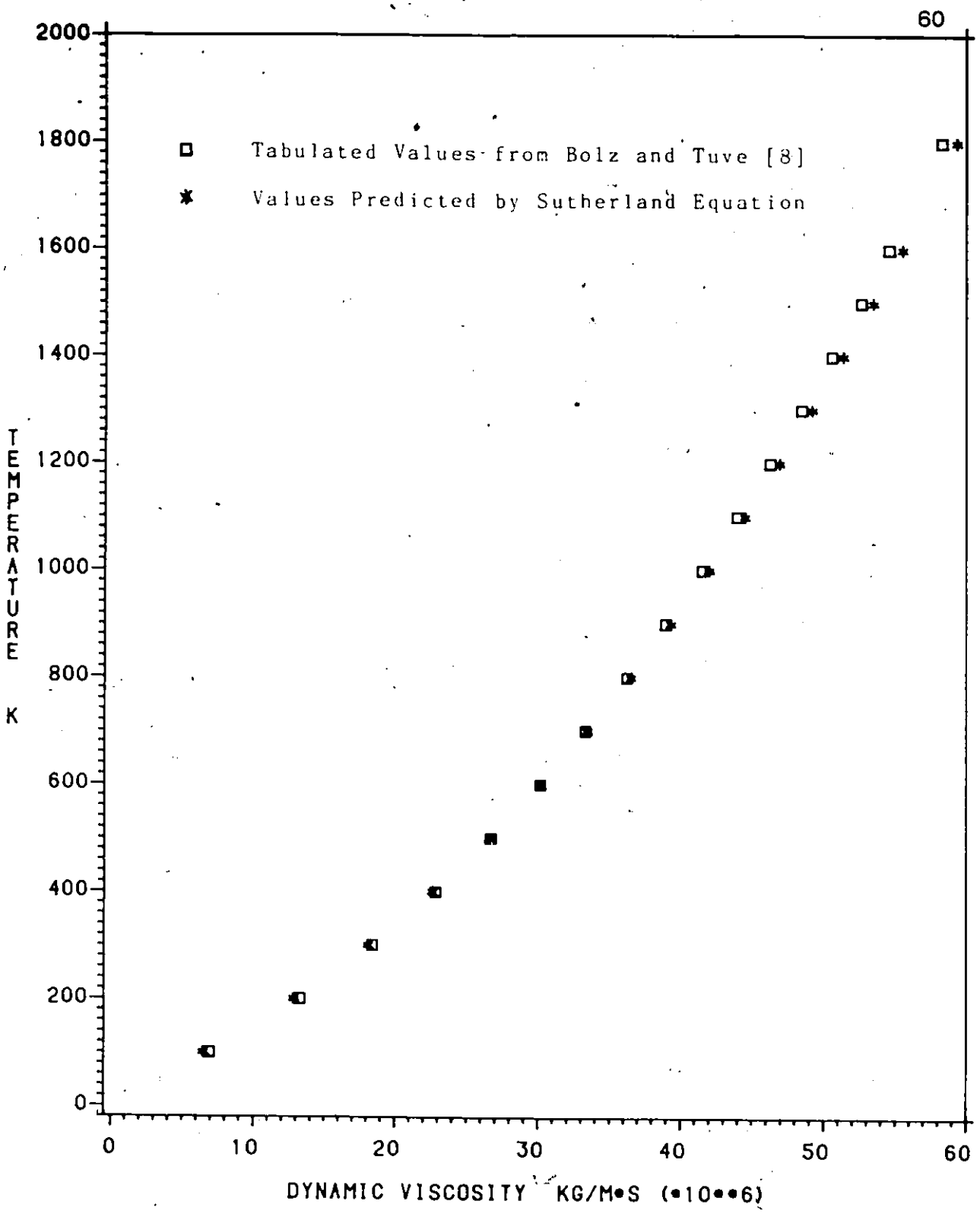

Figure 17: Comparison of Dynamic Viscosity Using Tabulated and Predicted Values

Chapter V

NUMERICAL RESULTS

5.1 TEST CASES

To verify the program, a series of test cases were run: isothermal,developing pipe flow; fully developed pipe flow with constant wall temperature; and fully developed pipe flow with constant heat flux.

5.1.1 Developing Isothermal Pipe Flow

The program was used to solve isothermal developing pipe flow and the results compared to published data. The grid spacing and the geometry were similar to the furnace tube dimensions: 28 nodes in the axial direction (with variable spacing as discussed in section 4.2.4), 20 in the radial direction; 2 m length, 0.032 m inside radius. An inlet air flow at 800 K was introduced into the tube with a 0.795 m/s uniform velocity. These conditions resulted in a Reynolds number of 500, roughly in the range expected in the drop tube furnace. The program solved the axial and radial momentum equations and obtained a converged solution after 168 iterations. The calculated velocities and the distances were made dimensionless by the following expressions:

$$U = \frac{u}{u_o}$$

where u = velocity at point (x,r)

u_o = inlet velocity (average)

$$R = \frac{r}{r_o}$$

where r = radius

r_o = radius of tube

$$Z = \frac{200x}{r_o Re}$$

where x = axial distance from inlet

r_o = radius of tube

Re = Reynolds number

The arrangement of the grid results in axial velocities being solved for near rather than on the centre-line; this radial position was very close to the axis (r/r_o = 0.05). Figure 18 shows the developing velocities at r/r_o = 0.05 that were obtained from the present work and compares them to the published results of Friedman et al [15]. A very close agreement is observed between the values. The work peformed by Friedman et al compares well with that of several other authors [1, 13, 27], and hence the velocity predictions of the present work were considered satisfactory. The solution of the momentum equations using a numerical scheme resulted in the initial velocity profiles developing a 'bump' near the wall (see Figure 19), as noted by several researchers [1, 15, 18, 27, 33] in developing pipe and channel flow. This 'bump' arises because the reduction of velocity in the boundary layer at the wall forces the velocity to increase outside the boundary layer This increase does not immediately spread over the whole profile, because the rate of spread is limited by laminar momentum diffusion, hence a velocity maximum arises. This phenomenum has not been observed experimentally because it is nearly impossible to produce a truly uniform inlet velocity (no inlet boundary layer).

5.1.2 Fully Developed Pipe Flow Subject to Heating

The program was used to solve developing temperature profiles in fully developed pipe flow with constant properties. This was carried out with the same geometry and grid spacing as the developing pipe flow discussed in the previous section (5.1.1).

5.1.2.1 Constant Wall Temperature

The velocity profile to be studied in the tube was a fully developed parabolic flow with an average velocity of 0.250 m/s. The air properties were evaluated at the inlet temperature which was at 300 K and the tube wall temperature was fixed at 1500 K. This resulted in an inlet Reynolds number of 950 and a Prandtl number of 0.700. The program was used to solve the energy equation only and a converged solution was reached after 2 iterations. The temperatures and distances were made dimensionless by the following expressions:

$$Z = \frac{1000x}{dRePr}$$

where x - axial distance from inlet

d - diameter of tube

Re - Reynolds number

Pr - Prandtl number

$$R = \frac{r}{r_o}$$

where r - radial position

r_o - radius of tube

$$\Theta = \frac{T - T_w}{T_o - T_w}$$

where T - temperature at point (x,r)

T_o - inlet temperature

T_w - wall temperature at (x,ro)

Two radial positions were examined: one position close to the axis (r/r_o = 0.05), and the other close to the wall (r/r_o = 0.9). The values obtained are compared to the finite difference solutions obtained by Grigull and Tratz [16] and are shown in Figure 20. There is very good agreement between the results and it can be concluded that the program can predict the temperatures accurately.

5.1.2.2 Constant Heat Flux

In a similar test, a fully developed constant property parabolic flow through a tube was subjected to constant heat flux heating. The tube had the same geometry and grid spacing as in the constant wall temperature tests. The average velocity was 0.25 m/s and the properties were evaluated at the inlet temperature of 300 K; this gave a Reynolds number of 950. The heat flux into the tube was 1093 W/m**2 and the Prandtl number was 0.708. The program was used to solve the energy equation only and the solution converged after 2 iterations. The resulting temperatures and the distances were made dimensionless by the following expression:

$$Z = \frac{1000x}{dRePr}$$ see section 5.1.2.1

$$R = \frac{r}{r_o}$$ see section 5.1.2.1

$$\Theta = \frac{T_w - T}{(T_w - T_a)_\infty}$$ where T_w - wall temperature at (x,ro)

T - temperature at (x,r)

$$(T_w - T_a)_\infty = \frac{3\dot{q}_w d}{k}$$

where $\dot{q}_w$ - heat flux

d - diameter of tube

k - thermal conductivity

As the distance x approaches infinity, the temperature profile becomes fully developed. The difference between the wall and the centre-line temperature is

constant and can be expressed in terms of the diameter, the heat flux and the thermal conductivity [16], and this expression was used to non-dimensionalize the temperature. Two radial positions were examined: one position is very close to the centre-line (r/r_o = 0.05), the other very close to the tube wall (r/r_o = 0.90). The results are shown in Figure 21 and compared to the solutions obtained by Grigull and Tratz. There is very good agreement with the published results and it can be concluded that the program can accurately predict the temperatures with constant heat flux.

5.2 THE FURNACE FLOW FIELD

As satisfactory results had been obtained for the different test cases of pipe flow, the boundary conditions were now changed to conform to the actual furnace geometry. The primary flow of air was chosen as 10.0 g/min, corresponding to a roughly stoichiometric air quantity for a coal feed rate of 1.0 g/min; this resulted in a 4.4 m/s average primary air velocity entering the furnace. The primary tube in the burner was assumed to be long enough to allow the primary flow to achieve a fully developed parabolic profile. The flow visualization experiments led to the conclusion that the flow through the furnace would be stable if the secondary flow velocity profile entering the furnace was uniform and the flow fell within the range of the stability diagram. Two air numbers (total air mass / stoichiometric air mass) were chosen: 5:1 and 10:1, giving secondary to primary air mass flow ratios of 4:1 and 9:1. The temperature of the primary flow entering the furnace was assumed to be 300 K.

The program was used to solve the flow field in the furnace using this data. Since the coal particles were assumed to travel along the axis of the

furnace, the centre-line flow velocities and temperatures were of the most interest. For a 300 K inlet, the calculated temperature values at the axis of the furnace were low compared to a typical combustion temperature for coal (900 - 1100 C),thus it was felt that the secondary air flow would need a certain degree of preheating.

A study of the effect of varying certain parameters was conducted as follows:

1. Secondary flow temperature at 300 (no preheating) and with preheating to 450, 600, 750, 900, 1050 and 1200 K before entering the furnace.
2. Air number equal to 5 and 10 (secondary mass/primary mass ratio equal to 4 and 9)
3. Temperature of the surrounding glow bars (heating elements) at 1400 K and 1700 K.

Because flow recirculation induced by buoyancy was deemed to increase dispersion of the primary coal stream, one aim of this study was to determine under which conditions such recirculation could be avoided. It was felt that the effects of bucyancy which could lead to recirculation would be stronger at lower preheat temperatures; therefore, the secondary air preheat temperature was reduced in steps of 150 K from 1200 K down to the temperature where recirculation was first noted. As soon as recirculation was apparent, calculations were halted, because lowering the preheat temperature further would only enhance recirculation. The minimum preheat temperature was 300 K. The velocity profiles under different conditions are illustrated in Figures 22 to 43. In order to make the illustrations clear, only a selected number axial positions were chosen to show the developing profiles along the furnace tube

length. The axial positions are at 0.010, 0.052, 0.250, 0.595, 1.000, 1.500, and 2.000 m measured from the furnace tube inlet plane.

5.2.1 Flow Field Study – Glow Bar Temperature 1700 K

For the first set of tests, the inlet mass flow of the secondary air was specified as 40.0 g/min. The primary air mass flow was fixed at 10 g/min; therefore, the mass secondary/mass primary (ie M–S/M–P) was equal to 4.0. The resulting axial velocity profiles are illustrated in Figures 22 to 26. As the preheat temperature increases, the centre–line velocity decreases. The buoyancy forces are greater at the lower preheat temperature because of the greater temperature differences between the wall and the incoming flow. Since the momentum forces and the buoyant forces oppose each other, a deceleration of the flow at the wall is observed, and this in turn causes an acceleration of the flow in the tube centre. The minimum preheat temperature required to avoid flow reversal was found to be close to 600 K; below this point flow reversal near the wall results. The velocity of the flow reversal is small compared to the final centre–line velocity (0.1%) and the furnace could probably be operated with a secondary preheat temperature of 600 K without a significant increase in dispersion of the primary jet. Even without flow reversal, buoyancy is seen to result in a much thicker wall boundary layer than is found in isothermal, developing flow.

For the second set of tests, the inlet mass flow of the secondary air was specified as 90.0 g/min (ie M–S/M–P = 9.0). The results are shown in Figures 27 to 33. The larger inlet mass (momentum) flux reduces the effect of buoyancy and lowers the shear stress between the secondary and primary

flow,both of which result in higher velocities on the tube axis. There is no recirculation apparent for any of the preheat temperatures with a 90.0 g/min flow rate. For both secondary flows, the velocities near the axis change little with secondary inlet temperature; this suggests that particle transit times will not be strongly affected by preheating.

5.2.2 Flow Field Study – Glow Bar Temperature 1400 K

The same set of conditions in the previous section were examined at a lower glow bar temperature. The results with the lower glow bar temperature and 40 g/min air flow are shown in Figures 34 to 36; those with a 90.0 g/min air flow are shown in Figures 37 to 43. If the velocity profiles with a 1400 K glow bar temperature are compared to the velocity profiles with a 1700 K glow bar temperature using the same inlet conditions, very little difference is apparent. The effect of buoyancy is seen to be slightly stronger at the lower glow bar temperature, if results at 1700 K are compared to results for the same inlet conditions at 1400 K. One might expect that an increase in the glow bar temperature would result in a greater distortion near the furnace wall, but the reverse was observed The glow bars heat the incoming gas, which decreases in density and accelerates to conserve mass. Momentum increases with the square of the velocity while buoyancy increases with the difference in temperatures; thus the momentum forces increase somewhat more rapidly than the buoyancy forces as the temperature is increased. The momentum of the gas flow is greater at the higher glow bar temperature, thus the effects of buoyancy are reduced. This effect is small, but can be seen most clearly by comparing results for M-S/M-P = 9.0 with Tinsec = 300 K at the two glow bar

temperatures. A reversal of the flow near the wall was noted with 90.0 g/min at 300 K but it was small compared to the final centre line velocity (0.1%). This reversal resulted from the relatively low flow velocities and large buoyant forces. The buoyancy effect at 1400 K is particularly strong for the 40.0 g/min flow rate with a low preheat temperature. (see Figure 34) These conditions represent the lowest momentum forces and the greatest buoyancy forces.

5.3 PARTICLE VELOCITY AND TEMPERATURE

Four different sizes of particles that were considered representative of the size to be tested in the furnace were examined; these were 10, 30, 100, 300 um particles. The temperature increase and furnace residence times of these particles were examined under each of the flow conditions studied in the previous section. A series of heating curves were obtained and are shown in Figures 44 to 65. Particle heating rates were examined in preheated flows up until recirculation was noted; therefore, particle heating rates for some of the flows at lower preheat temperatures are not given.

5.3.1 Particle Heating - Glow Bar Temperature 1700 K

The four sizes of coal particls were introduced into the furnace flow with a 40.0 g/min secondary mass flow rate at preheat temperatures of 600 to 1200 K (see Figures 44 to 48). The five curves represent the gas centre-line temperature and the four particle temperatures. Before the centre-line gas can increase in temperature, the heat from the furnace walls must penetrate the surrounding secondary flow; therefore, preheating the secondary flow will allow

the temperature of the central primary stream to increase more rapidly. As the particles enter the furnace, the initial particle heating is dependent on the particle size. The 10 um particle has the largest initial temperature increase while the 300 um particle has the smallest initial temperature increase. This pattern of heating for the different particles remains the same for each preheat temperature. The 10 um particle then heats very quickly because of small thermal inertia, and follows the centre-line temperature closely. The 10 um particle also has the largest convective heat transfer coefficient because of its small diameter, and most of the heat it receives by radiation is convected to the surrounding cooler gas. As the preheat temperature is increased, the 10 um particle approaches the centre line gas temperature more closely. The 30 and 100 um particles follow a similar pattern for each preheat temperature. The convective heat transfer coefficient becomes less as the diameter becomes greater; therefore, radiation from the furnace walls becomes relatively more important, and the final temperature of these particles rises with increasing particle size. The 300 um particle has the lowest initial heating rate; because of its large mass, it requires a large quantity of heat to heat up, and spends most of its time undergoing transient heating. With a preheat temperature of 750 K, the temperature of the 300 um particle actually falls below the surrounding gas temperature; the particle is then heated by both radiation and convection. By the end of the furnace, the particle temperature has increased to a temperature close to that of the 100 um particle. Higher preheat temperatures yield similar results.

The same size particles were introduced into a 90.0 g/min secondary air mass flow with preheating from 300 to 1200 K. The results are shown in Figures 49 to 55. Much lower particle temperatures were achieved because of

the higher secondary mass flow rates. With the 90.0 g/min mass flow, the preheating of the secondary flow does not have a strong effect on the heating history; radiant heating is the main factor responsible for particle heating. At gas preheat temperature of 900 K and higher, the temperature of the 300 um particle falls below the gas centre-line temperature, hence receiving energy by both radiation and convection.

5.3.2 Particle Heating = Glow Bar Temperature 1400 K

The four particles were introduced into the flow field obtained at a 40.0 g/min secondary air flow with a preheat of 900 to 1200 K. (see Figures 56 to 58) The 10, 30 and 100 um particles follow the gas centre-line temperatures very closely; however, the 300 um particle spends almost all its time (except for a small initial distance) below the furnace gas temperature being heated by radiation and convection. In contrast to the results with a 1700 K glow bar temperature, the 300 um particle reaches the lowest final temperature of all the particles. The 100 um particle also exhibits a different behaviour than the results at 1700 K glow bar temperature; its temperature falls below that of the 30 um particle in the initial region of the furnace (0.5 m). An increase in the preheating from 900 to 1200 results in the temperature of the 100 um particle falling below the gas centre-line temperature; however, this particle eventually reaches the highest particle temperature. The radiation produced by the furnace walls is much less but the convective heat transfer coefficient essentially remains the same, therefore the particles remain closer to the gas temperature.

The four particles were subjected to a 90.0 g/min secondary air mass flow rate with preheating from 300 to 1200 K. (see Figures 59 to 65) The 10 and 30 um particles have curves similar to those of the other test conditions. The thermal inertia of the 100 and 300 um particles is more noticable at the 1400 K glow bar temperature. Much lower particle temperatures are achieved at the 1400 K glow bar temperature. These results indicate the considerable loss of radiation heat transfer to the particles at the lower glow bar temperature.

5.3.3 Particle Heating Rates

One of the objectives of this study was to find the particle heating rates under various flow and preheat conditions. The resulting heating rates for 10, 30, 100 and 300 um particles taken from the results discussed previously are shown in Figures 66 to 69, respectively. The heating rates were calculated by taking the temperature achieved by the particle after travelling 0.25 m in the furnace and dividing by the time taken to travel that distance. A distance of 0.25 metres was chosen because it represents a point of continual and relatively linear temperature rise for all particle sizes. In all the heating rate curves (Figures 44 to 65), the 1700 K glow bar temperature gives a greater heating rate than the 1400 K glow bar temperature at the same preheat temperature. This is expected owing to the greater energy received by radiation. All the heating rates increase with preheat temperature, and the rate of this increase is dependent on the particle size. The heating rate of the 10 um particle is affected most by the preheat temperature; the 300 um is affected the least, owing to the greater thermal inertia with large in particle diameters.

For all the particle sizes examined, the mass flow rate of the secondary flow has a very small effect. Both mass flow rates give very similar particle heating rates (see Figures 66 to 69). As particle size increases, the difference in heating rates between the two glow bar temperatures becomes greater. This is true for the 10, 30 and 100 um particles; however, owing to the large thermal inertia of the 300 um particle, the heating rate is somewhat less than for the 100 um particle.

Figure 70 illustrates the effect of secondary air preheating on the residence time of a 100 um particle. Increasing the preheat temperature results in a longer residence time for all flow rates because the centre-line velocity rises less (see Figures 22 to 43). The mass flow rate of the secondary air has a significant effect on the residence time. The larger mass flow rate has a high initial velocity and is accelerated further in the furnace tube. The smaller mass flow has a lower inlet velocity and is accelerated less in the furnace tube, thus the residence time is longer for the lower mass flow. Varying the glow bar temperature has a slight effect on the residence time. The higher glow bar temperature heats the flow to a higher temperature which leads to higher velocities and slightly shorter residence times.

Chapter VI

CONCLUSIONS AND RECOMMENDATIONS

The objective of this study was to develop a numerical model for the CCRL drop tube furnace. The model examined the effect of the secondary air mass flow rate, secondary preheat temperature and the glow bar (heating element) temperature. Inert, spherical coal particles with diameters of 10, 30, 100, 300 um were introduced into the furnace model and their velocities, temperature and heating rates were computed.

The first section of this report examined experimental results obtained from isothermal flow visualization tests. These results yielded two conclusions:

1. The use of a flow straightener at the secondary air inlet is necessary to obtain a desired flow pattern with low dispersion of the central primary jet.
2. The furnace should be operated within the range of the stability diagram (Figure 7).

Operating the furnace under the above conditions should result in the desired laminar flow pattern.

The finite difference model of the drop tube furnace was used in a parametric study to determine the effects of secondary mass flow, secondary preheat temperature and glow bar temperature. The results led to the following conclusions:

1. Higher glow bar temperatures resulted in greater centre-line velocities and temperatures; buoyancy effects were reduced at the higher glow bar temperature.

2. Higher secondary air mass flows resulted in larger centre-line velocities but lower centre-line temperatures; buoyancy effects were reduced with the larger mass flow.
3. Increasing the preheat temperature resulted in reduced buoyancy effects, higher centre-line temperatures and lower centre-line velocities.

The introduction of the four different particle sizes into the furnace flow field under various flow conditions showed certain trends:

1. Particle heating rates increased with rising secondary preheat temperatures.
2. The mass flow rate of the secondary air had a very slight effect on the heating rates.
3. Higher glow bar temperatures significantly increase particle heating rates.
4. Heating rates are chiefly governed by radiant heat transfer from the furnace wall.
5. Heating rates rose with larger particle diameters.

The residence time of a 100 μm particle was examined under various flow conditions. The following conclusions were drawn from the results:

1. A longer particle residence time was observed with larger preheat temperatures.
2. A larger secondary mass flow gives a decrease in particle residence time.
3. A higher glow bar temperature gave a small increase in particle residence time.

This model has been developed in conjunction with the actual drop tube furnace at CANMET research laboratories. Calculated values of temperature predicted by the numerical model will be compared to measurements made in the actual drop tube furnace. The experimental, cold flow apparatus used for the flow visualization tests will be used to measure the developing velocity profiles. These measurements will then be compared to the values predicted by the numerical model using the same inlet and boundary conditions (ie cold flow). Future research with the actual furnace and the numerical model will eventually lead to the development of a pulverized coal combustion model.

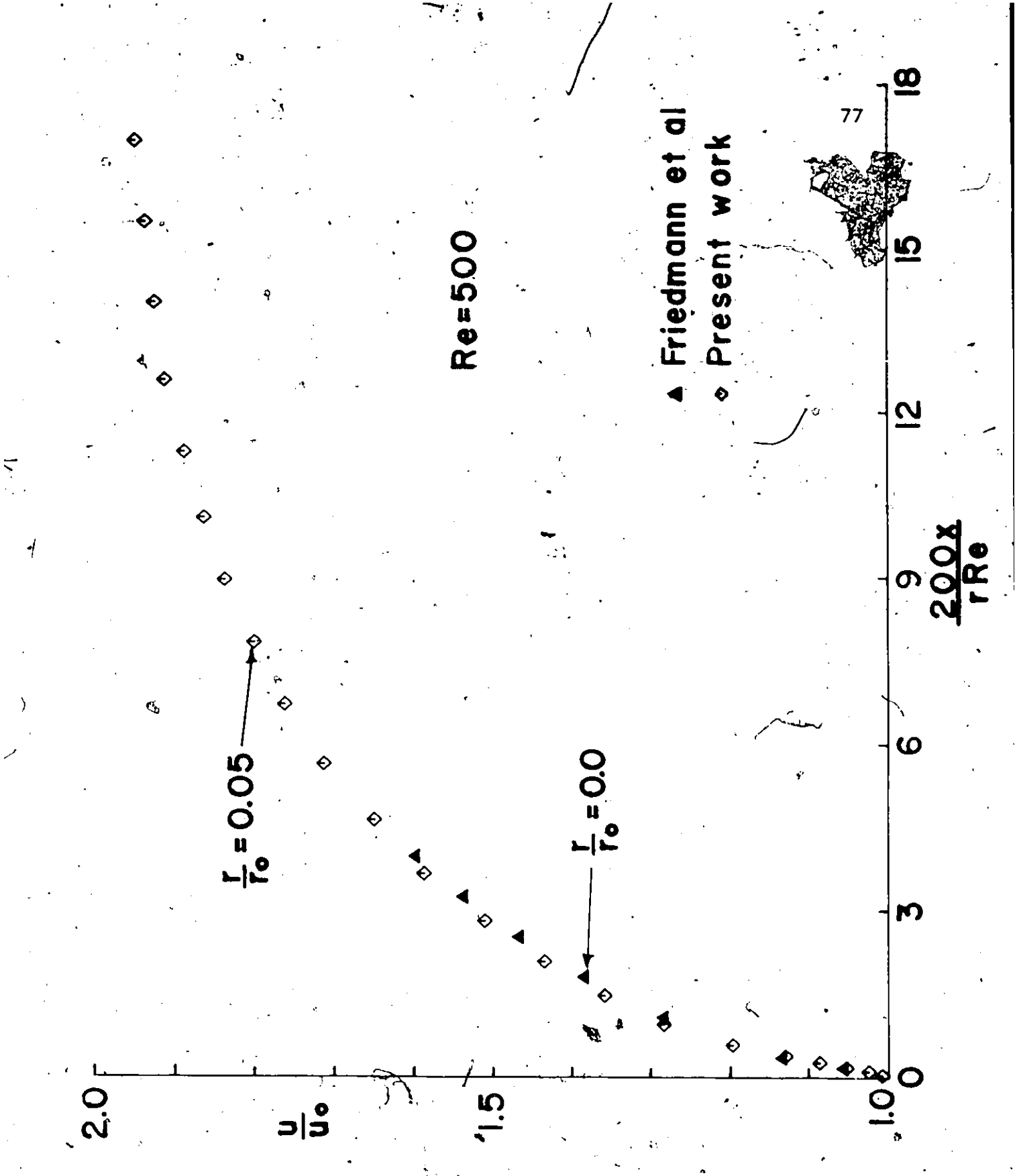

Figure 18: Comparison of Centre-line Velocities

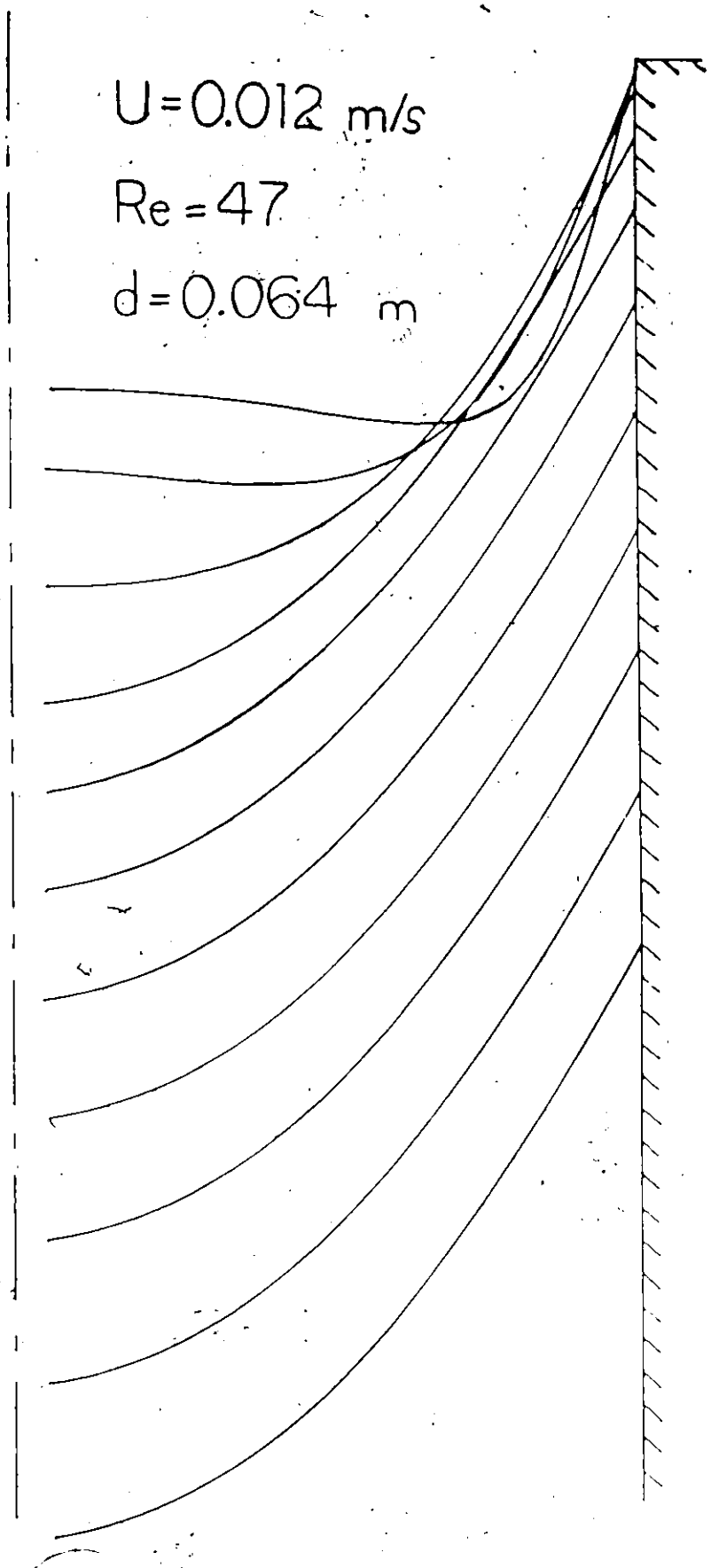

Figure 19: Developing Velocity Profiles in a Tube

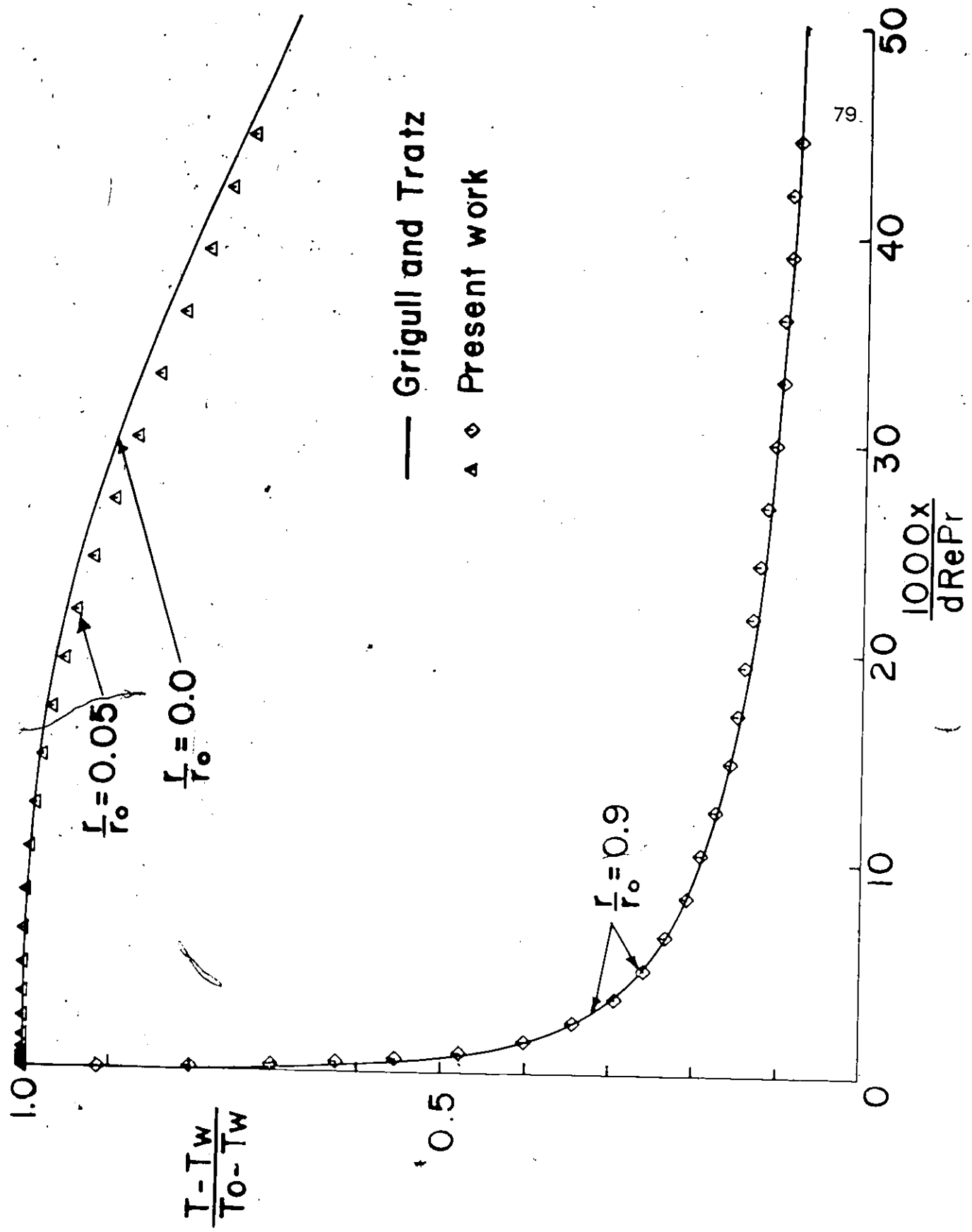

Figure 20: Comparison of Temperature – Constant Wall Temperature

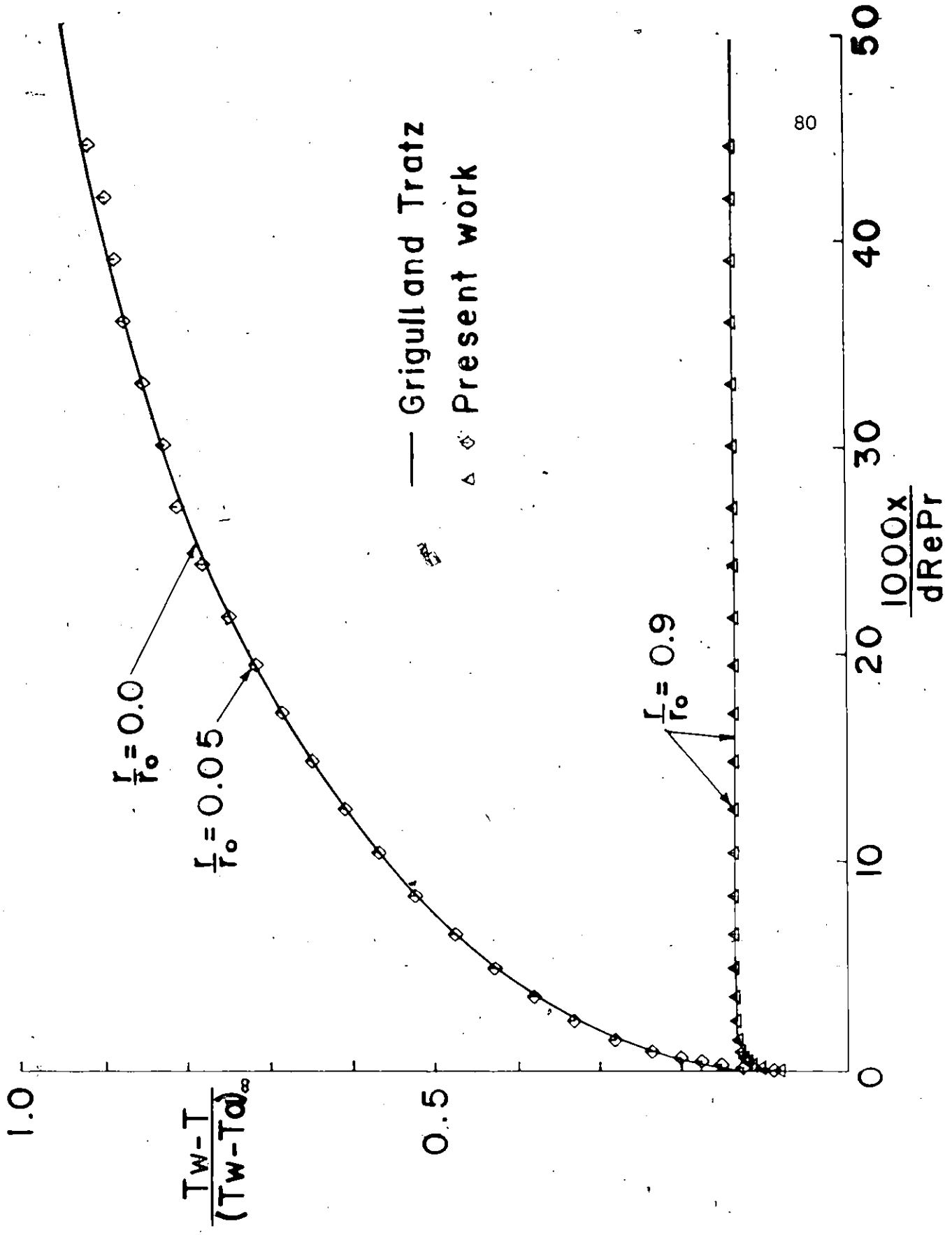

Figure 21: Comparison of Temperature – Constant Heat Flux

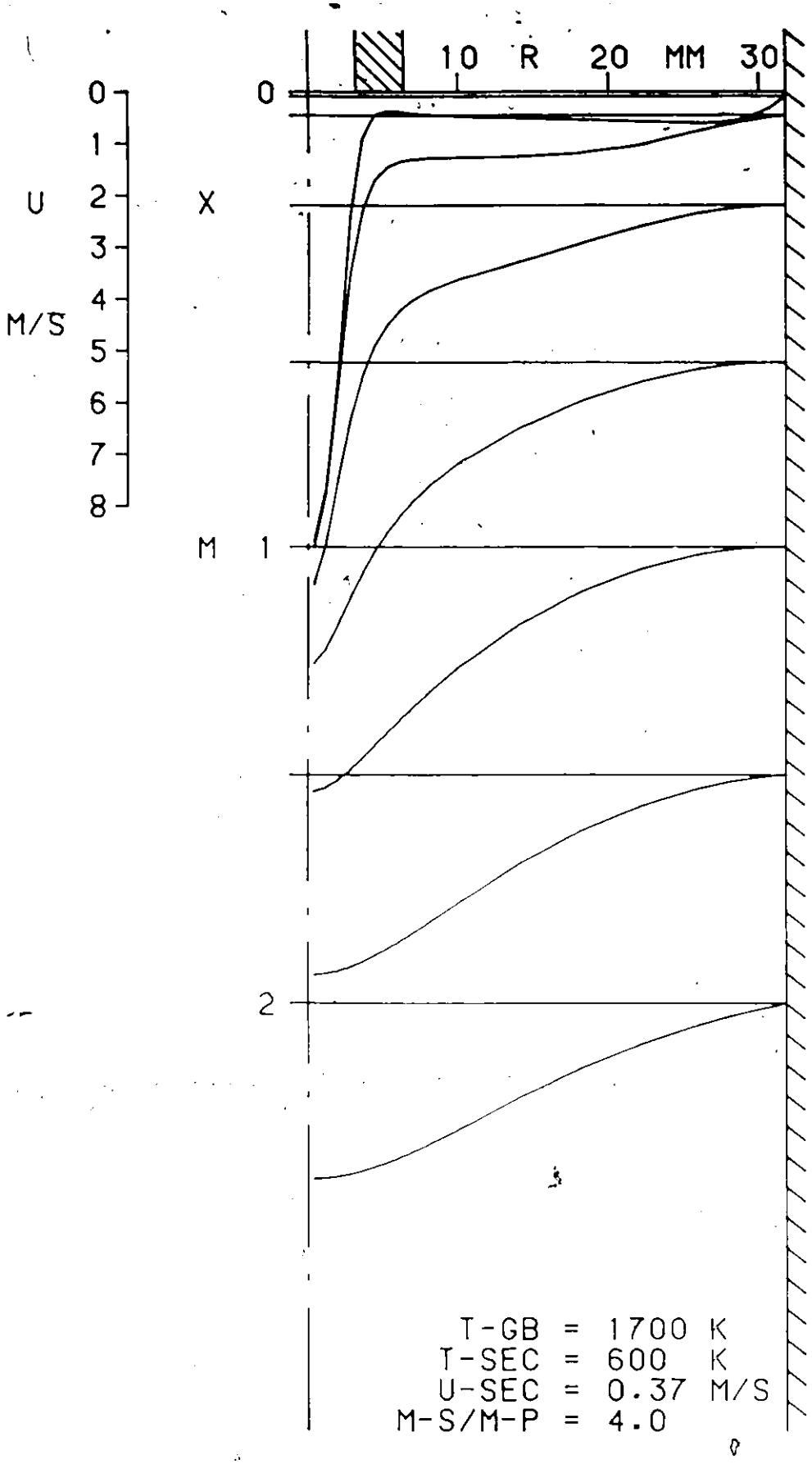

Figure 22: Velocity Profiles – Tgb=1700 K, Tinsec=600 K, M-S/M-P=4.0

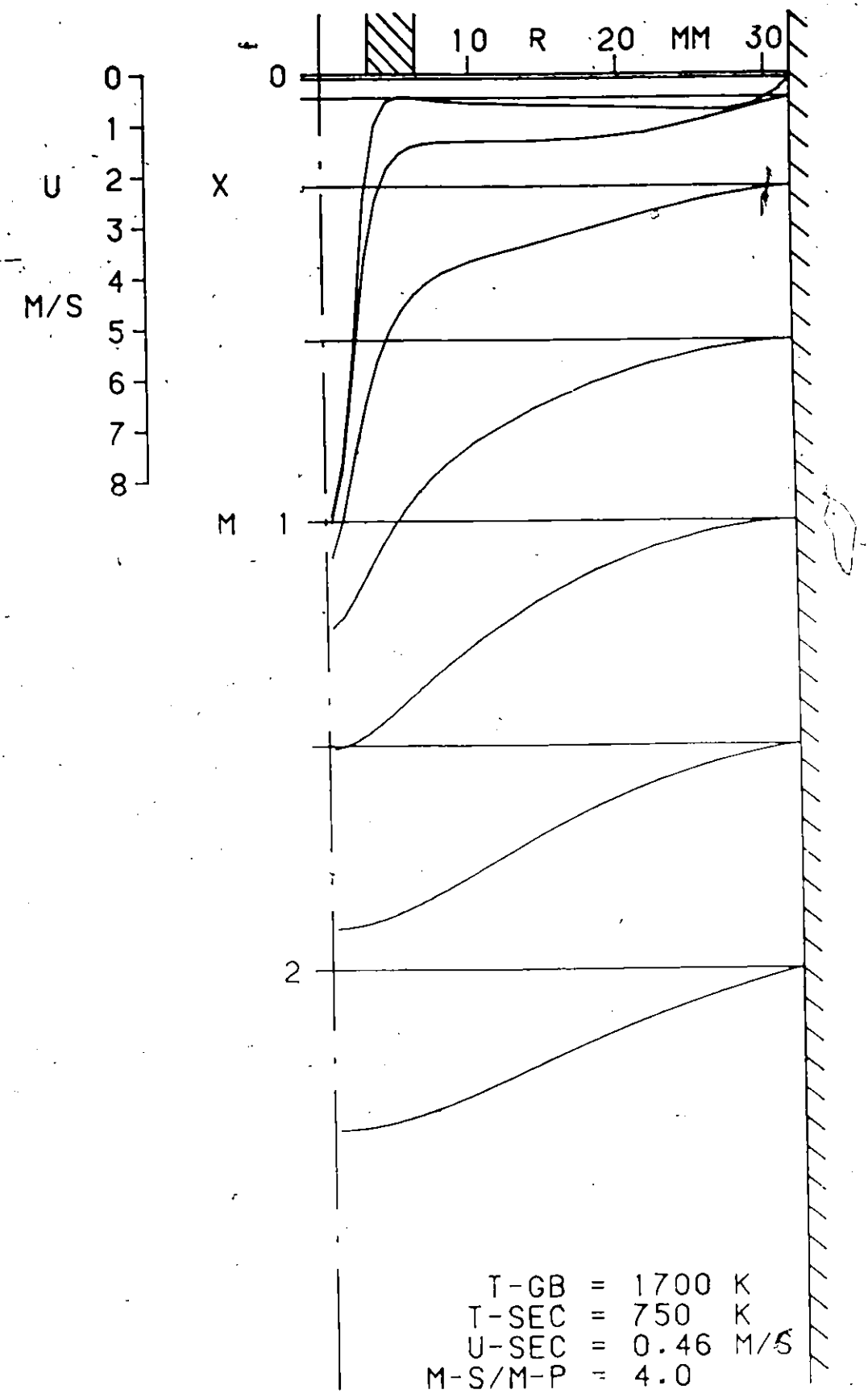

Figure 23: Velocity Profiles - Tgb=1700 K, Tinsec=750 K, M-S/M-P=4.0

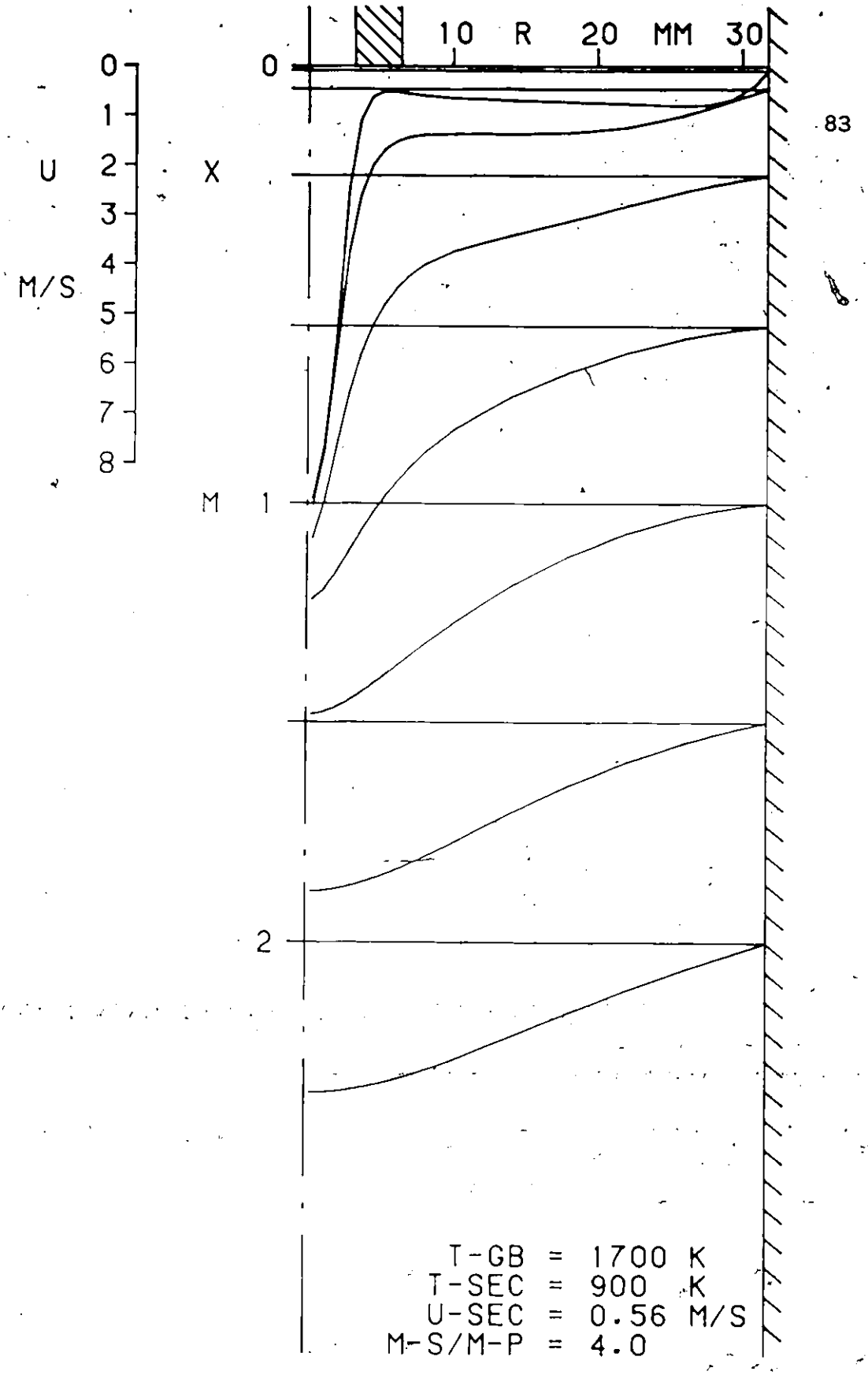

Figure 24: Velocity Profiles – Tgb=1700 K, Tinsec=900 K, M-S/M-P=4.0

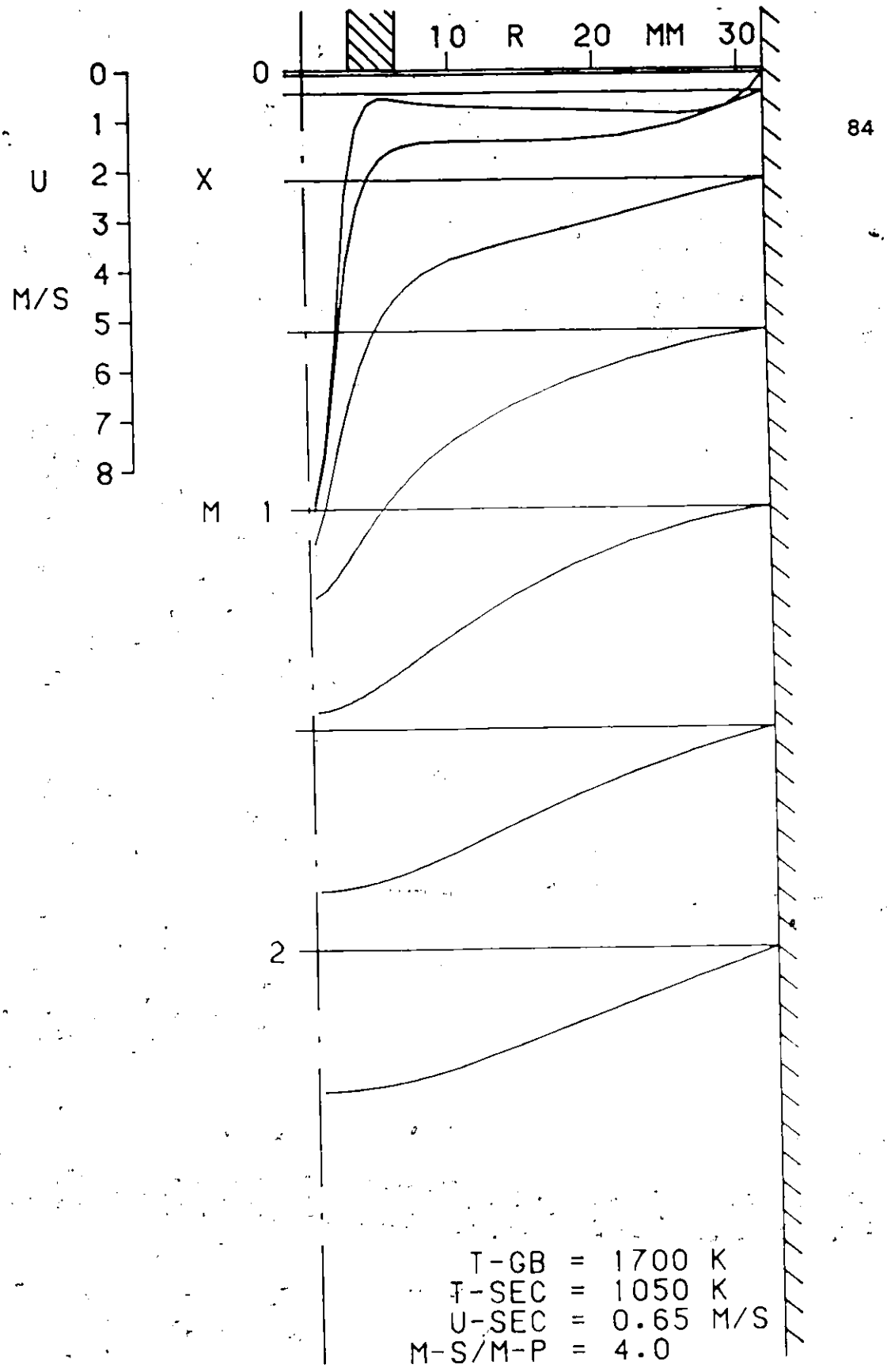

Figure 25: Velocity Profiles - Tgb=1700 K, Tinsec=1050 K, M-S/M-P=4.0

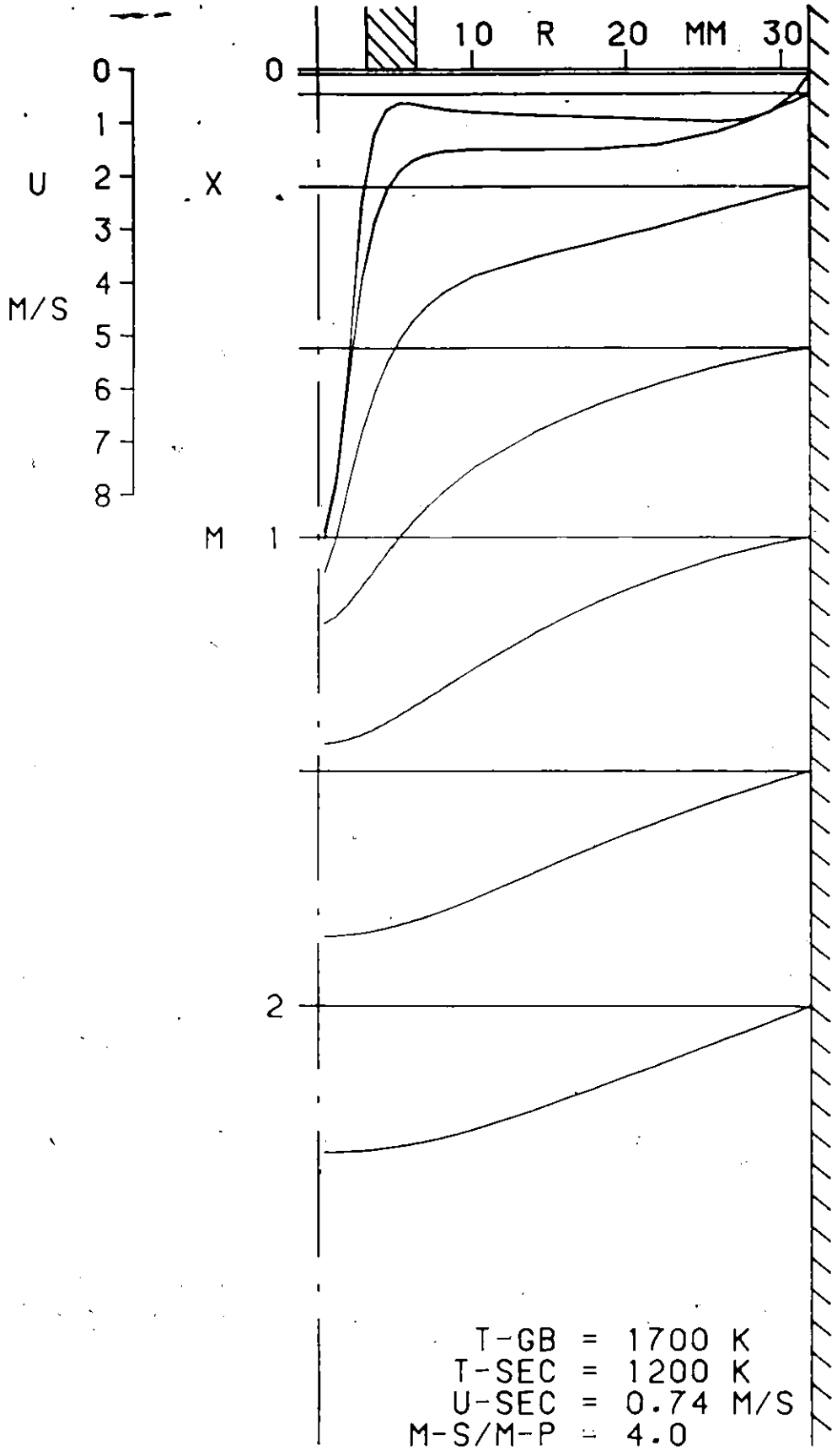

Figure 26: Velocity Profiles – Tgb=1700 K, Tinsec=1200 K, M-S/M-P=4.0

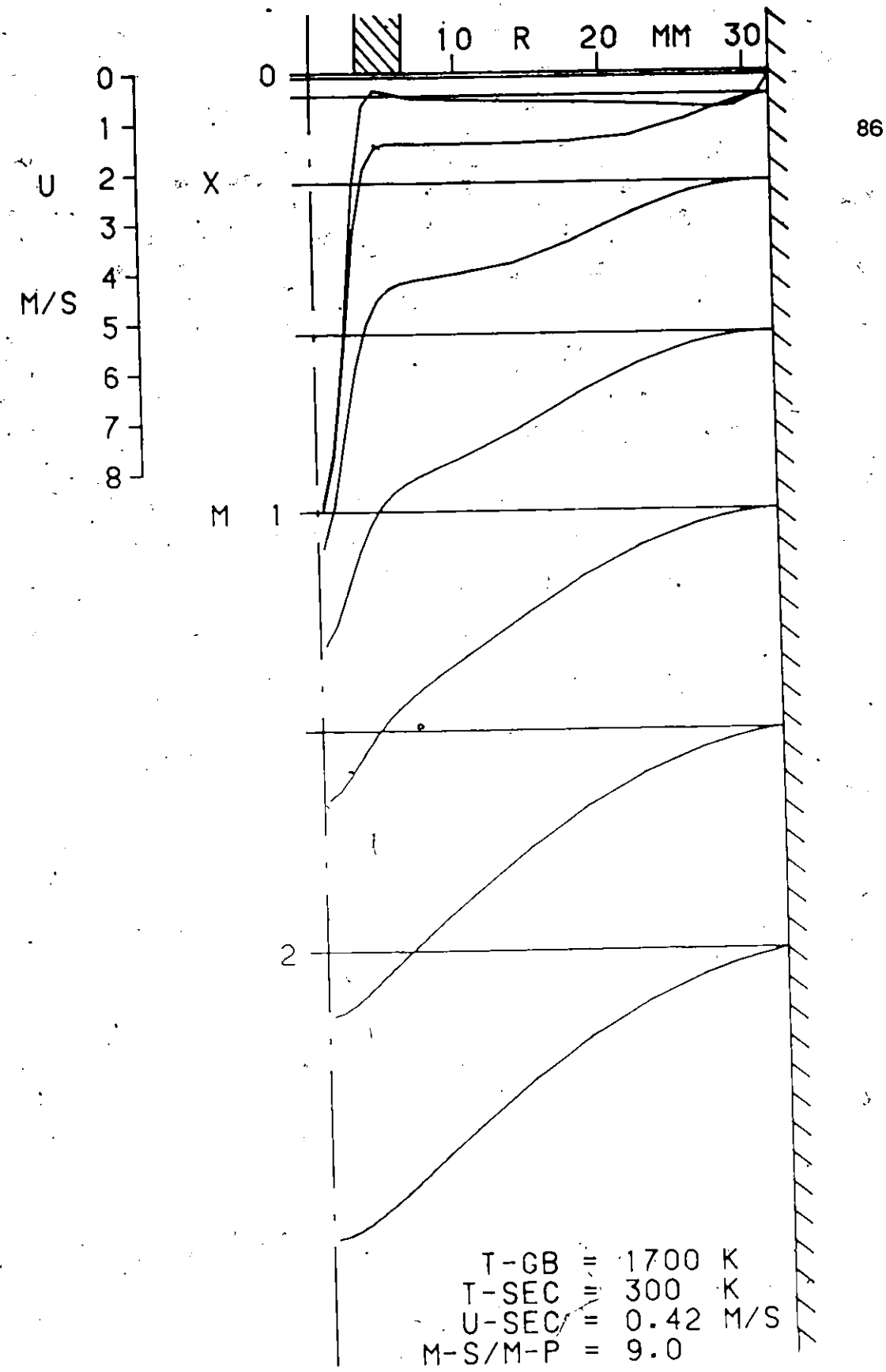

Figure 27: Velocity Profiles – Tgb=1700 K, Tinsec=300 K, M-S/M-P=9.0

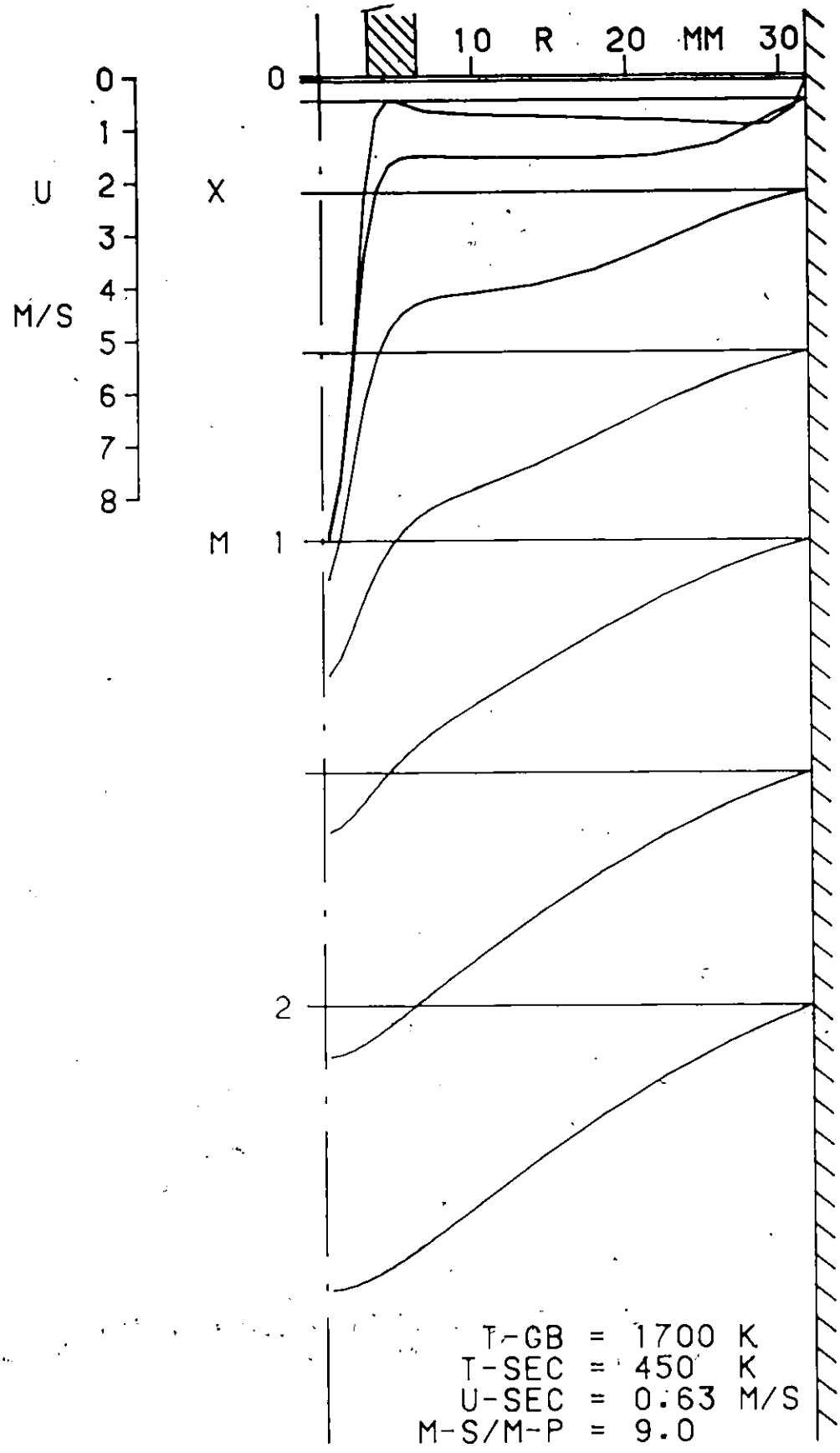

Figure 28: Velocity Profiles - Tgb=1700 K, Tinsec=450 K, M-S/M-P=9.0

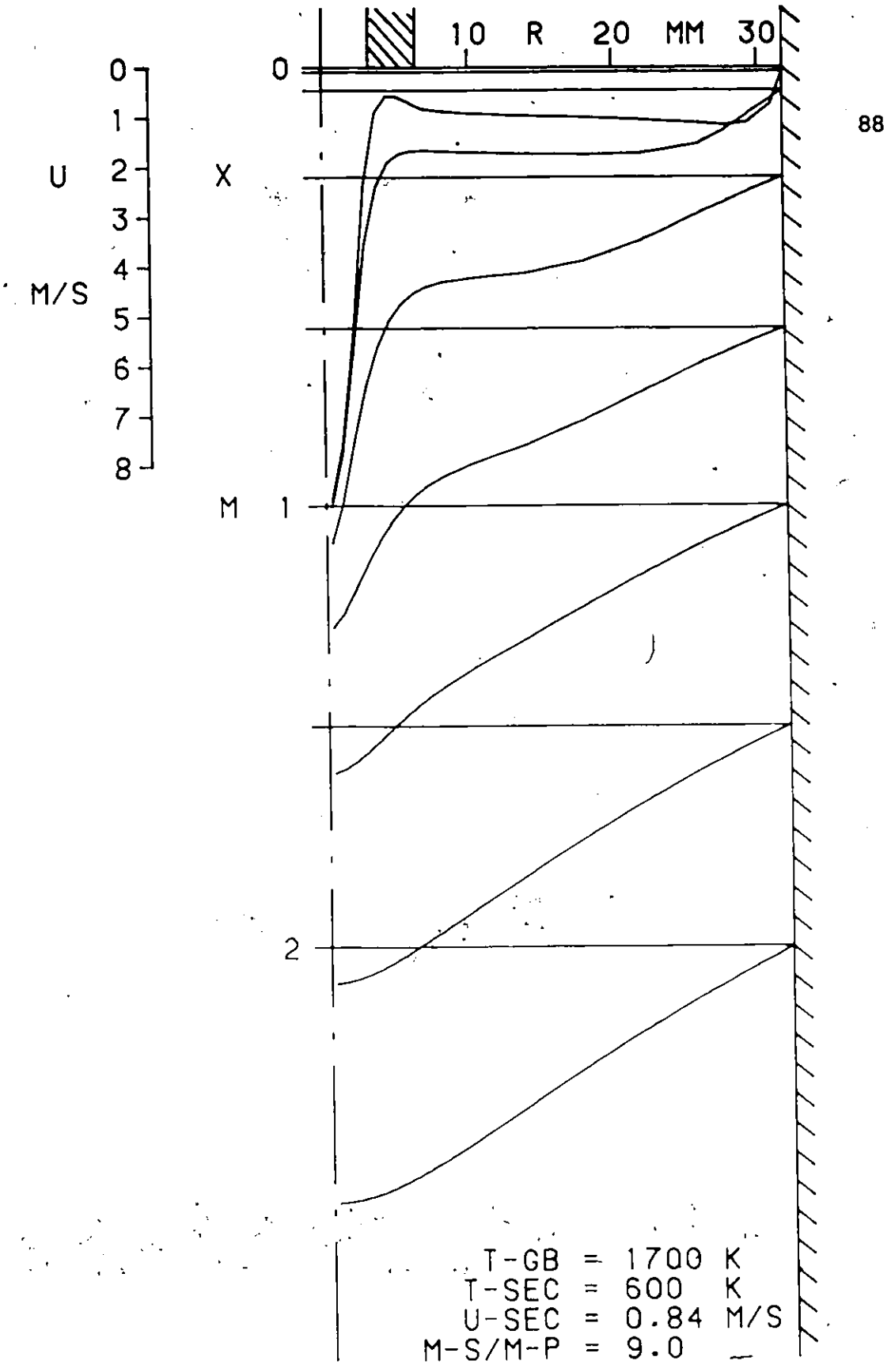

Figure 29: Velocity Profiles – Tgb=1700 K, Tinsec=600 K, M-S/M-P=9.0

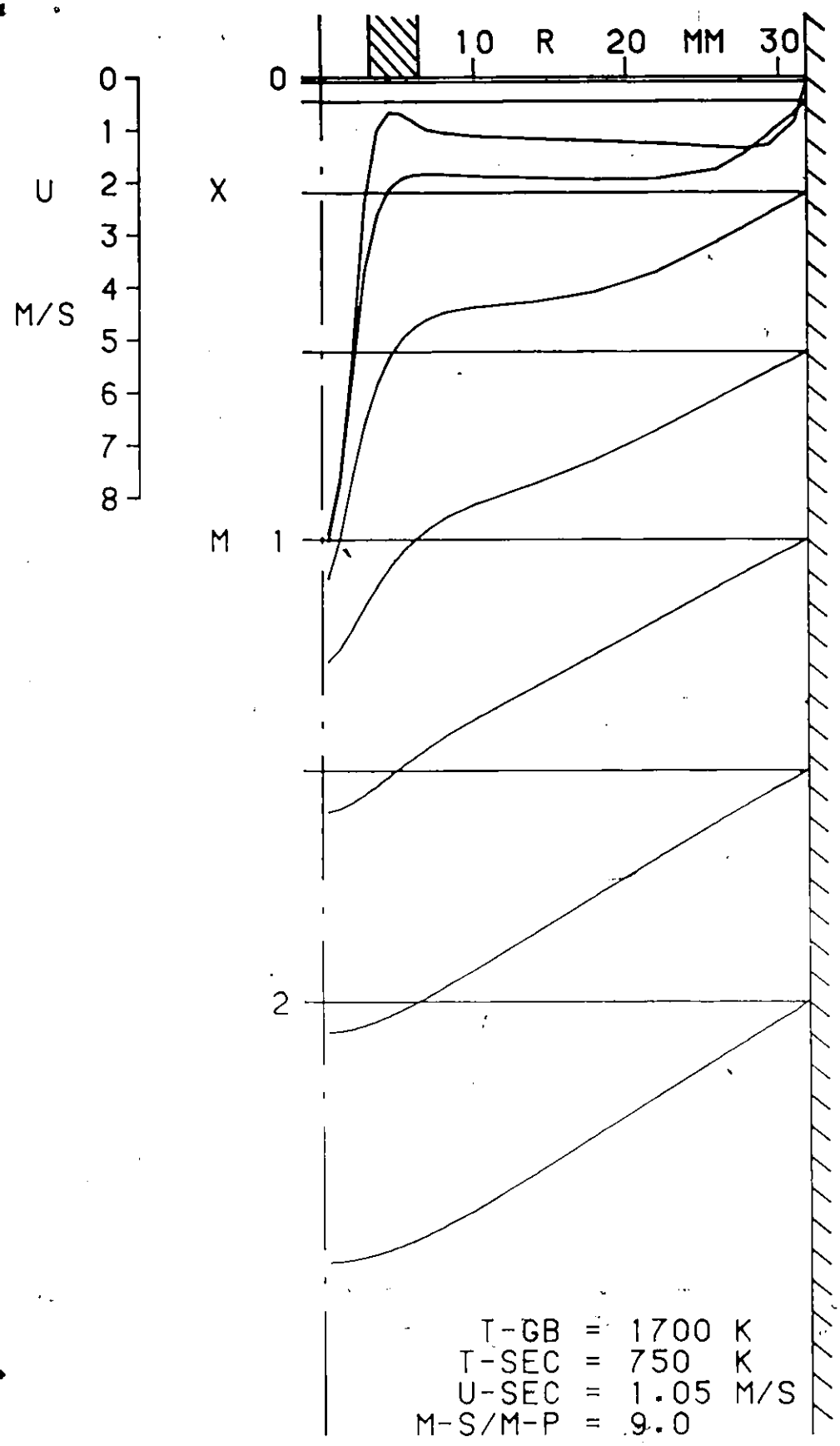

Figure 30: Velocity Profiles – Tgb=1700 K, Tinsec=750 K, M-S/M-P=9.0

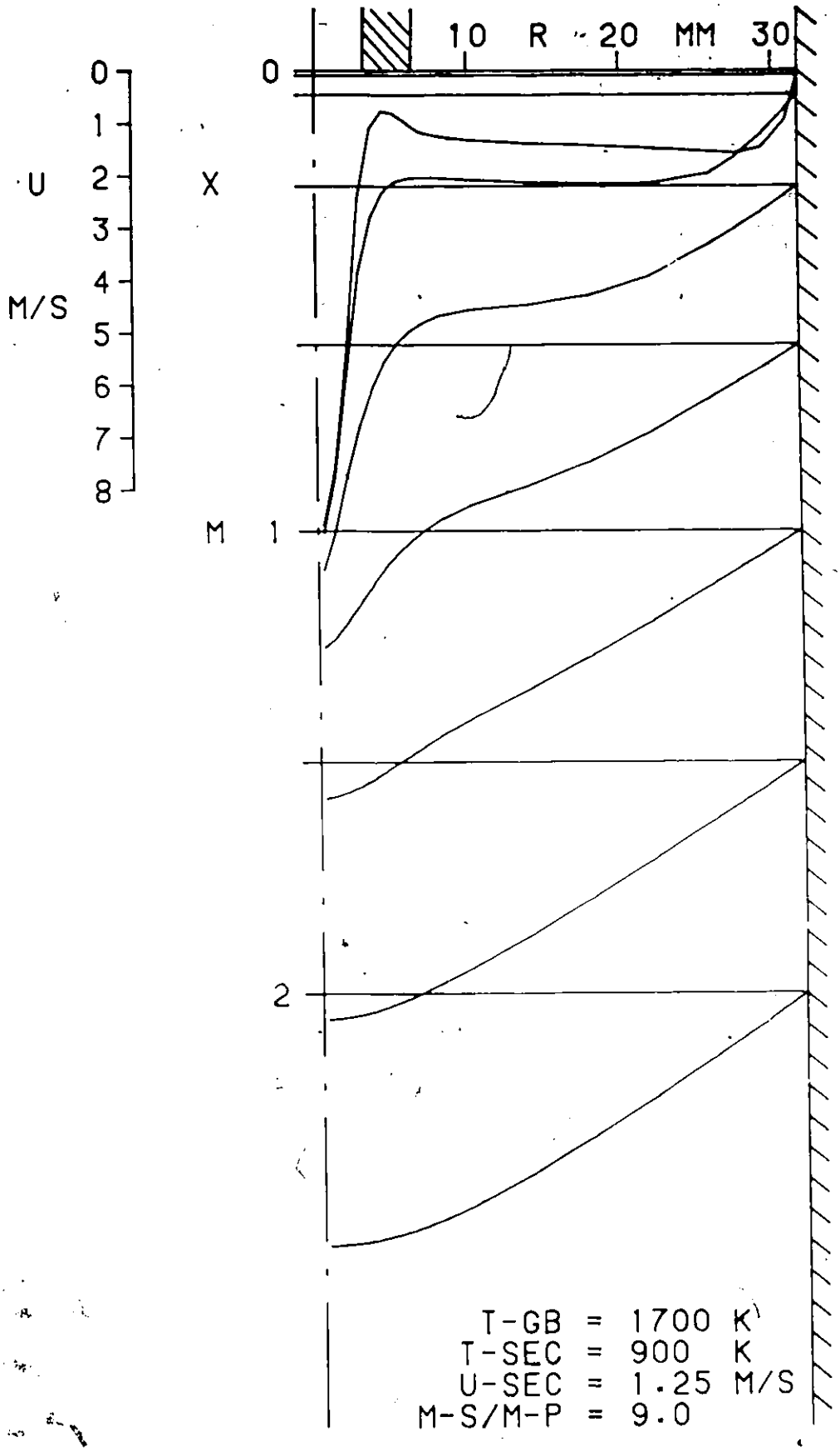

Figure 31: Velocity Profiles - Tgb=1700 K, Tinsec=900 K, M-S/M-P=9.0

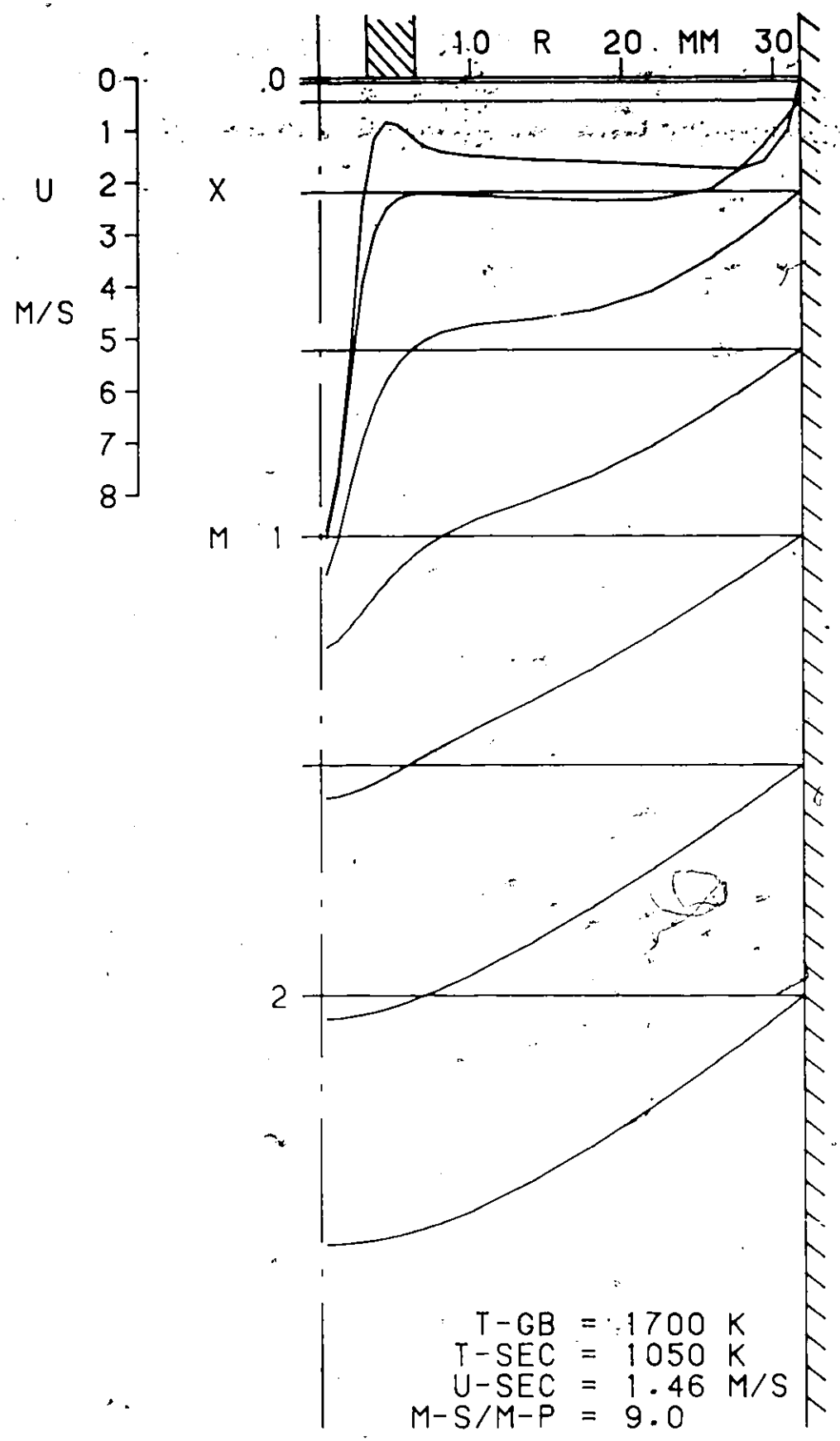

Figure 32: Velocity Profiles – Tgb=1700 K, Tinsec=1050 K, M-S/M-P=9.0

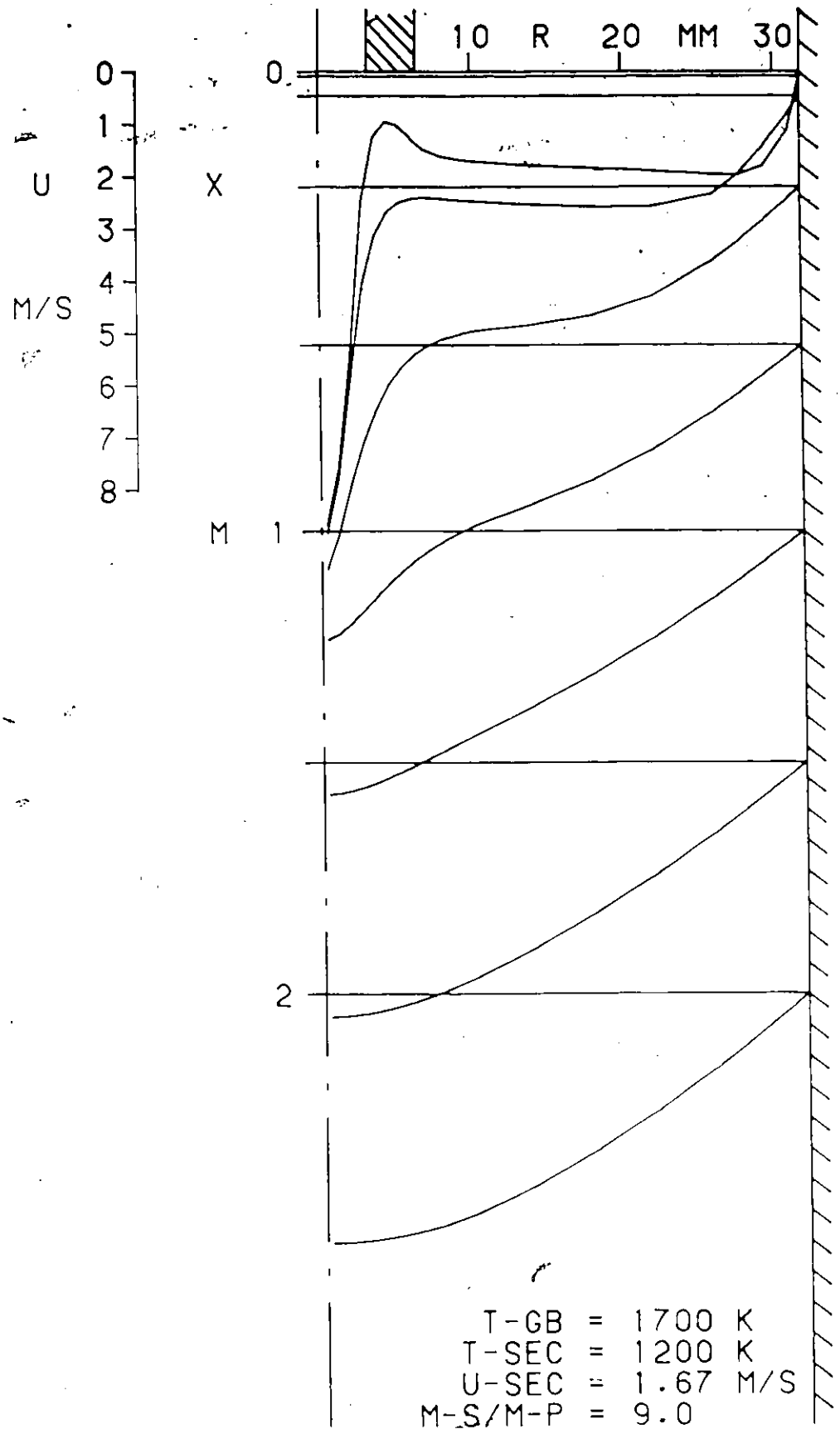

Figure 33: Velocity Profiles – Tgb=1700 K, Tinsec=1200 K, M-S/M-P=9.0

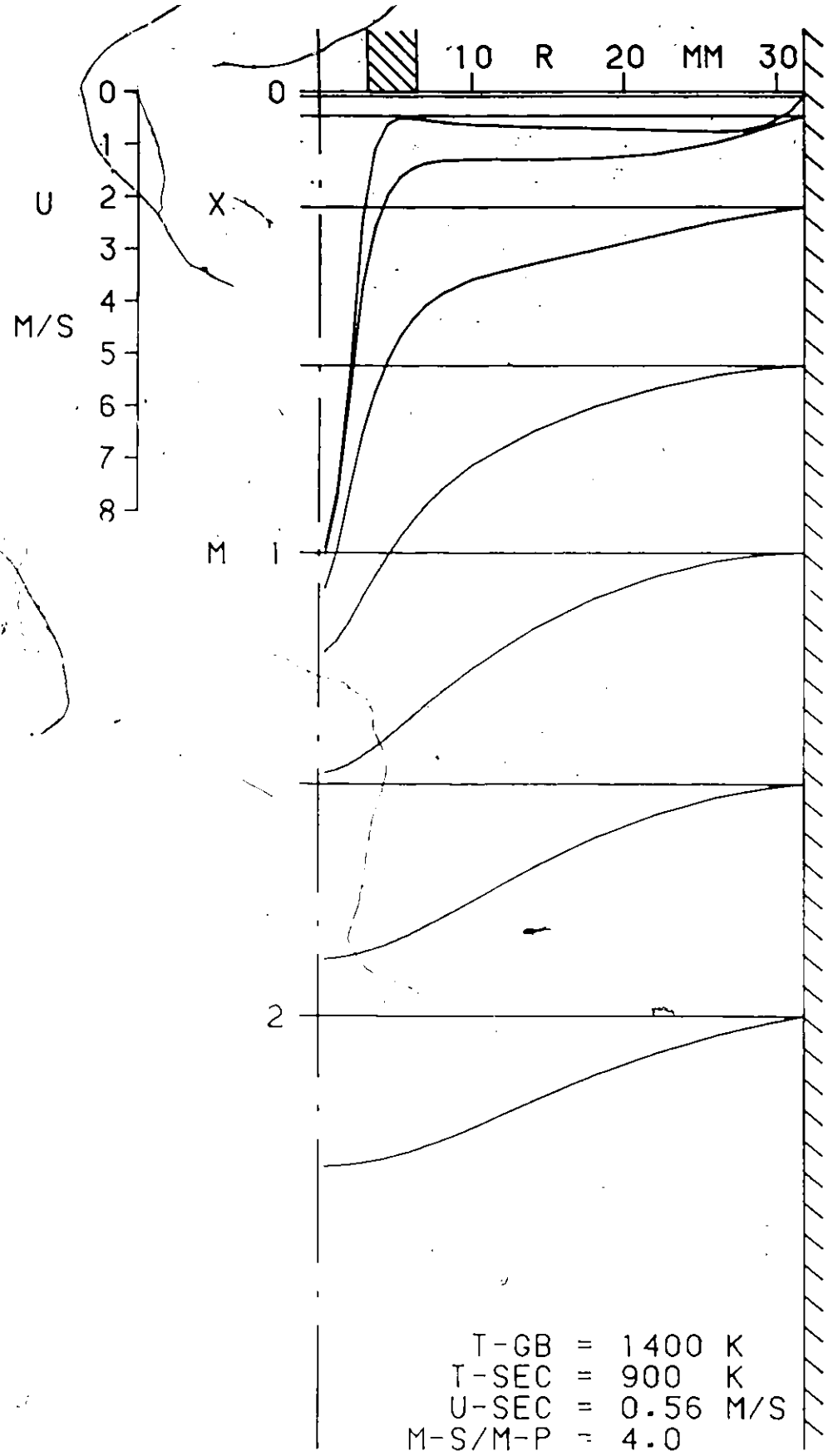

Figure 34: Velocity Profiles – Tgb=1400 K, Tinsec=900 K, M-S/M-P=4.0

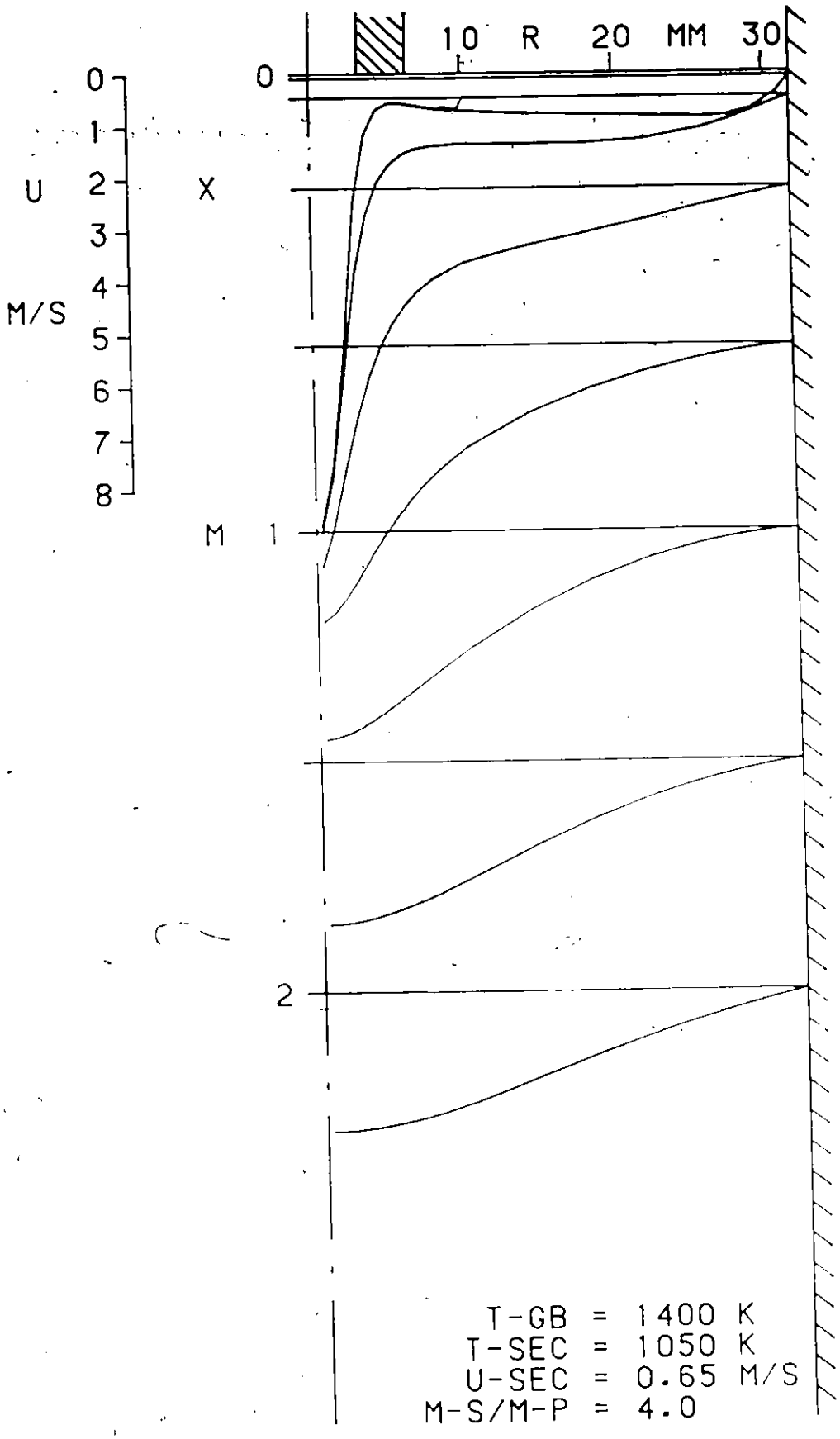

Figure 35: Velocity Profiles – Tgb=1400 K, Tinsec=1050 K, M-S/M-P=4.0

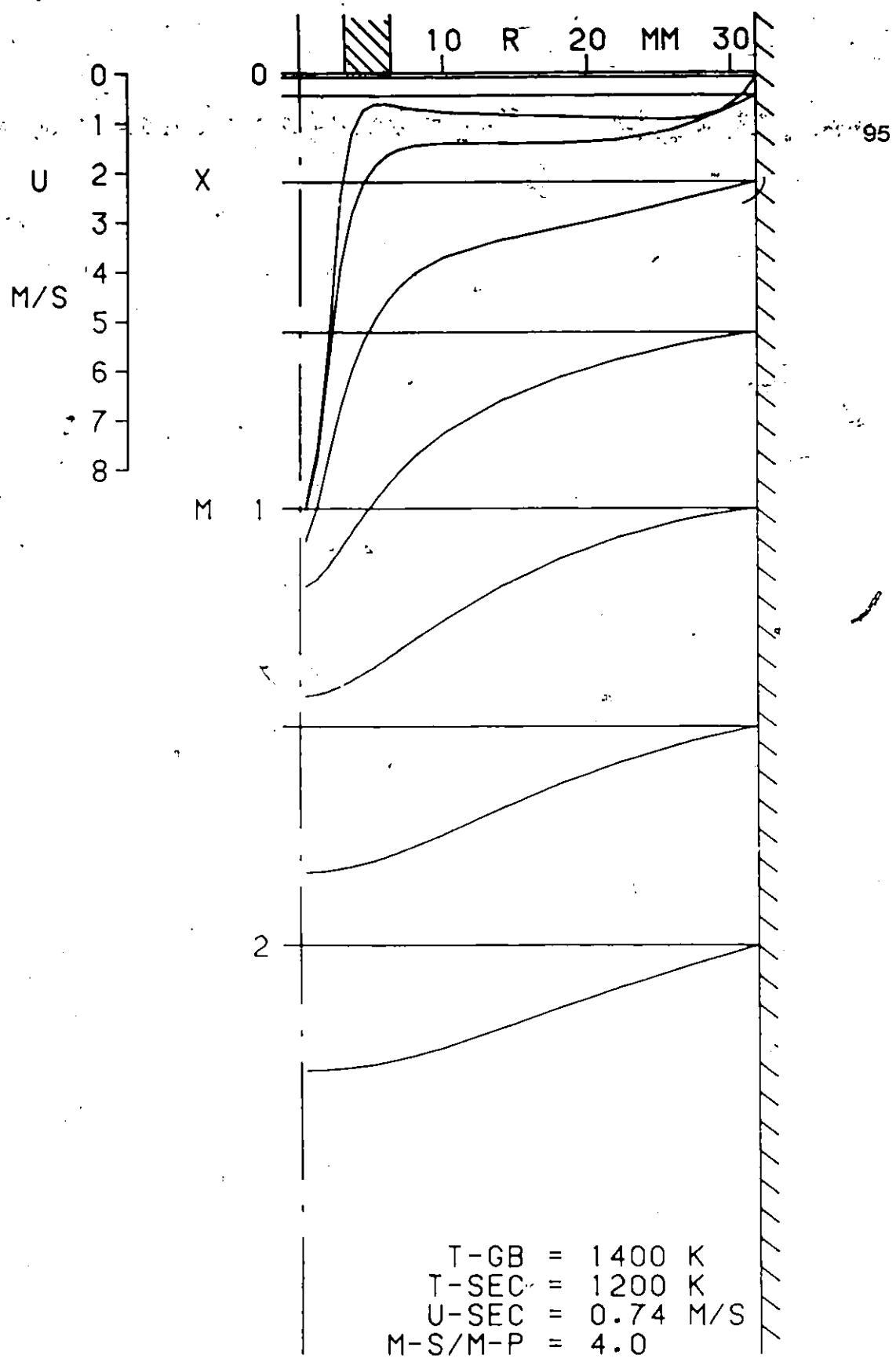

Figure 36: Velocity Profiles – Tgb=1400 K, Tinsec=1200 K, M-S/M-P=4.0

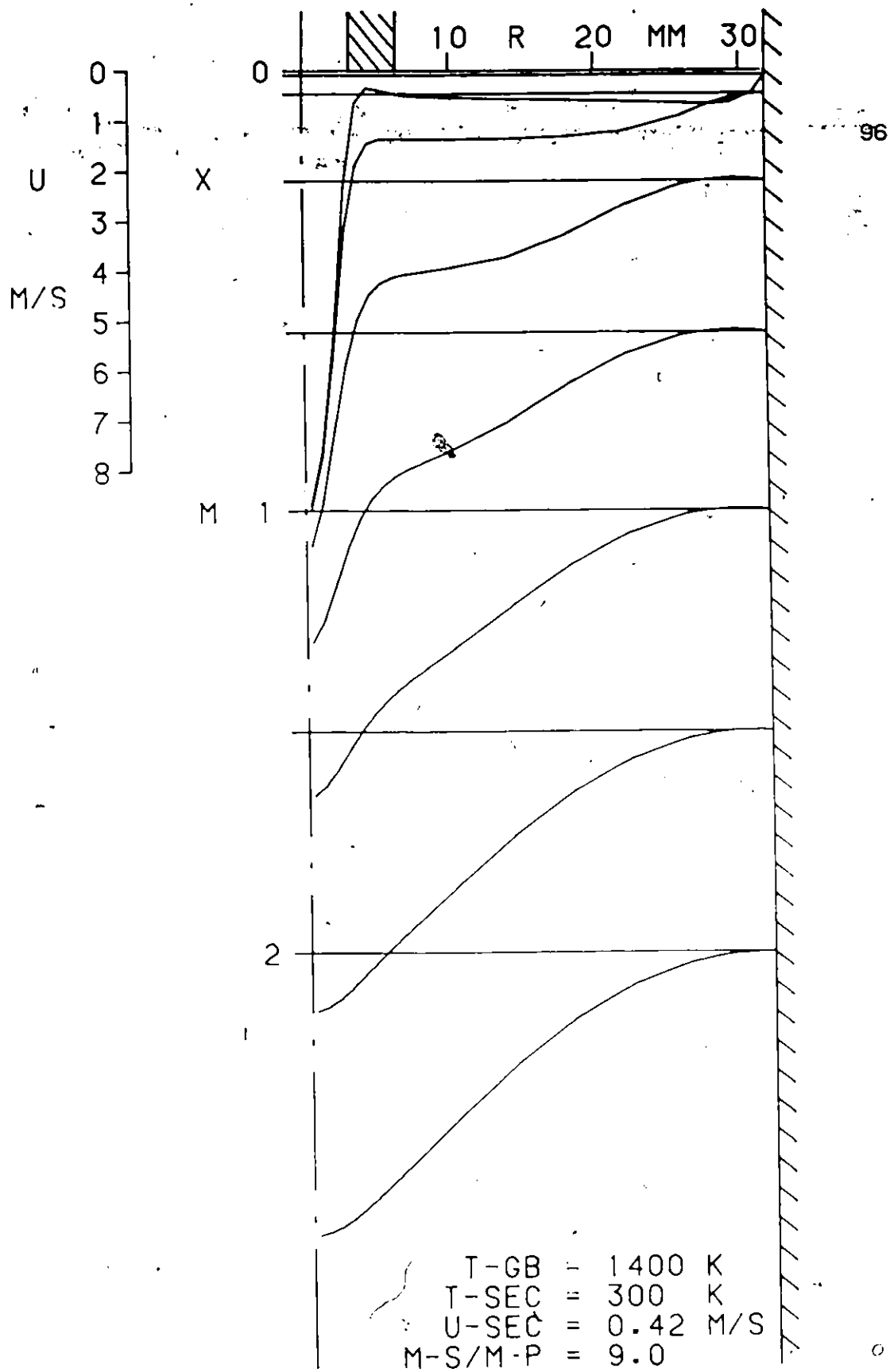

Figure 37: Velocity Profiles – Tgb=1400 K, Tinsec=300 K, M-S/M-P=9.0

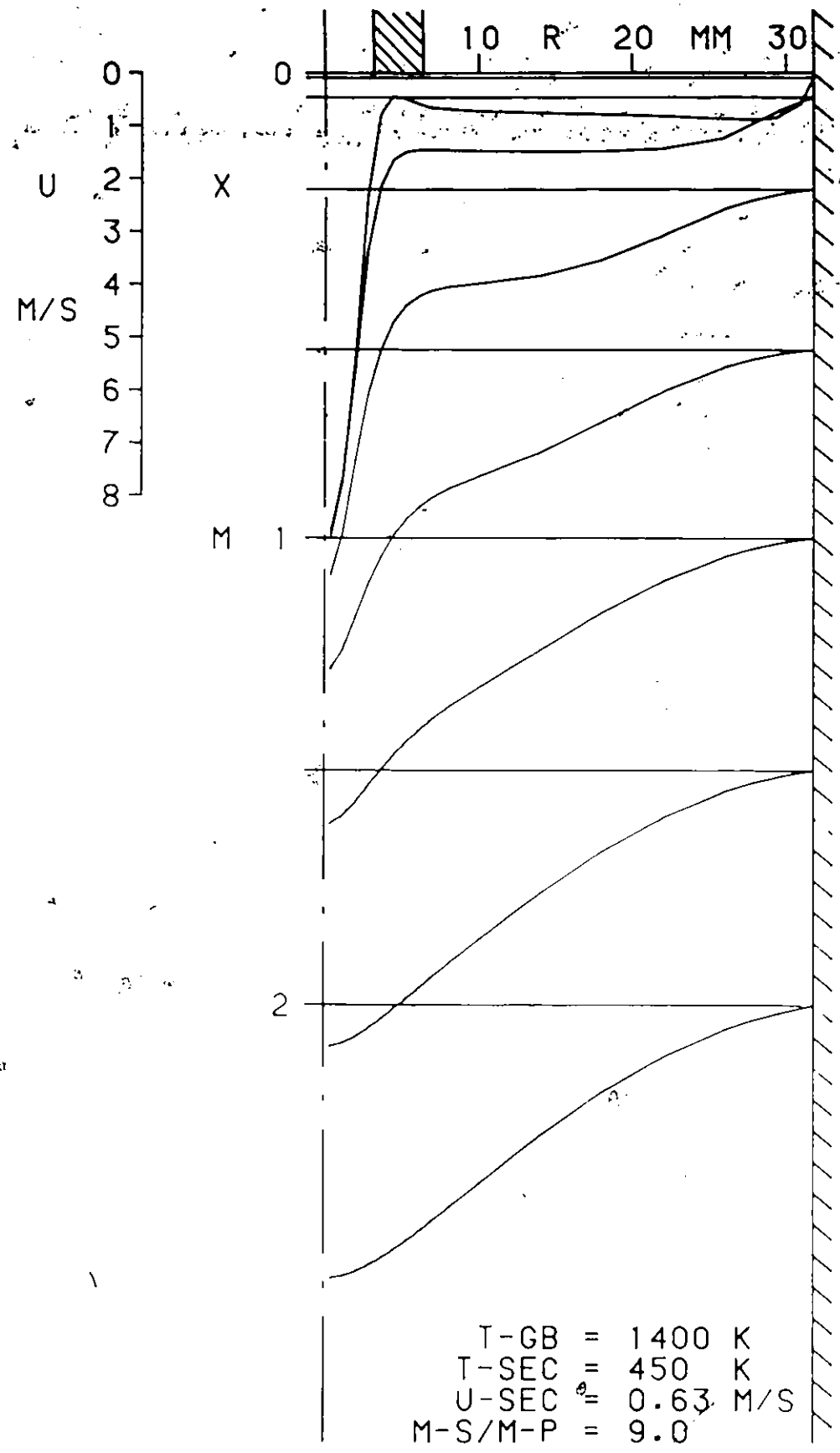

Figure 38: Velocity Profiles – Tgb=1400 K, Tinsec=450 K, M-S/M-P=9.0

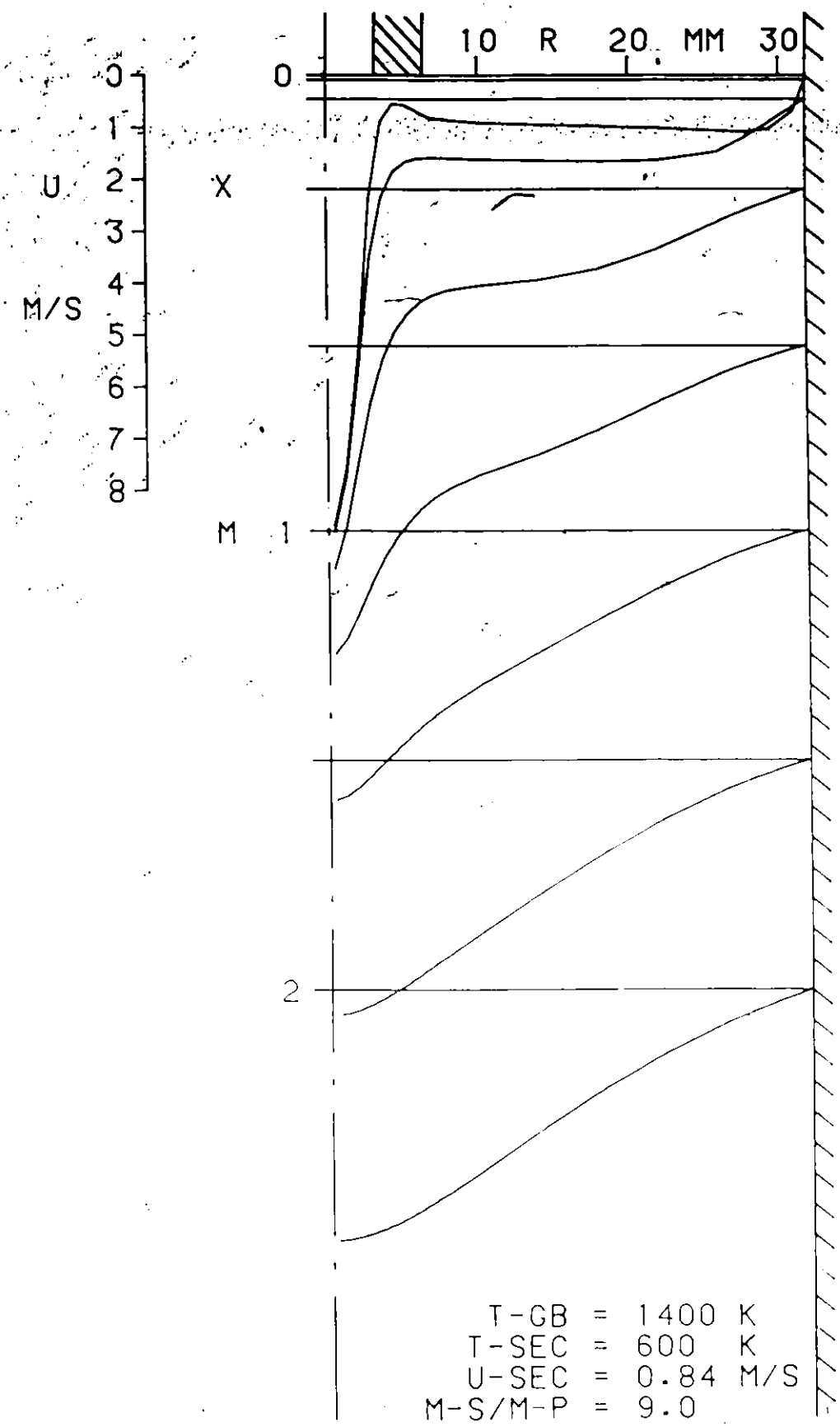

Figure 39: Velocity Profiles – Tgb=1400 K, Tinsec=600 K, M-S/M-P=9.0

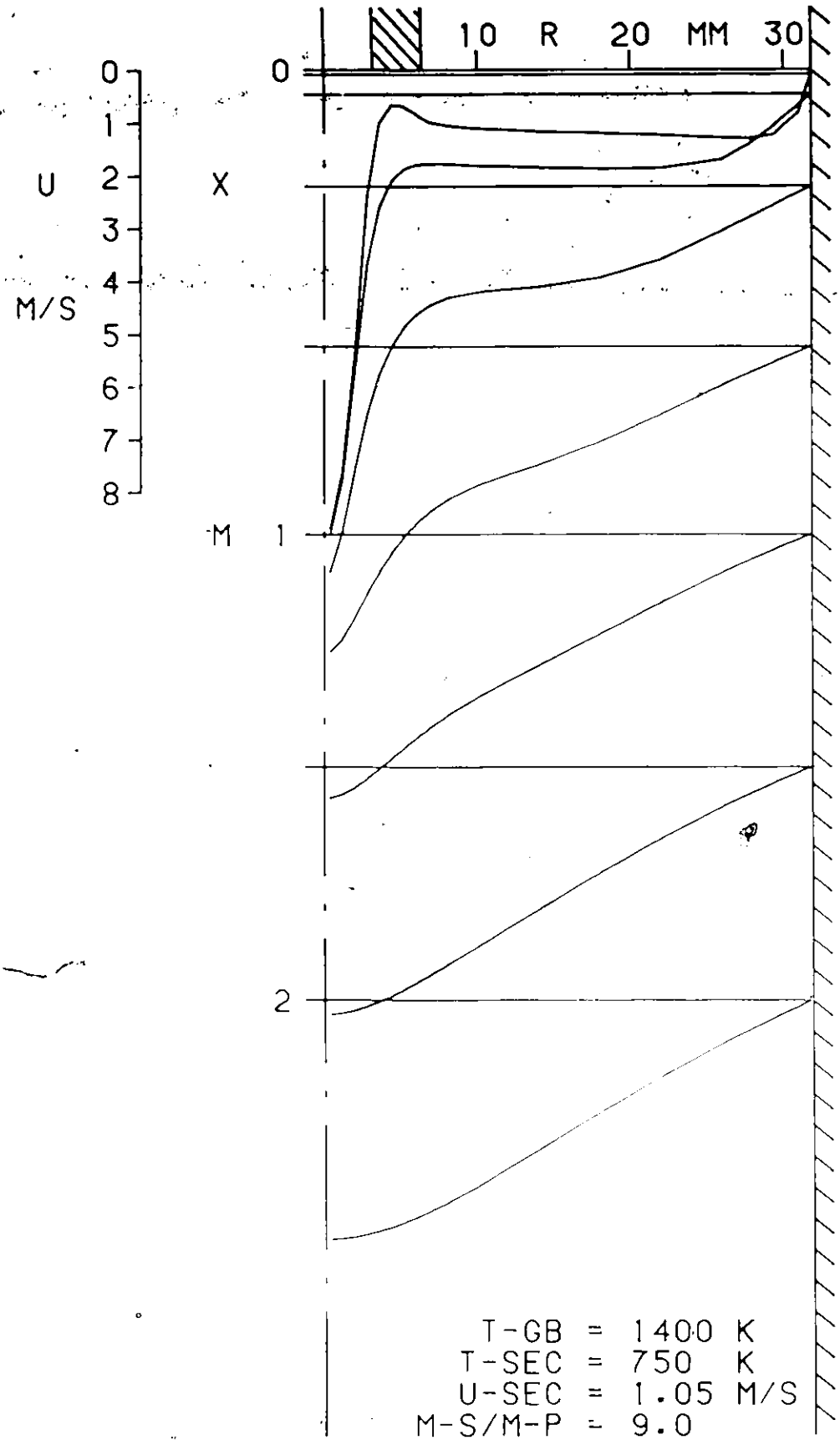

Figure 40: Velocity Profiles – Tgb=1400 K, Tinsec=750 K, M-S/M-P=9.0

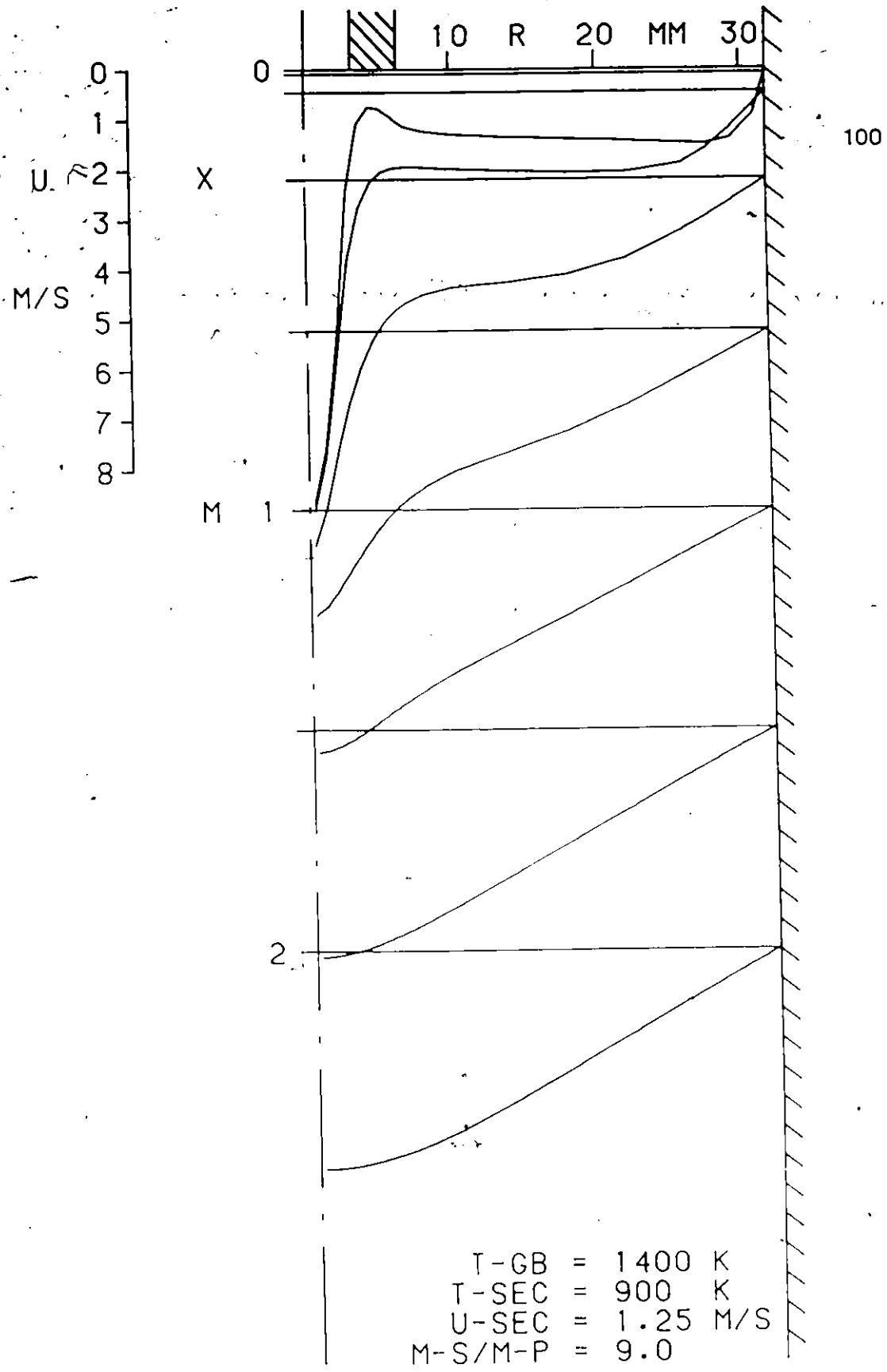

Figure 41: Velocity Profiles - Tgb=1400 K, Tinsec=900 K, M-S/M-P=9.0

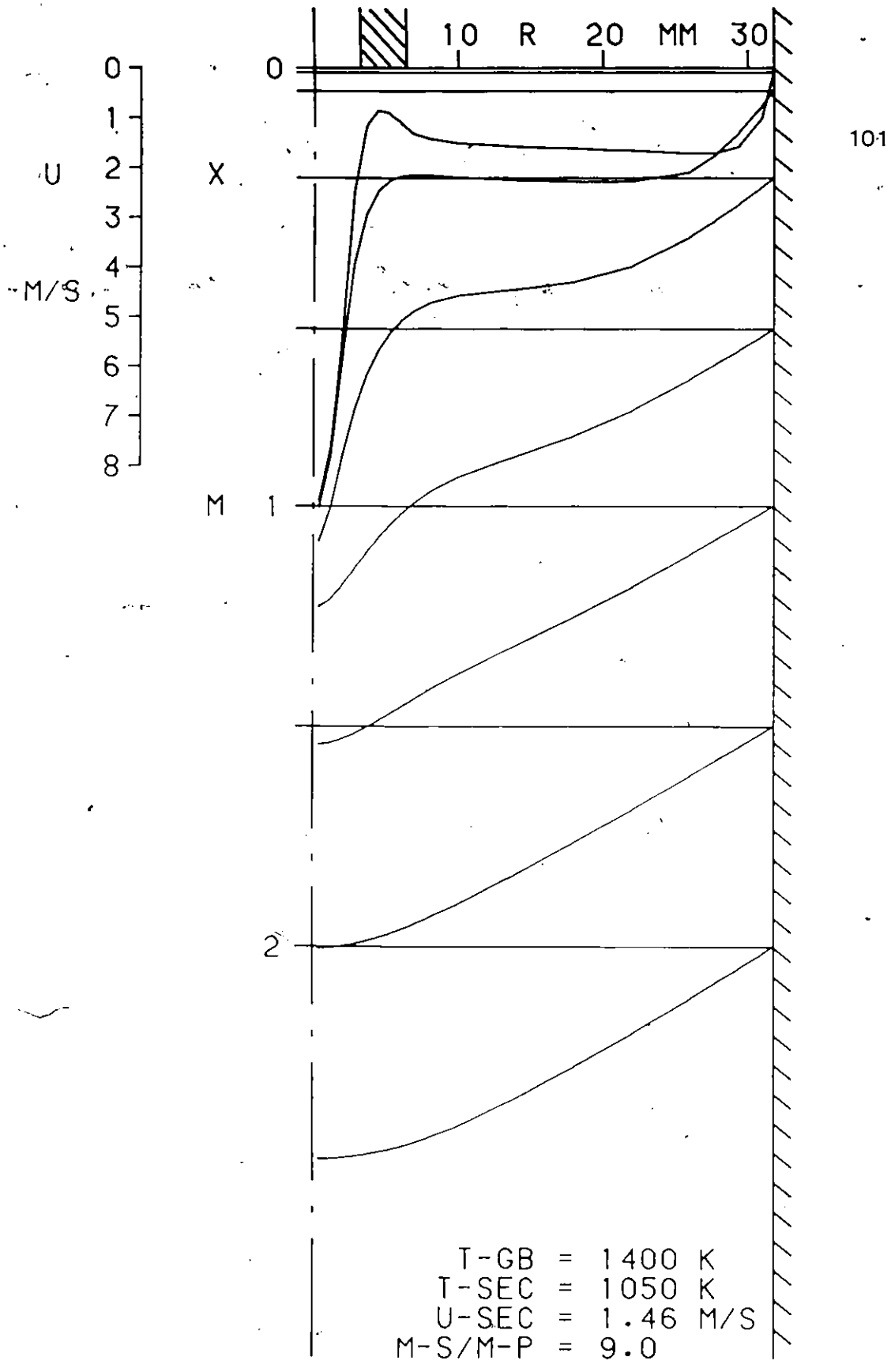

101

Figure 42: Velocity Profiles – Tgb=1400 K, Tinsec=1050 K, M-S/M-P=9.0

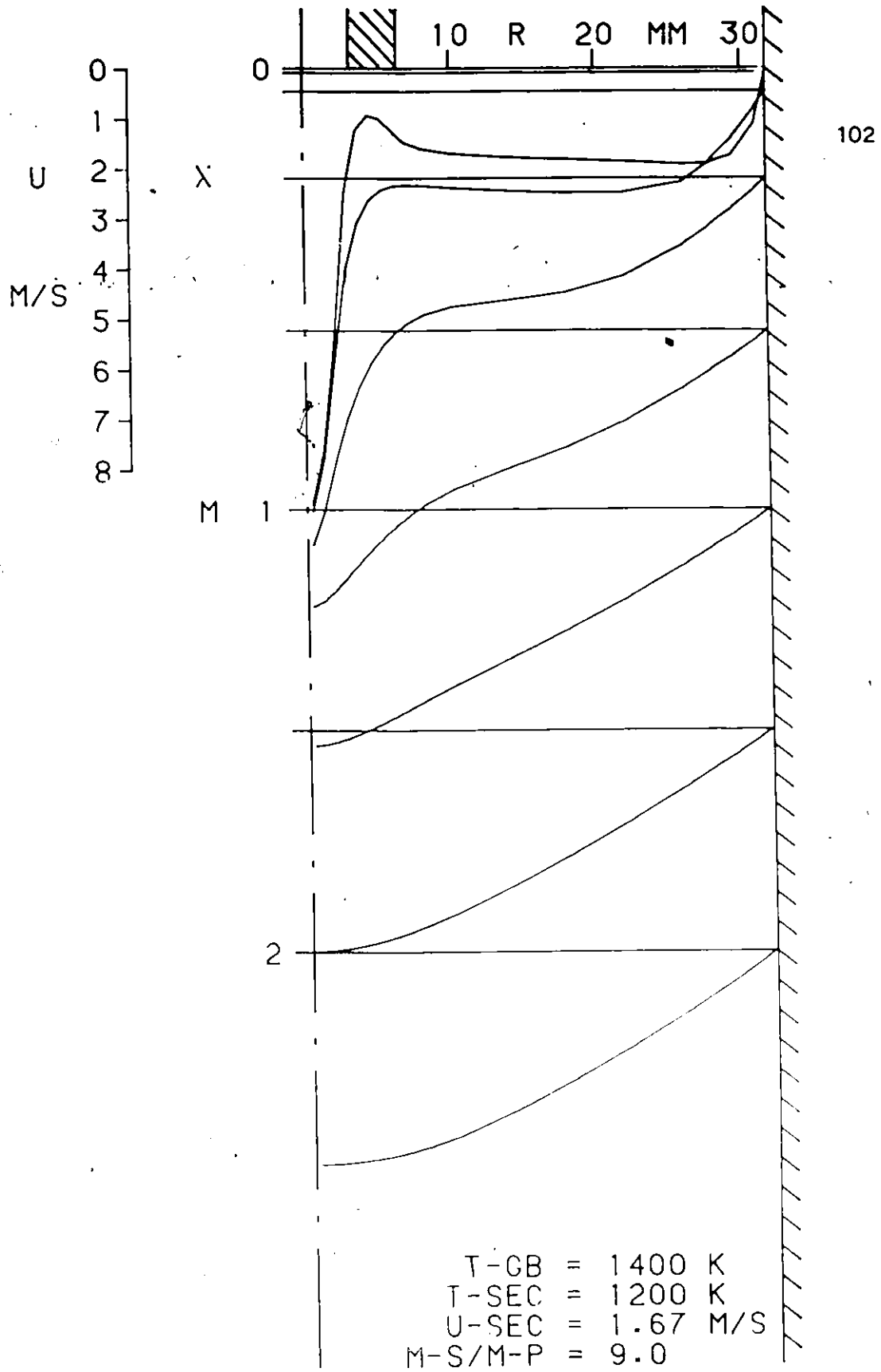

Figure 43: Velocity Profiles - Tgb=1400 K, Tinsec=1200 K, M-S/M-P=9.0

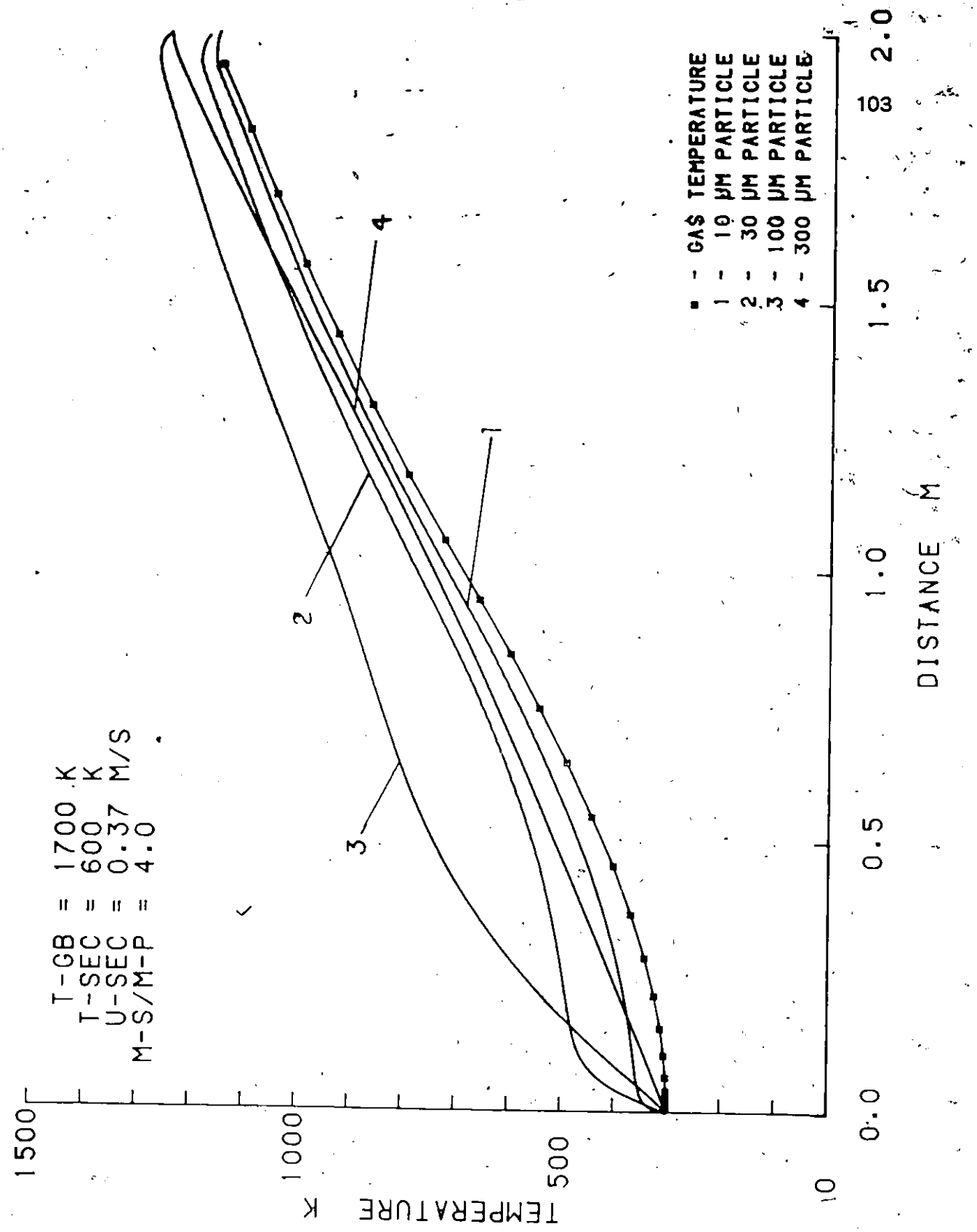

Figure 44: Particle Heating – Tgb=1700 K, Tinsec=600 K, M–S/M–P=4.0

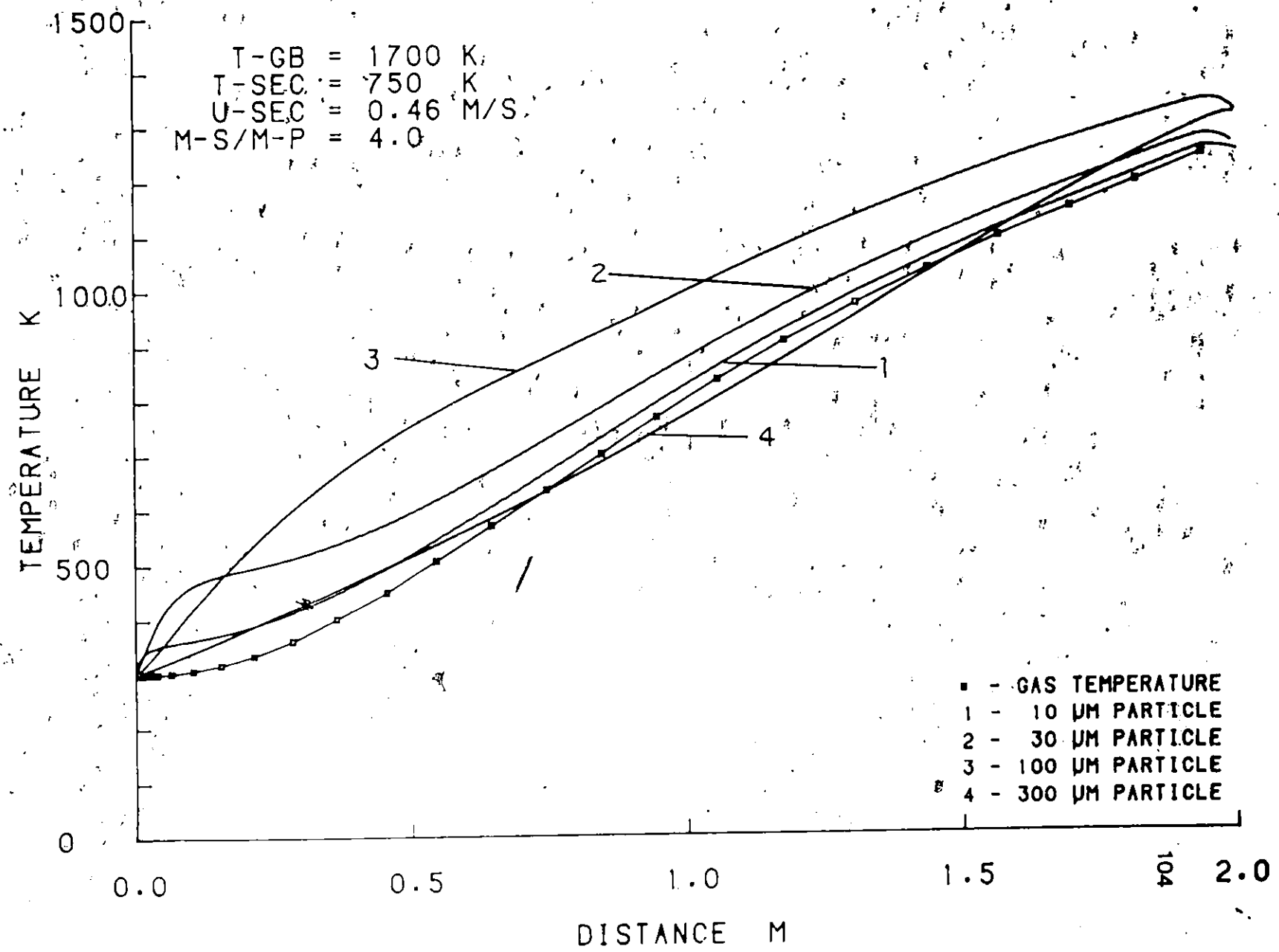

Figure 45: Particle Heating - Tgb=1700 K, Tinsec=750 K, M-S/M-P=4.0

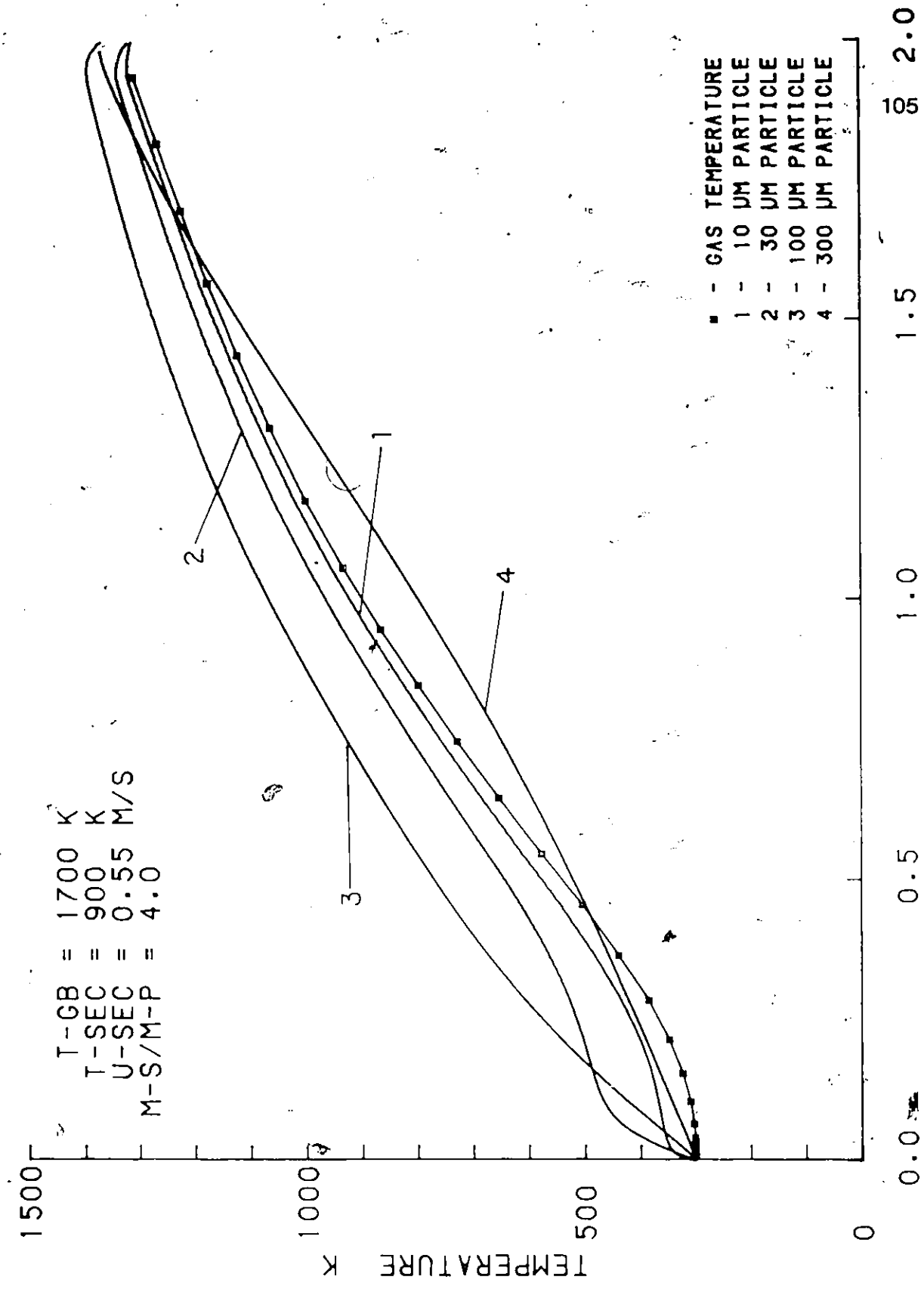

Figure 46: Particle Heating – Tgb=1700 K, Tinsec=900 K, M-S/M-P=4.0

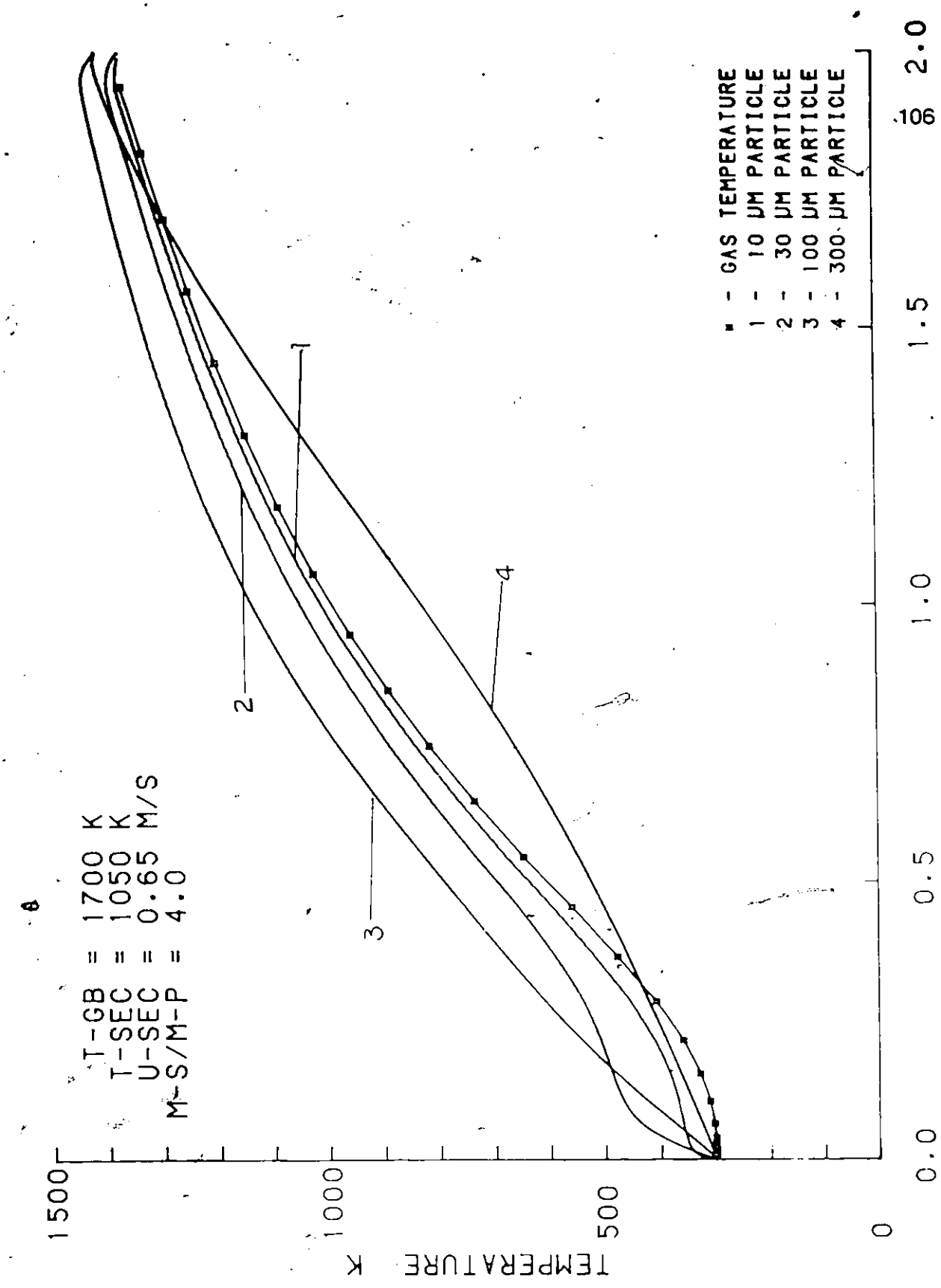

Figure 47: Particle Heating – Tgb=1700 K, Tinsec=1050 K, M-S/M-P=4.0

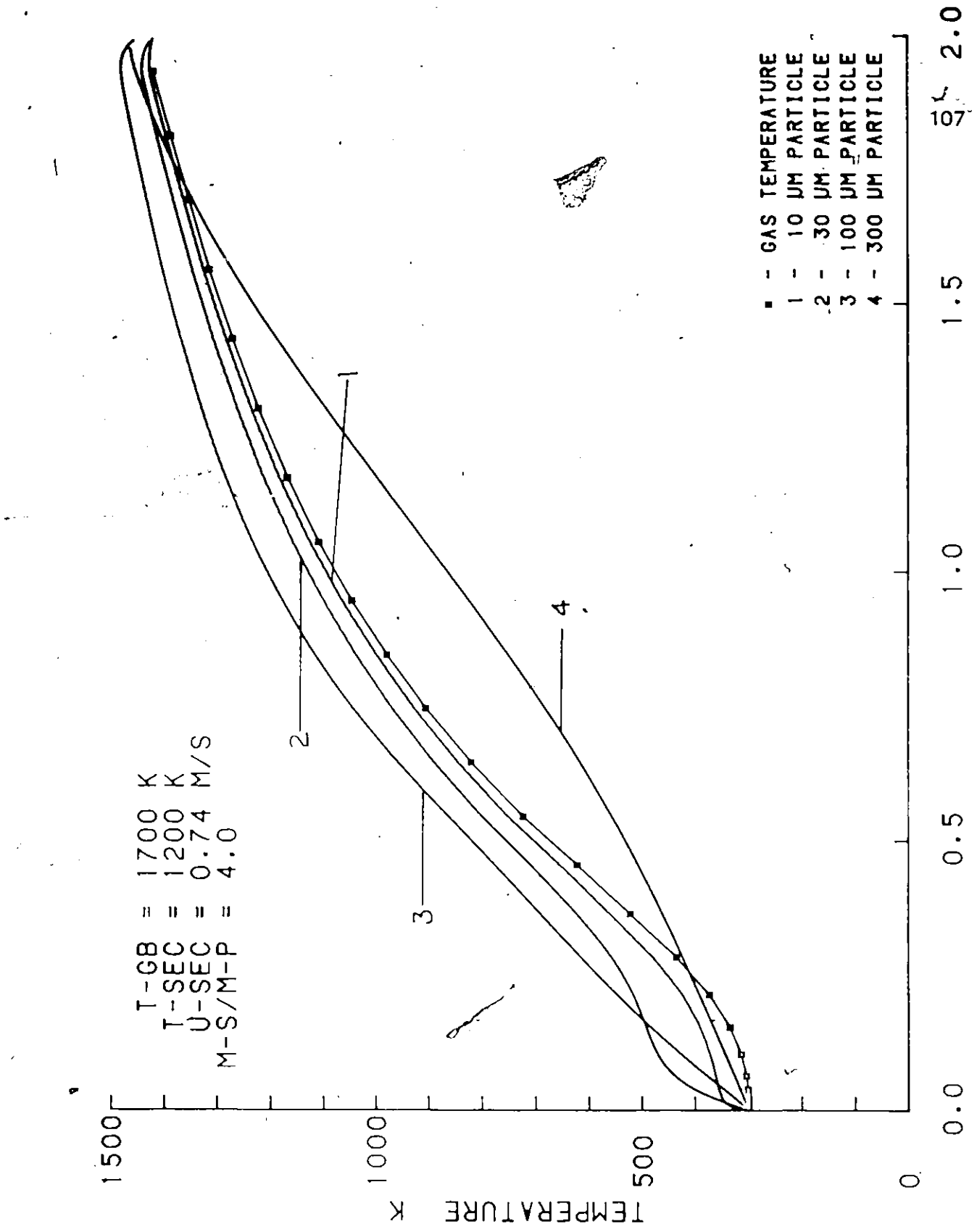

Figure 48: Particle Heating – Tgb=1700 K, Tinsec=1200 K, M-S/M-P=4.0

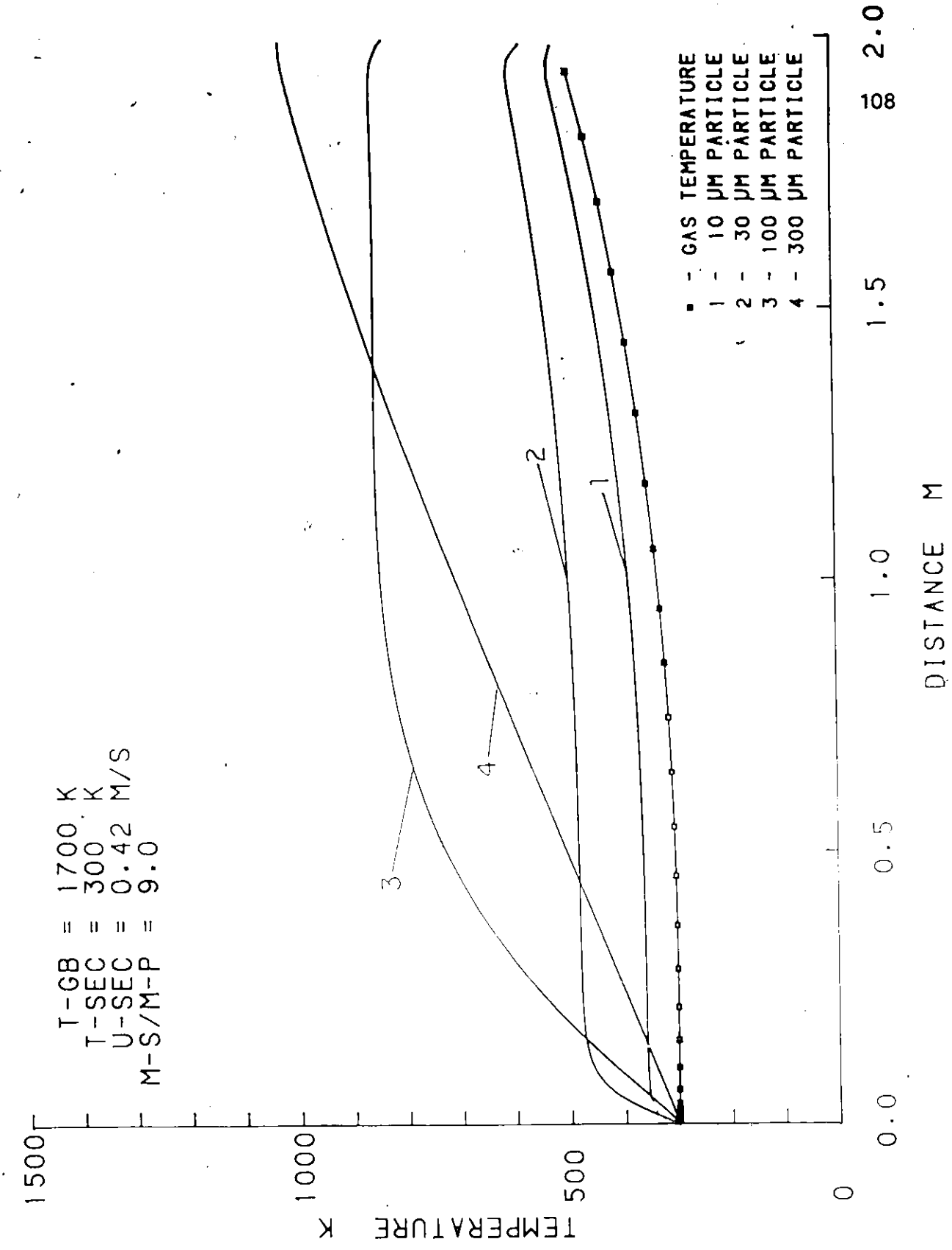

Figure 49: Particle Heating - Tgb=1700 K, Tinsec=300 K, M-S/M-P=9.0

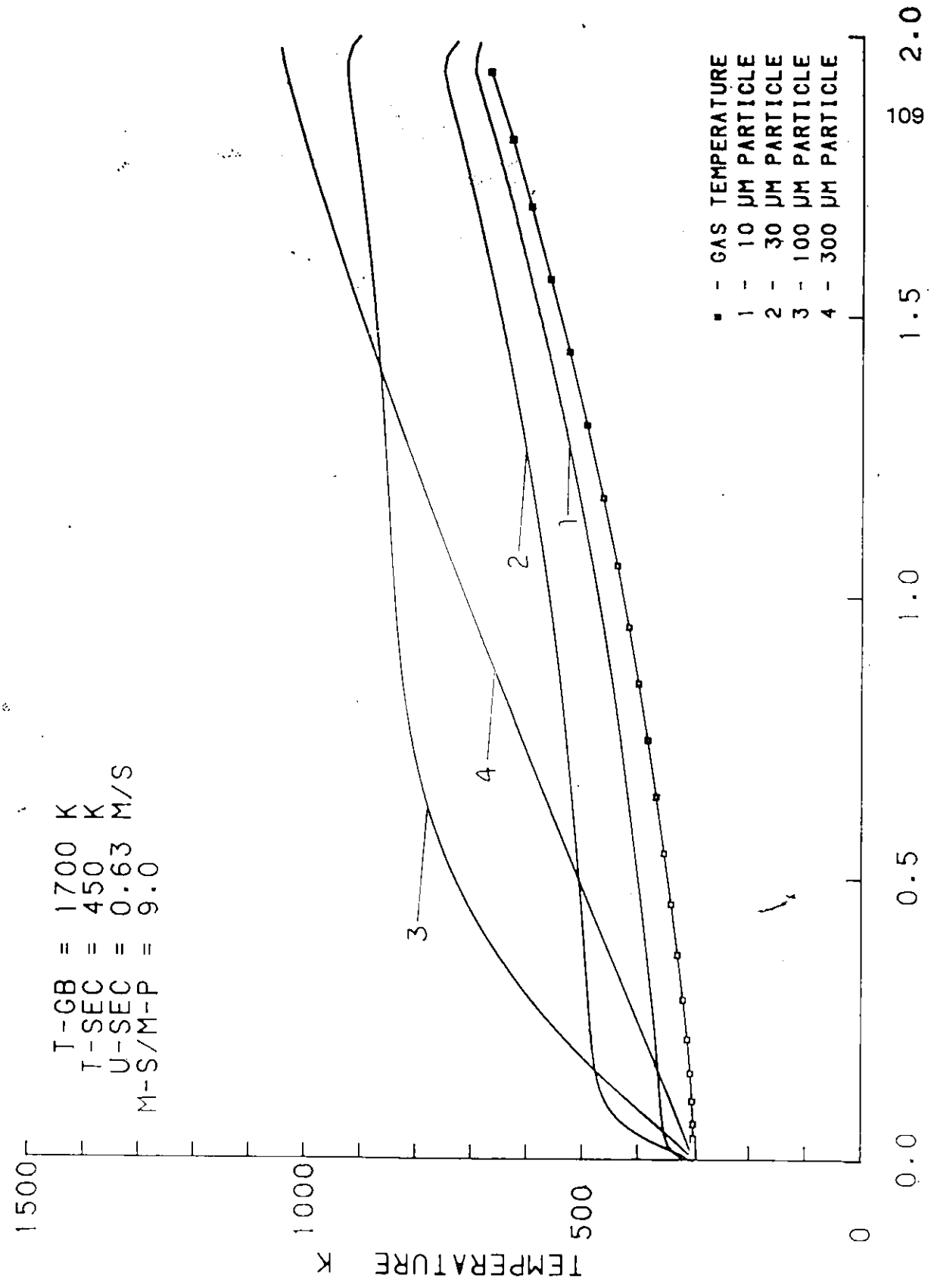

Figure 50: Particle Heating - Tgb=1700 K, Tinsec=450 K, M-S/M-P=9.0

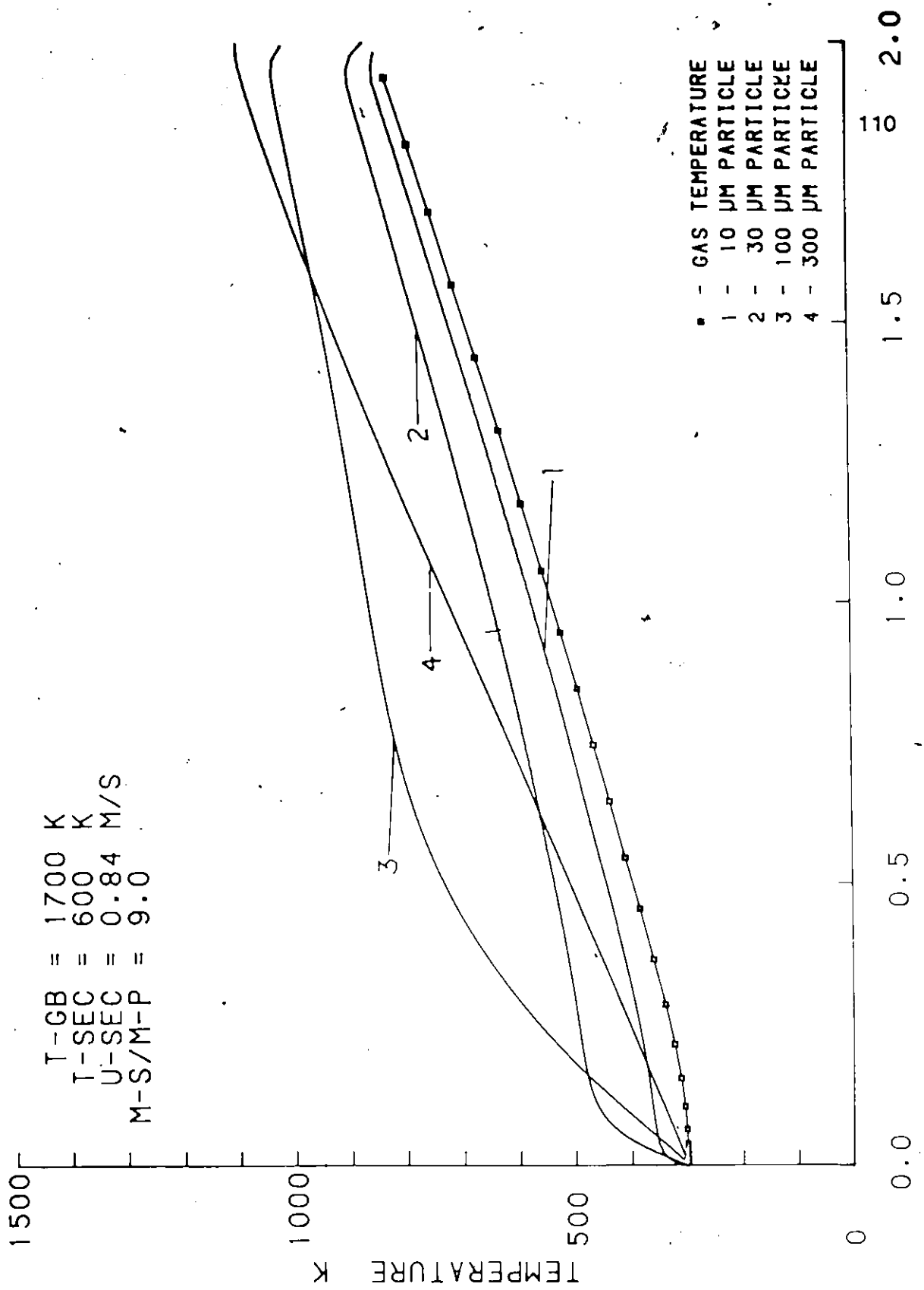

Figure 51: Particle Heating – Tgb=1700 K, Tinsec=600 K, M-S/M-P=9.0

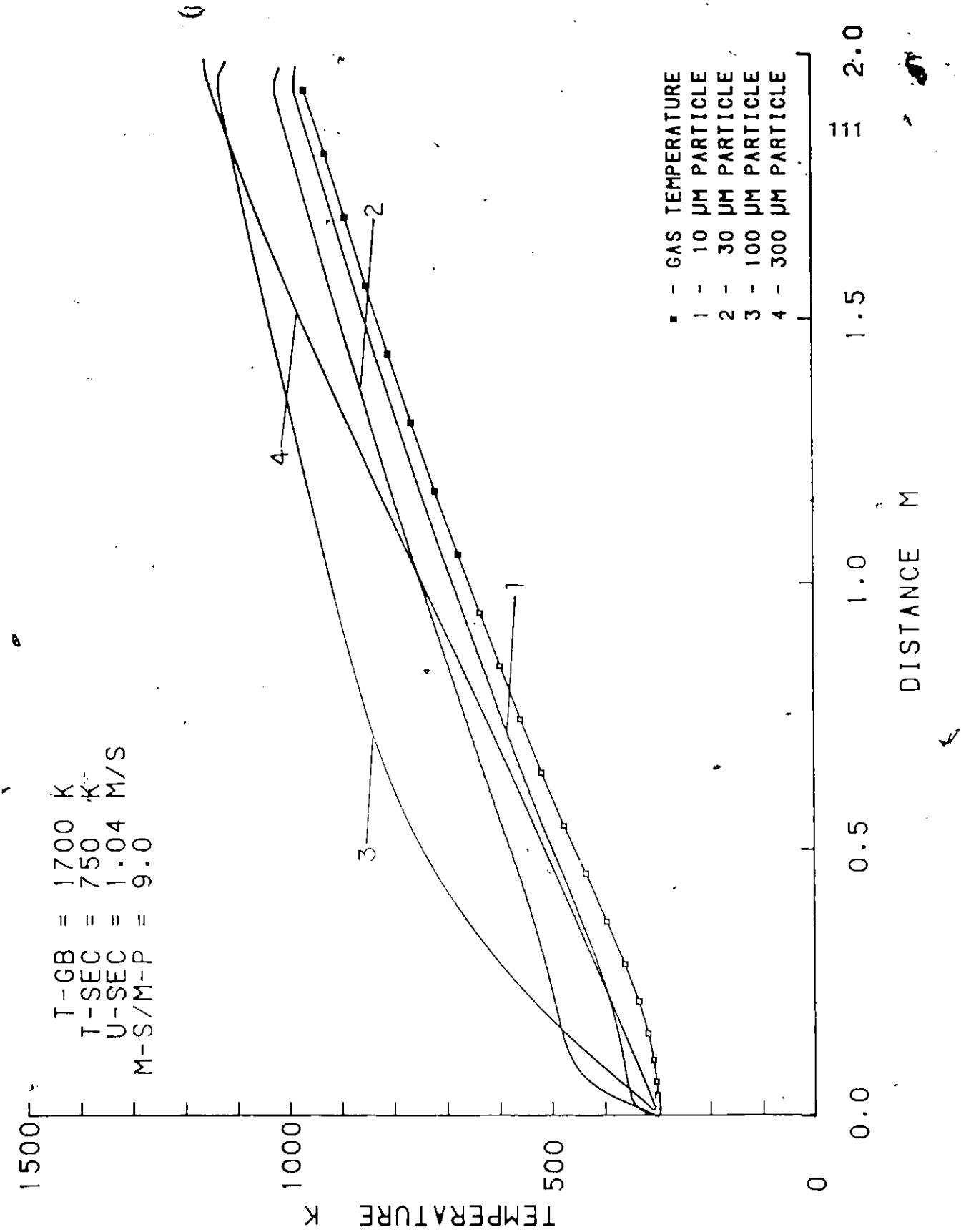

Figure 52: Particle Heating – Tgb=1700 K, Tinsec=750 K, M-S/M-P=9.0

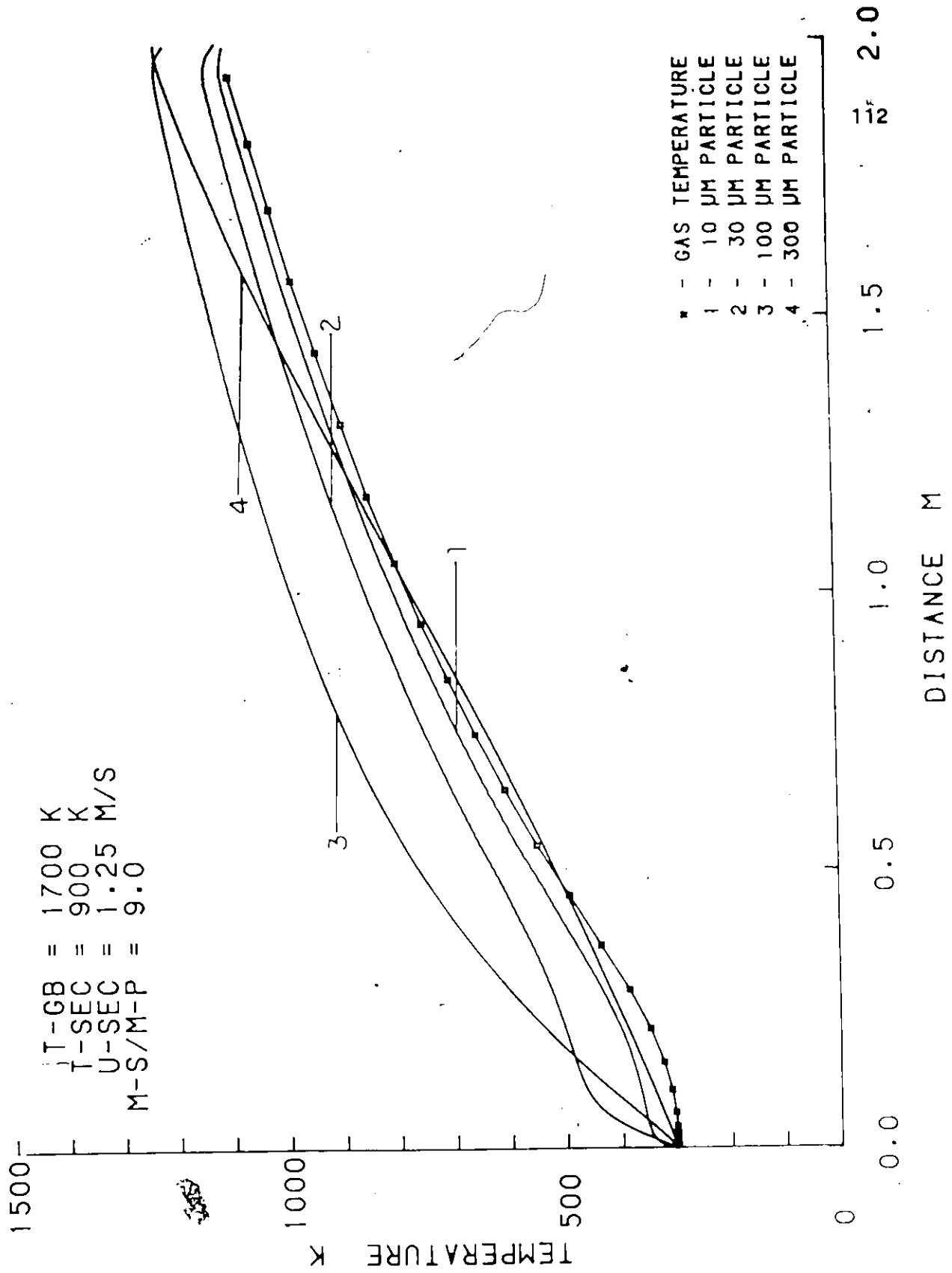

Figure 53: Particle Heating – Tgb=1700 K, Tinsec=900 K, M-S/M-P=9.0

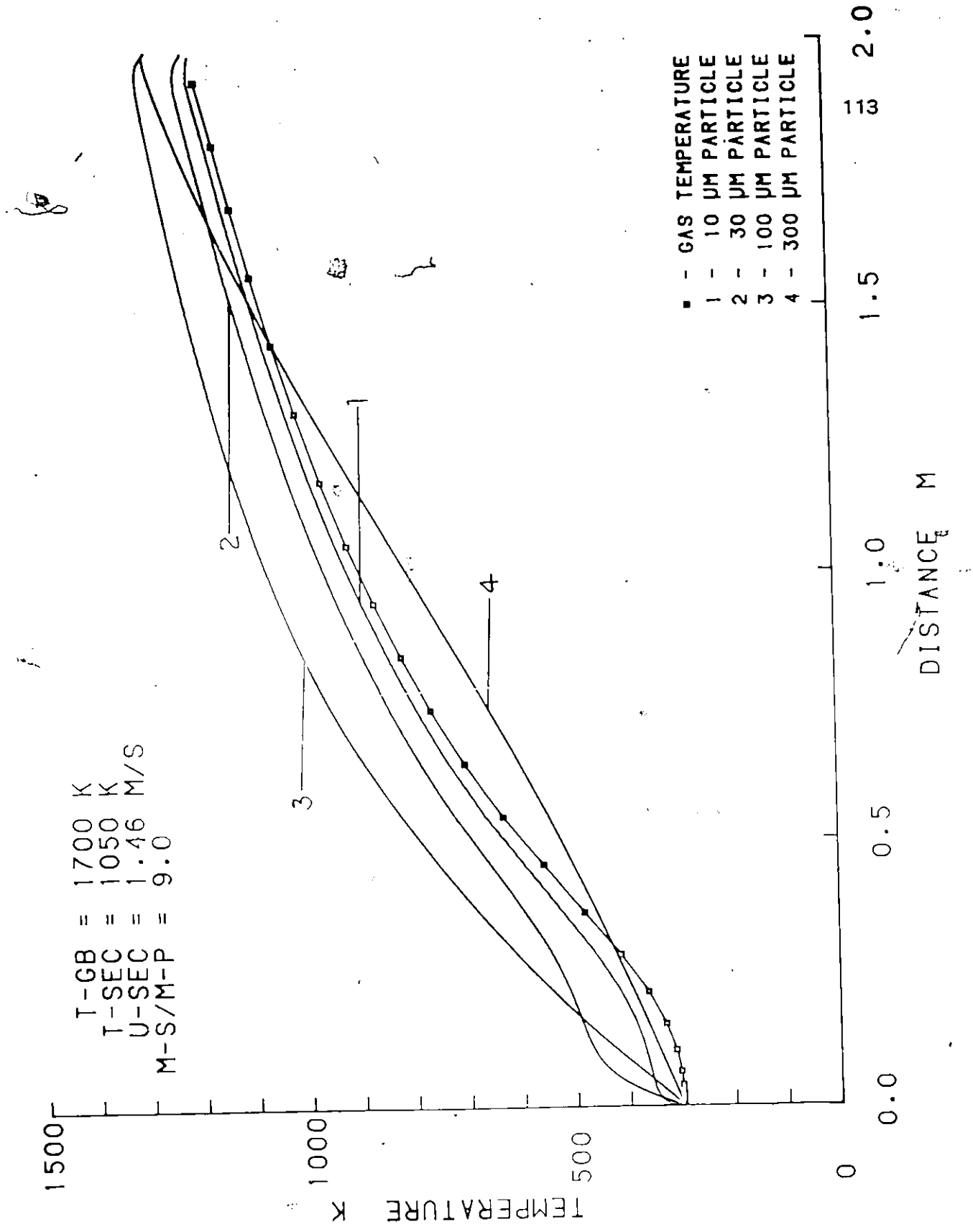

Figure 54: Particle Heating - Tgb=1700 K, Tinsec=1050 K, M-S/M-P=9.0

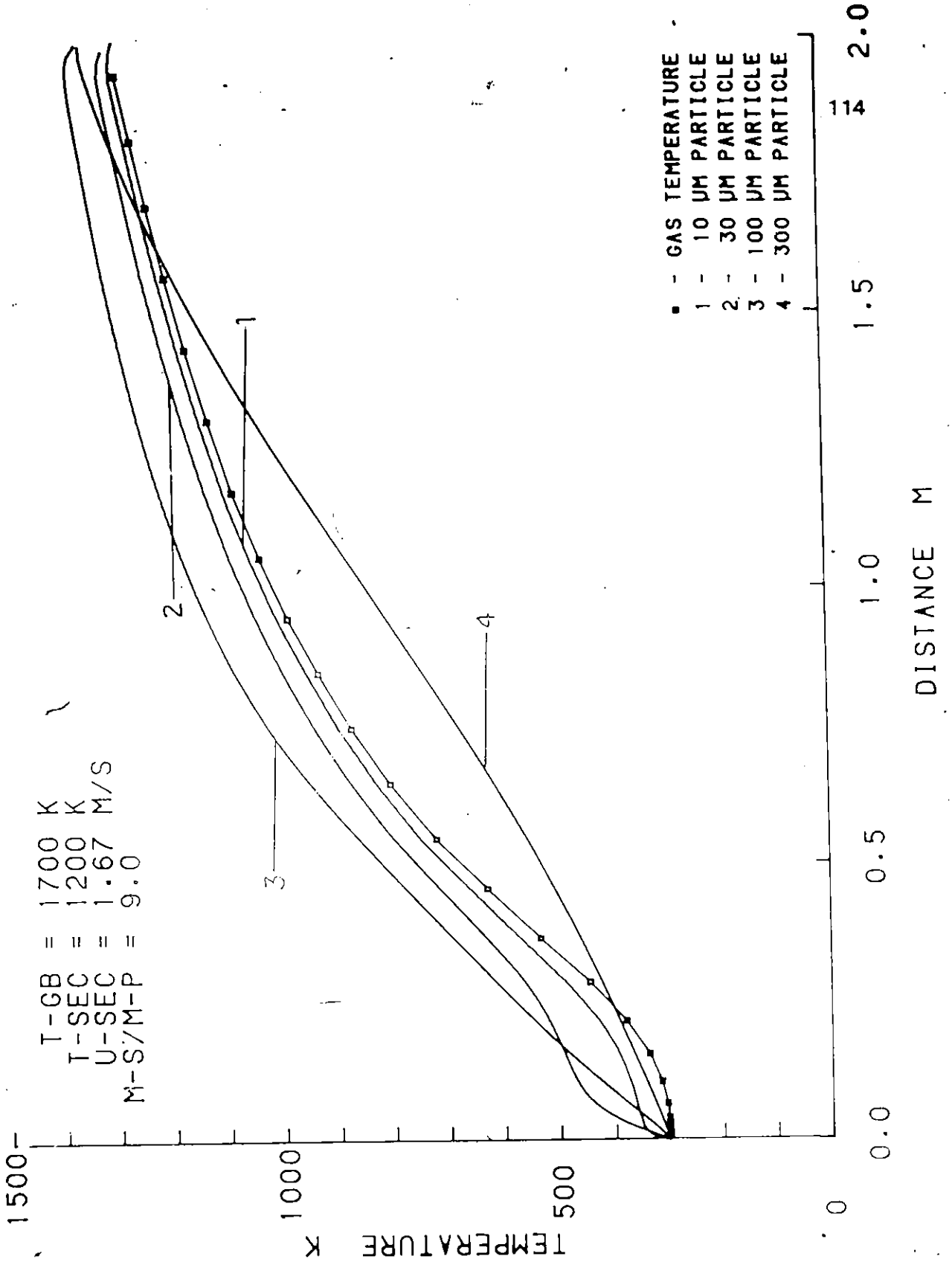

Figure 55: Particle Heating – Tgb=1700 K, Tinsec=1200 K, M-S/M-P=9.0

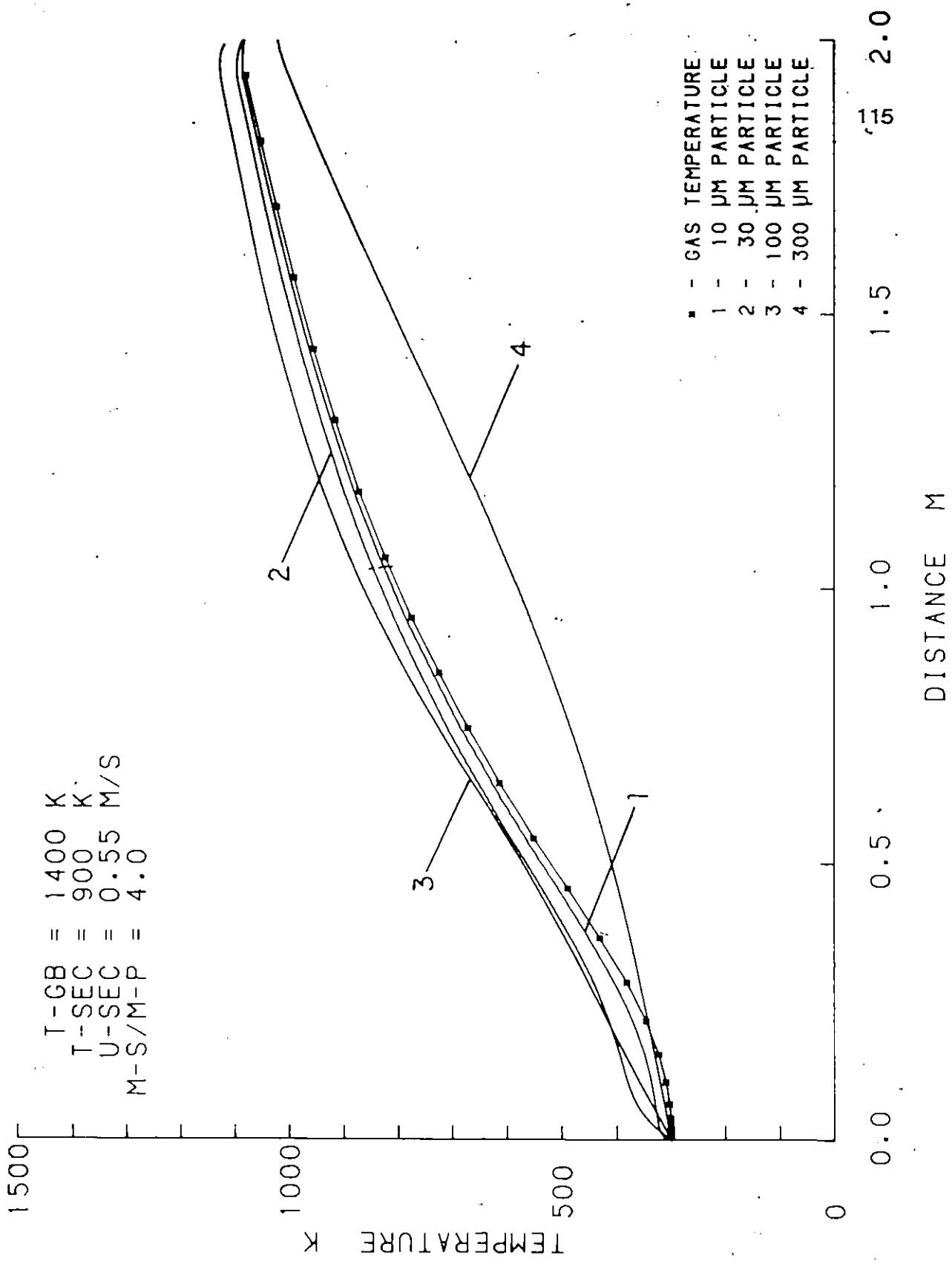

Figure 56: Particle Heating - Tgb=1400 K, Tinsec=900 K, M-S/M-P=4.0

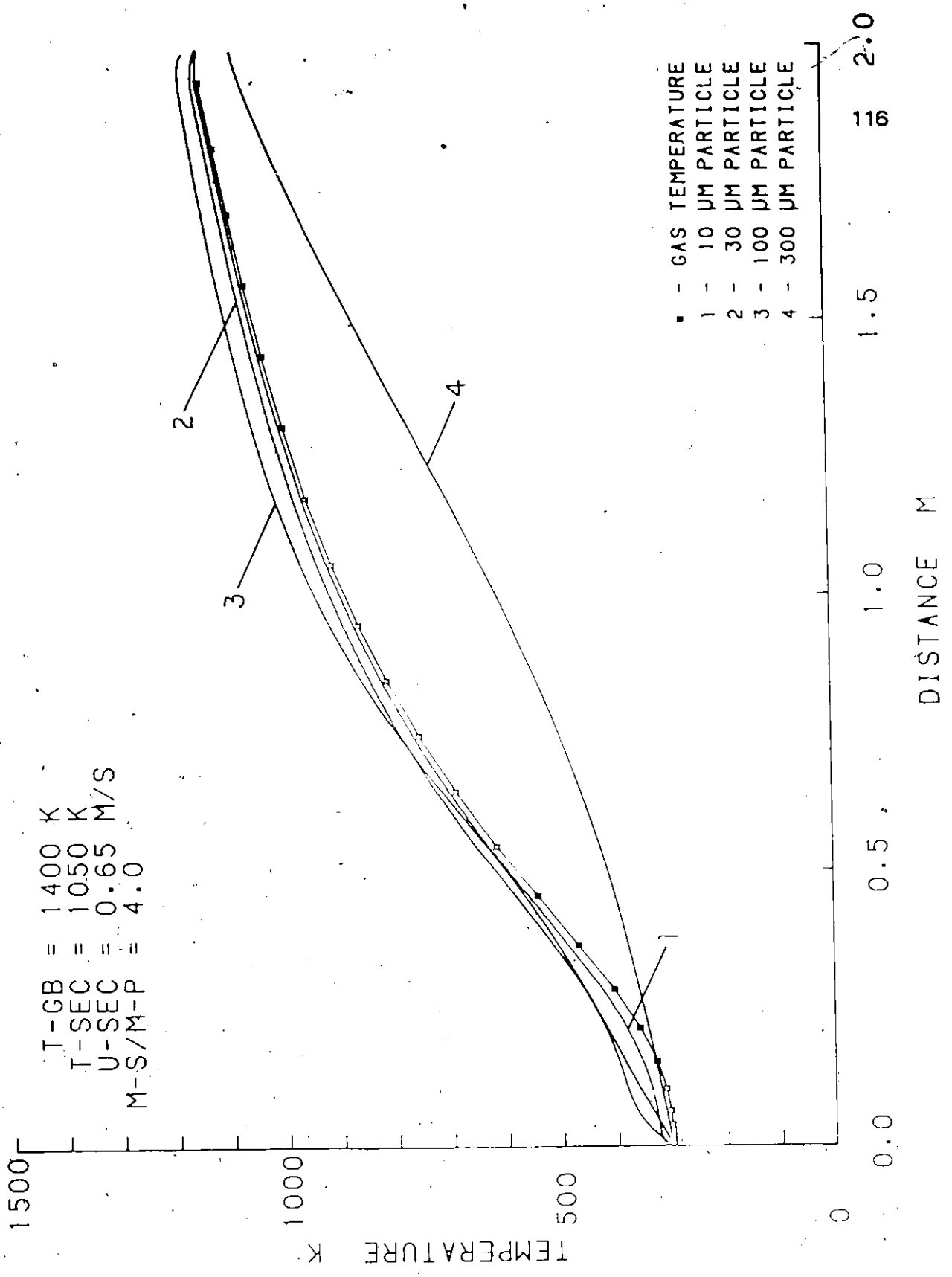

Figure 57: Particle Heating - Tgb=1400 K, Tinsec=1050 K, M-S/M-P=4.0

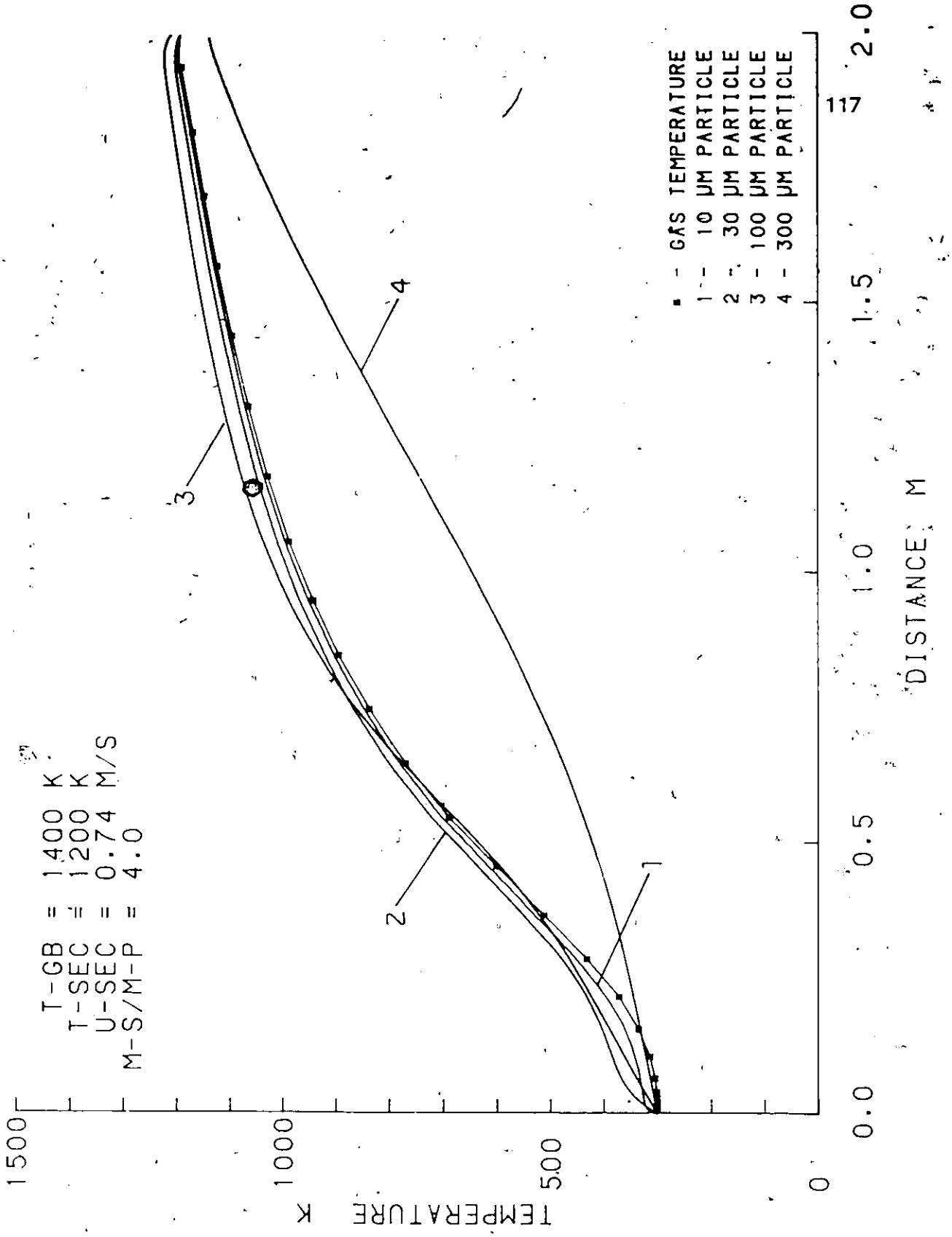

Figure 58: Particle Heating – Tgb=1400 K, Tinsec=1200 K, M-S/M-P=4.0

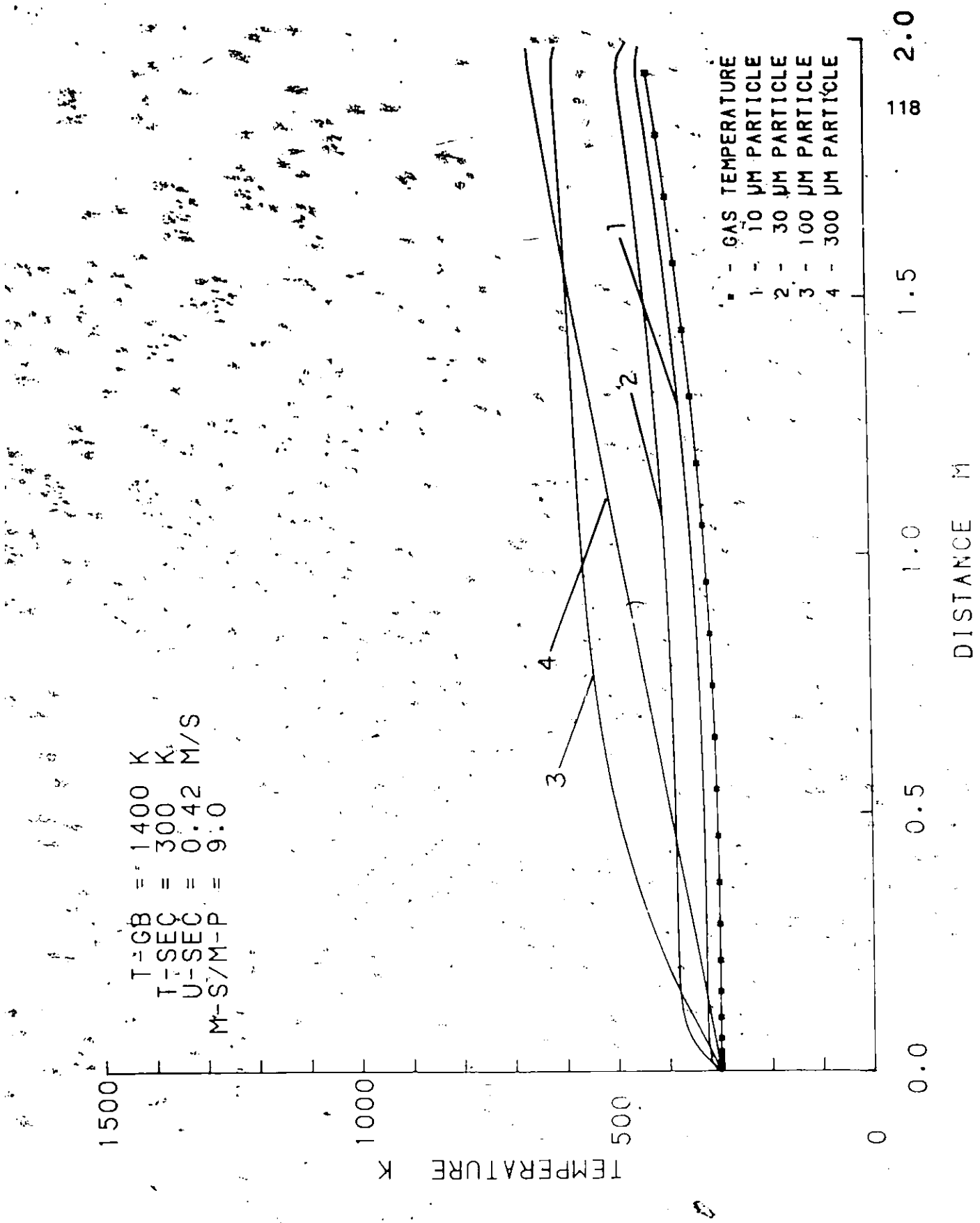

Figure 59: Particle Heating - Tgb=1400 K; Tinsec=300 K, M-S/M-P=9.0

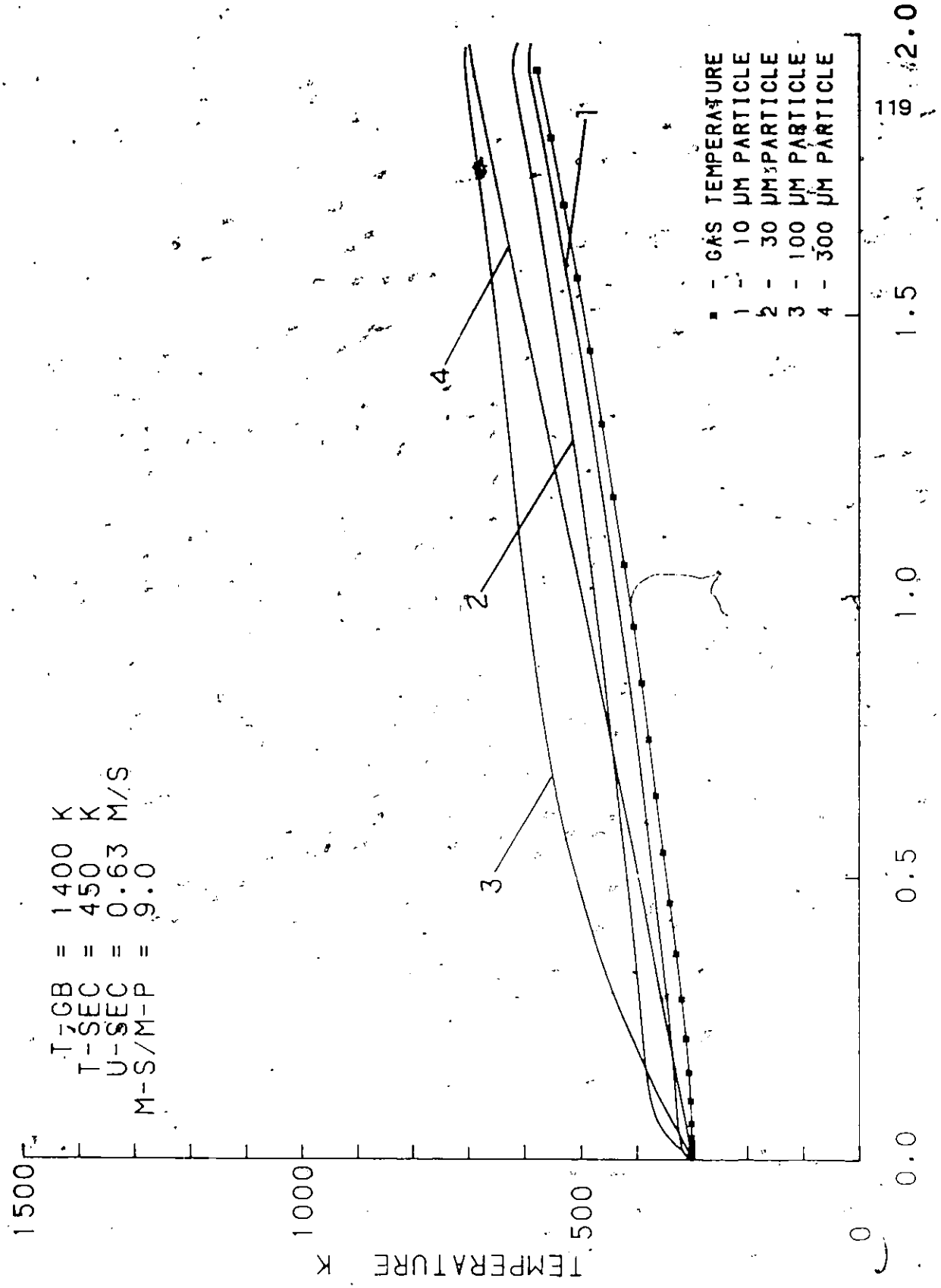

Figure 60: Particle Heating - Tgb=1400 K, Tinsec=450 K, M-S/M-P=9.0

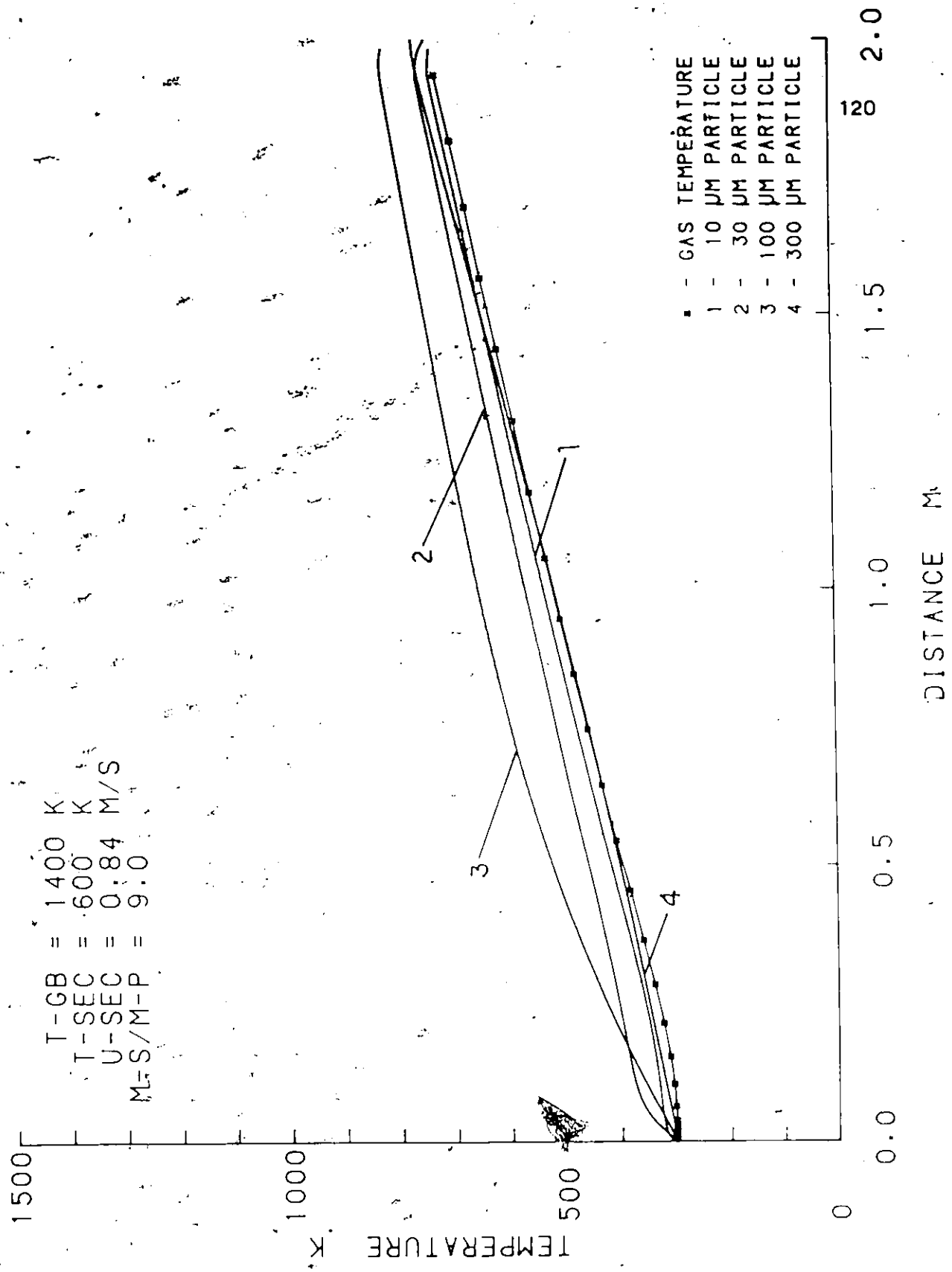

Figure 61: Particle Heating – Tgb=1400 K, Tinsec=600 K, M-S/M-P=9.0

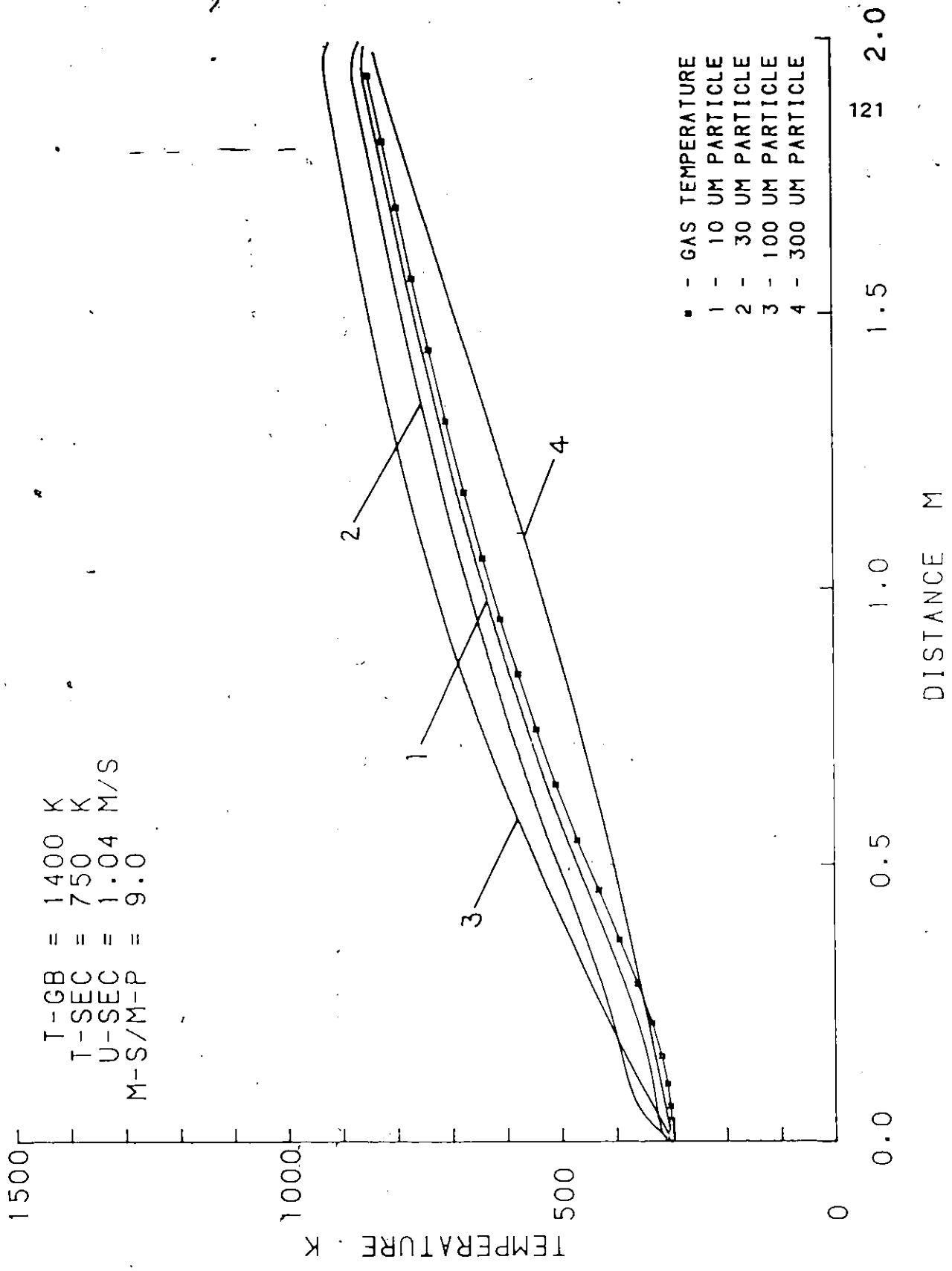

Figure 62: Particle Heating – Tgb=1400 K, Tinsec=750 K, M-S/M-P=9.0

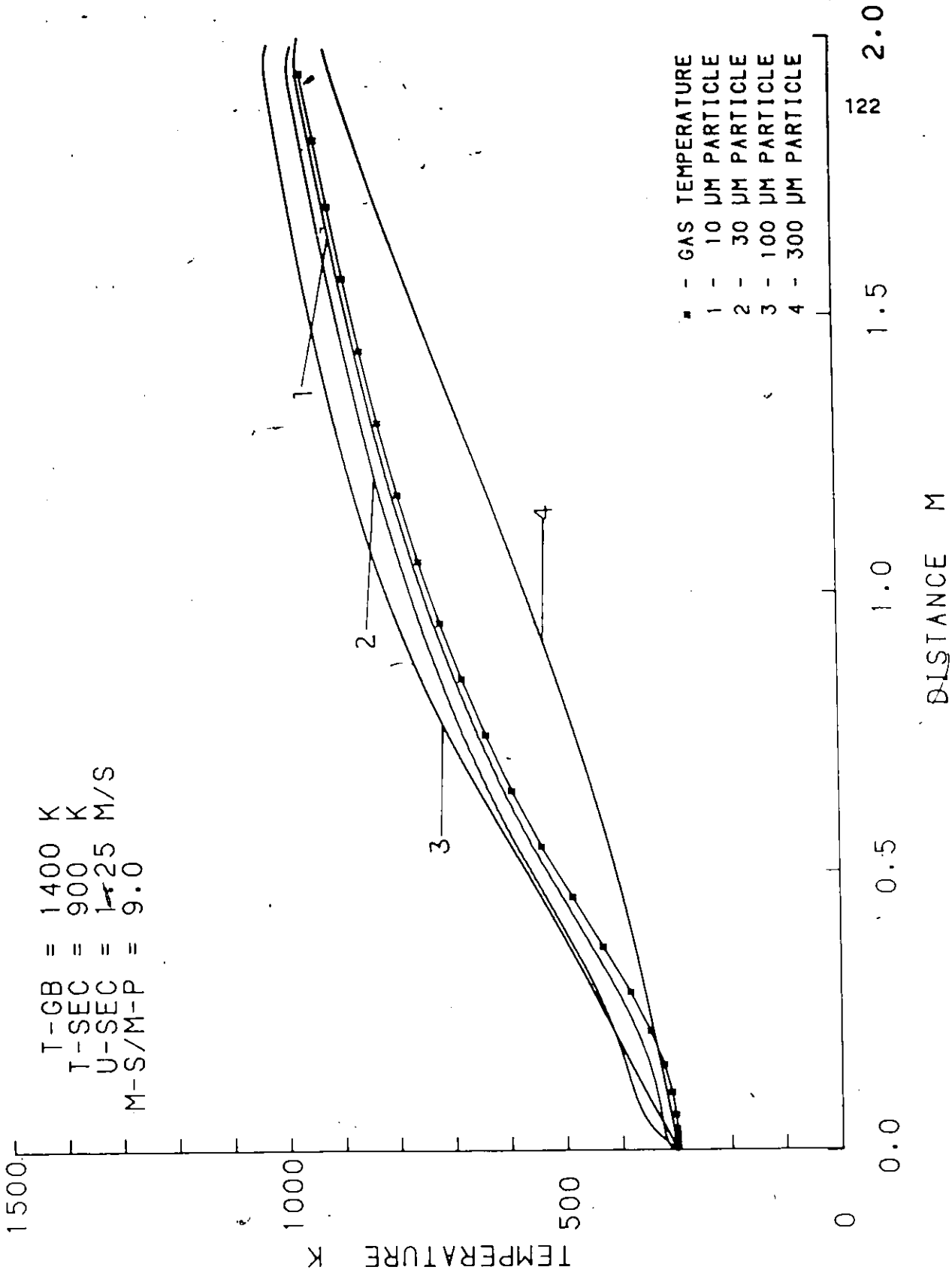

Figure 63: Particle Heating - Tgb=1400 K, Tinsec=900 K, M-S/M-P=9.0

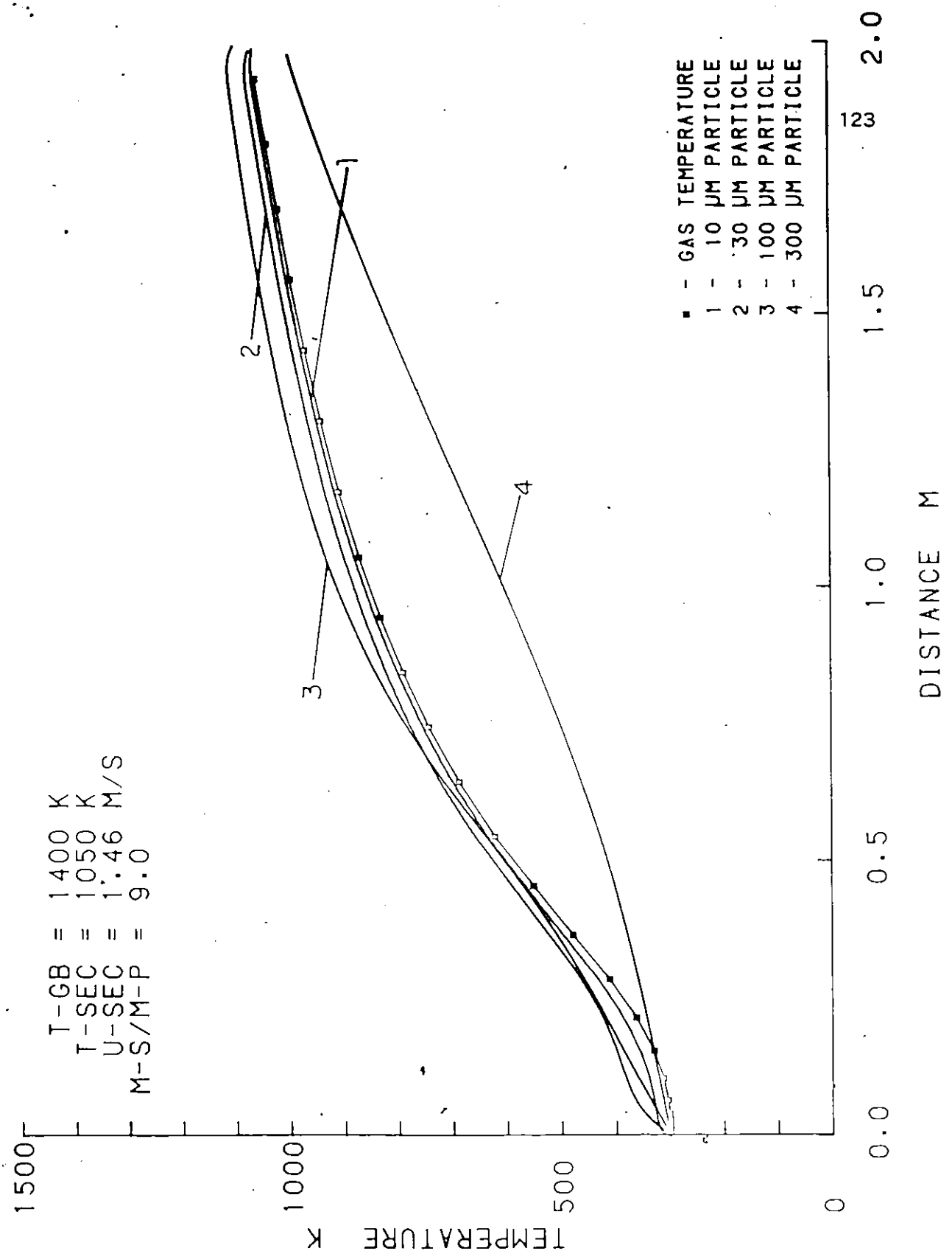

Figure 64: Particle Heating – Tgb=1400 K, Tinsec=1050 K, M-S/M-P=9.0

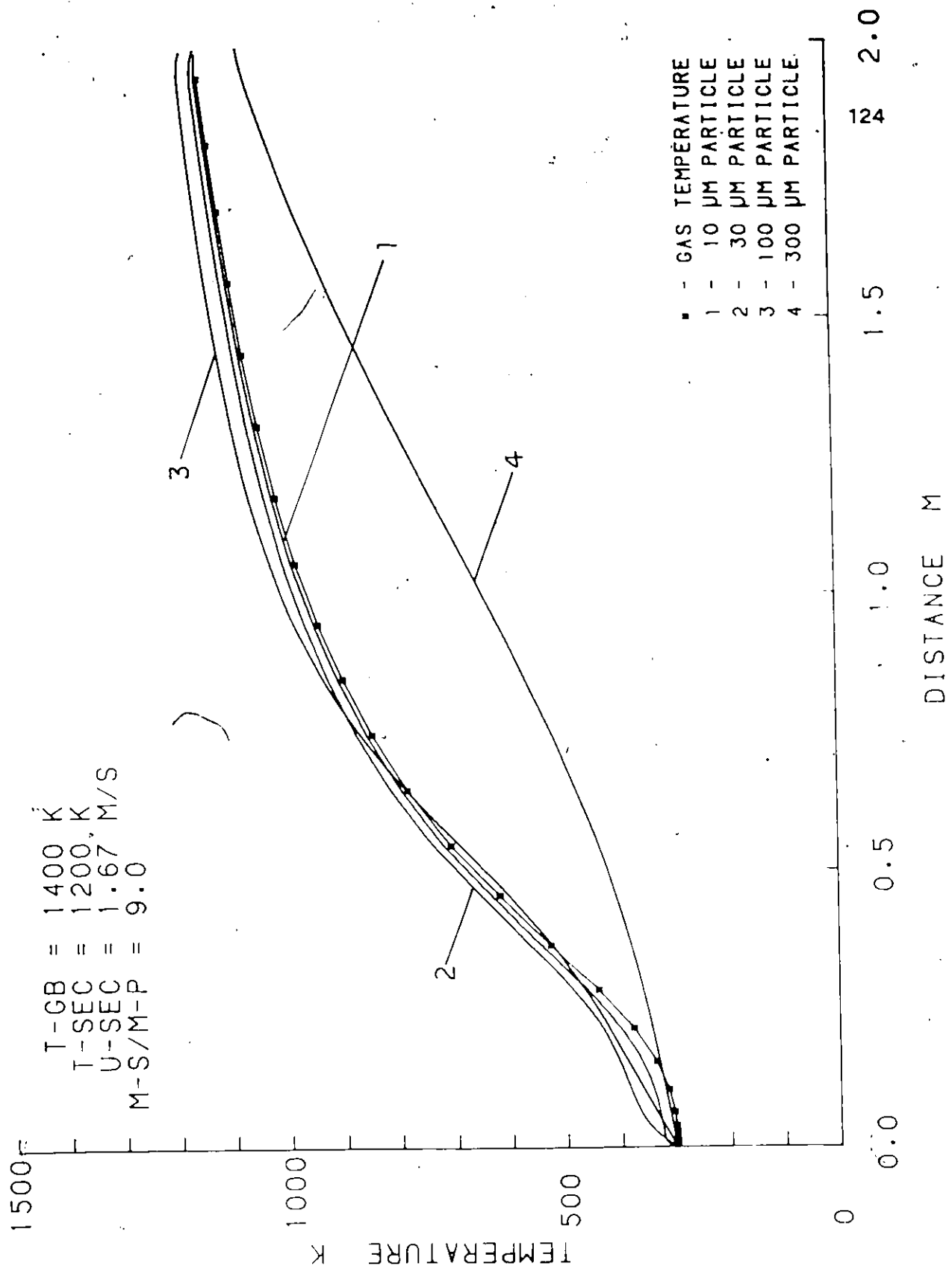

Figure 65: Particle Heating – Tgb=1400 K, Tinsec=1200 K, M-S/M-P=9.0

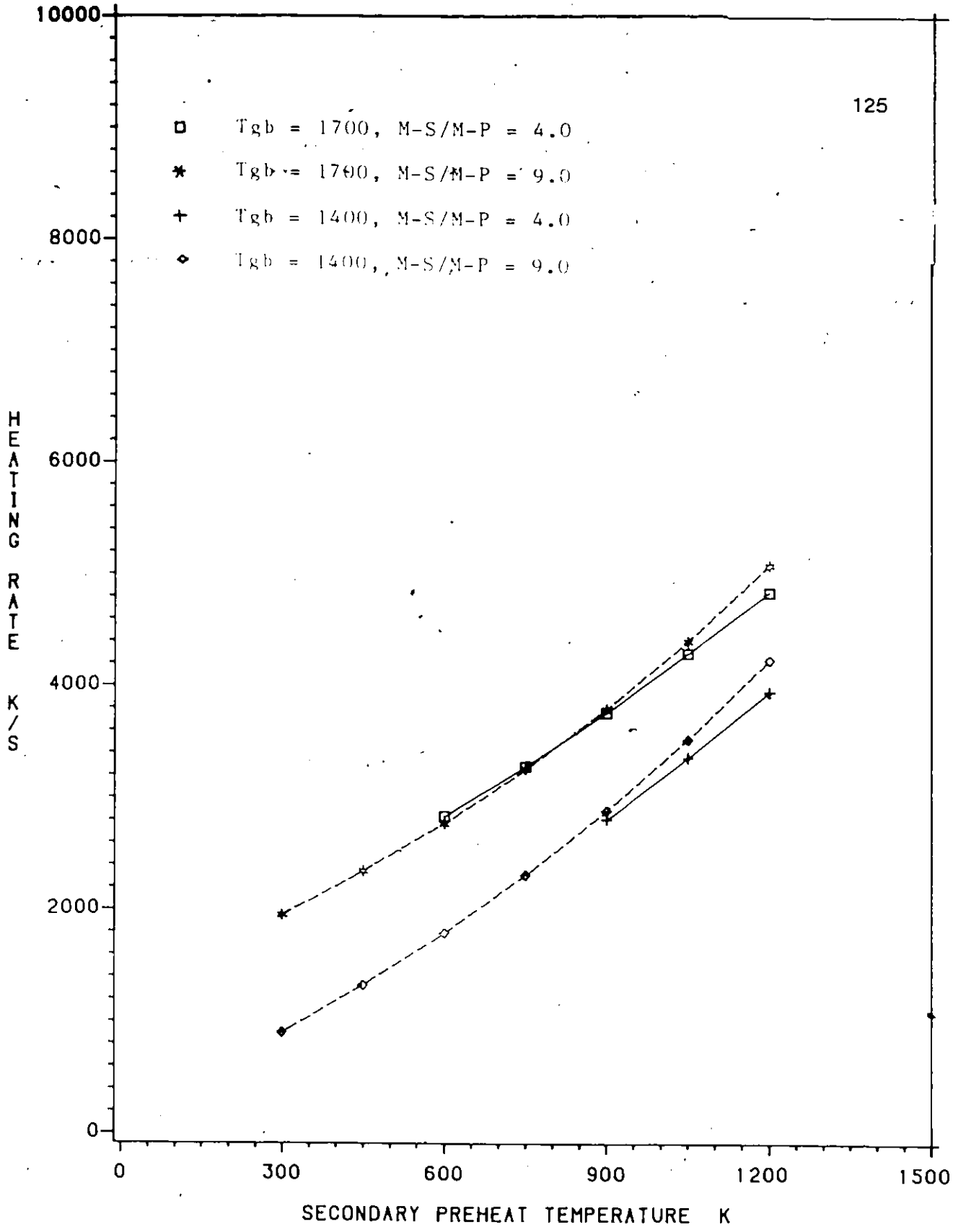

Figure 66: Rate of Temperature Rise for 10 μm Particle

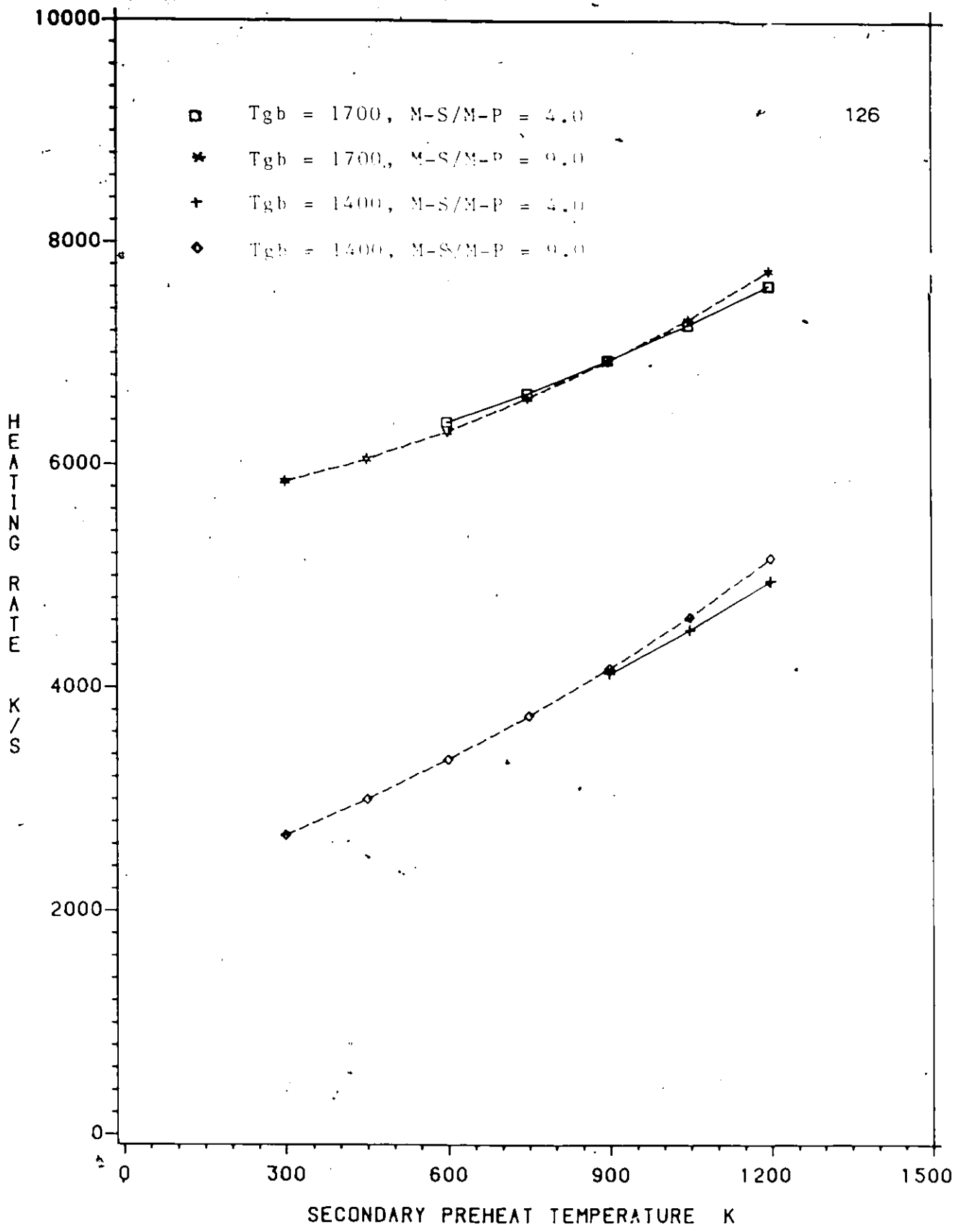

Figure 67: Rate of Temperature Rise for 30 μm Particle

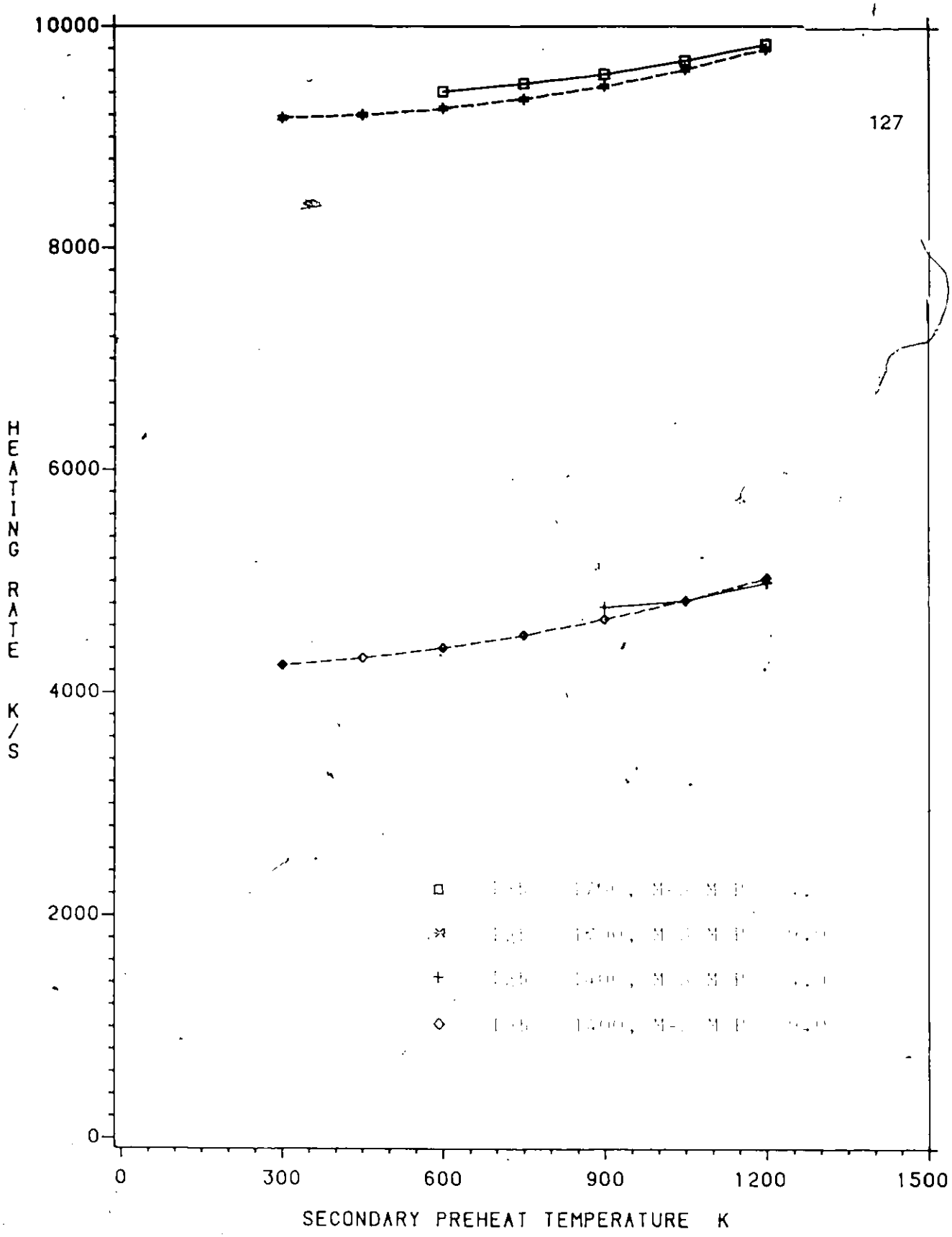

Figure 68: Rate of Temperature Rise for 100 μm Particle

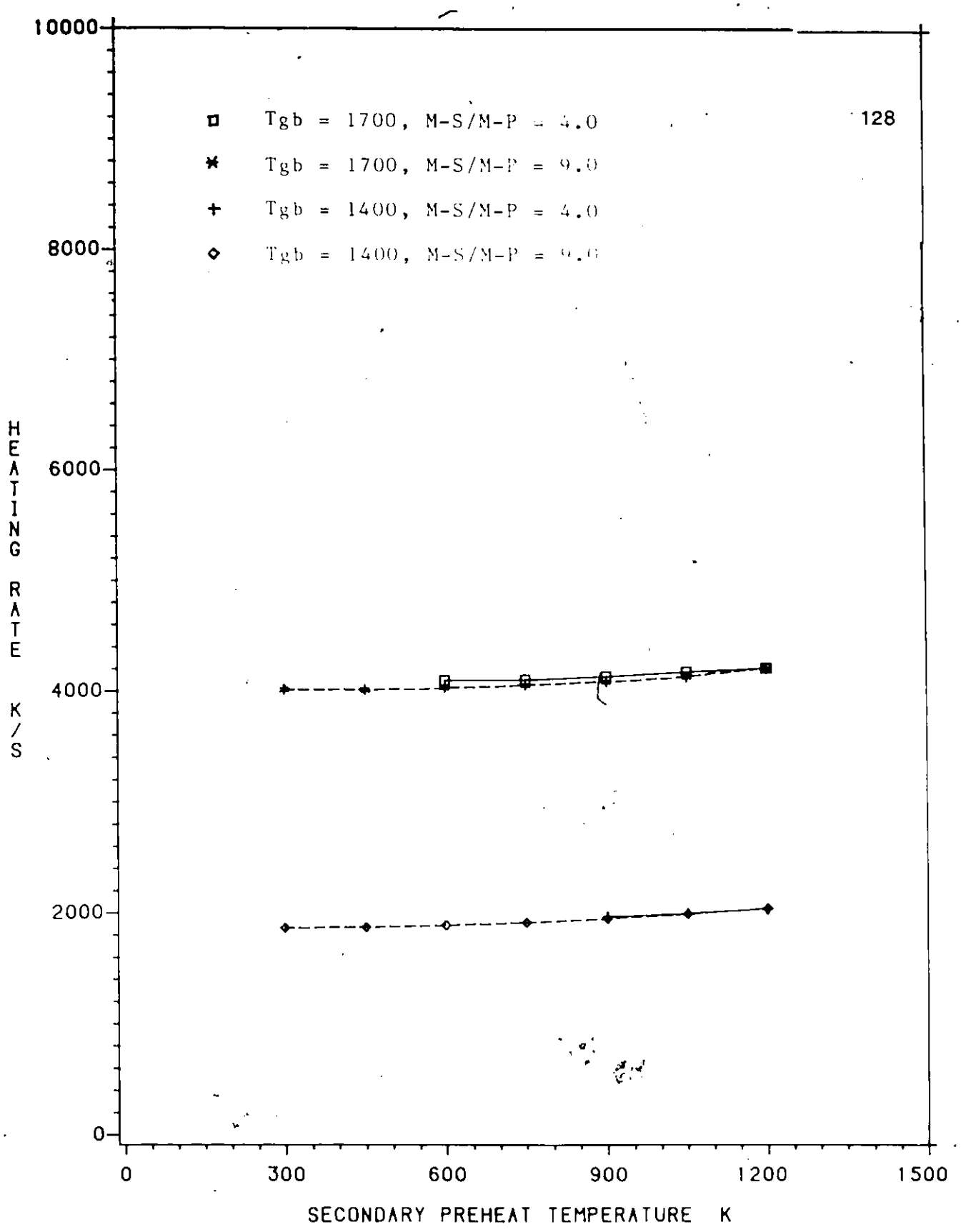

Figure 69: Rate of Temperature Rise for 300 μm Particle

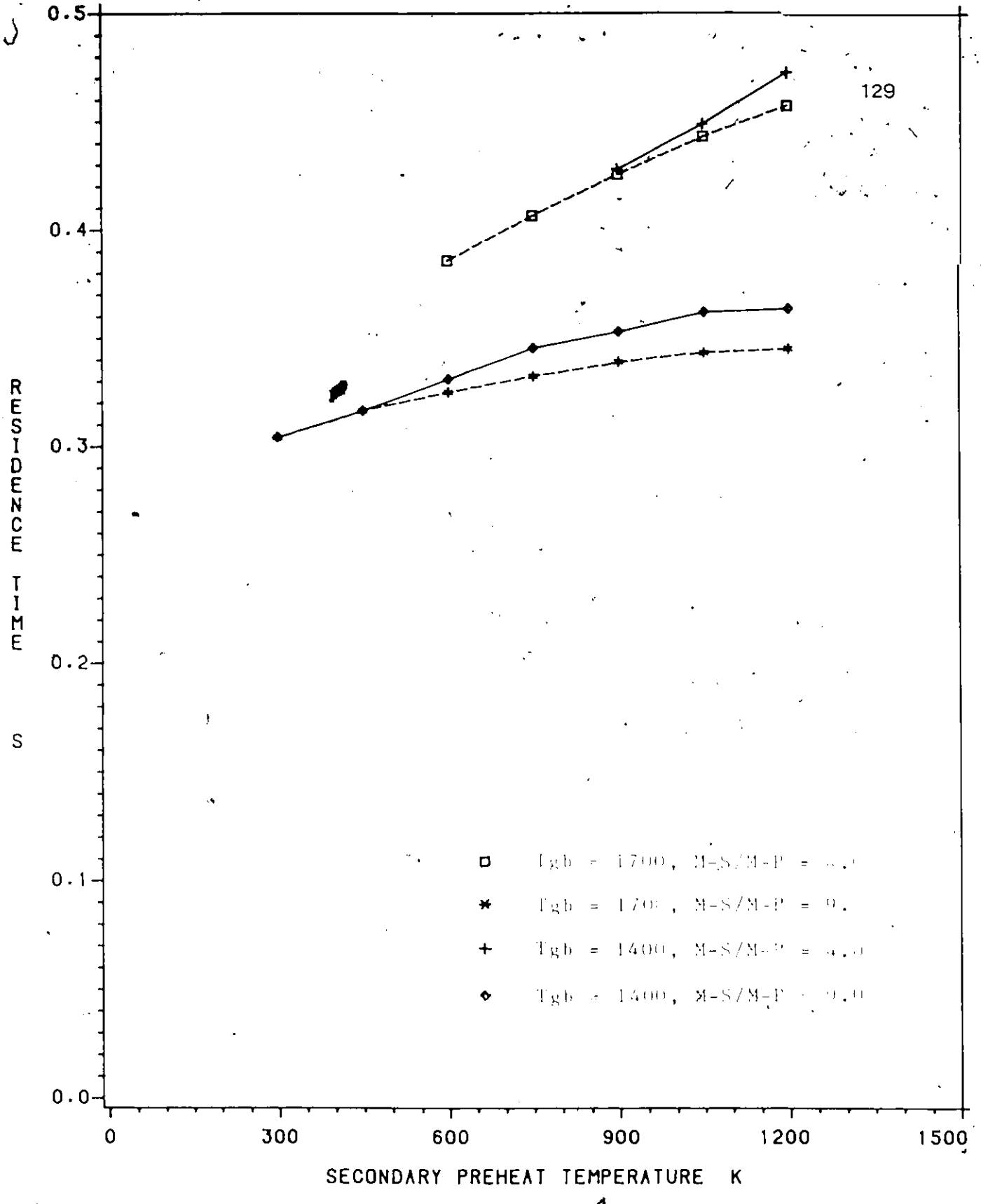

Figure 70: Residence Time for a 100 μm Particle

Appendix A

PARTICLE DENSITY

One of the assumptions made in developing the particle heating model was that the concentration of particles was small and that the effect of the particles on each other could be neglected. The furnace is a long narrow 2m long, 0.064m I.D. cylinder through which coal and air are passed. The air flow rates were based on a specified flow rate of coal. The total volume of coal and the number of size graded coal particles at any time can be calculated as follows:

Desired mass flow rate of coal:

1 g/min = 0.01667 g/s

Average velocity of coal through furnace:

4.4 m/s

Average residence time of coal in furnace:

(2m)/(4.4 m/s) = 0.4545 s

Total mass of coal in furnace at any time:

(0.01667 g/s)(0.4545 s)

= 7.576 *10**-3 g

Total volume of coal in furnace at any time:

(mass of coal)/(density of coal)

density of coal = 1300 kg/m**3

total volume = 5.828 *10**-9 m**3

Volume of each of the different sized spherical particles:

10 μm = 5.236 *10**-16 m**3

30 μm = 1.414 *10**-14 m**3

100 μm = 5.236 *10**-13 m**3

300 μm = 1.414 *10**-11 m**3

Number of particles of each diameter in furnace at any time:

(desired volume of coal)/(volume of particle)

-for a 100 μm particle

(5.828 *10**-9)/(5.236 *10**-13)

= 1.113 *10**4 particles

Similarly, number of particles in furnace at any time:

10 μm particle = 1.113 *10**7 particles

30 μm particle = 4.122 *10**5 particles

300 μm particle = 4.12 *10**2 particles

The furnace consists of a 2m long cylinder. If the furnace is sliced into a series of disks, then a certain number of particles can be said to occupy each disk. If the thickness of a slice is large compared to the diameter of the particle, then the concentration of the particles is small and cloud effects can be neglected.

For a 100 μm particle:

Thickness of slice = (furnace length)/(number of particles)

=(2m)/(1.113 *10**4 particles)

=0.000180 m

Number of particle diameters/slice

$$= (0.000180)/(0.000100)$$

$$= 1.8$$

Thickness of slice is 1.8 particle diameters and one 100 μm particle occupies each slice. The assumption that the particles are spaced sufficiently apart with low particle concentration can be said to be valid.

Similarly,

10 μm particle = 0.018 particle diameters/slice thickness

30 μm particle = 0.16 particle diameters/slice thickness

300 μm particle = 16 particle diameters/slice thickness

For the 10 and 30 μm particle sizes, the slice thickness is smaller than the particle diameter; therefore, more than one particle will have to occupy each slice.

10 μm = 56 particles/slice thickness

30 μm = 6.3 particles/slice thickness

The concentration of the 10 and 30 μm particle is still relatively small when spread out over the cross-sectional area of the slice (slice diameter based on diameter of primary inlet = 6400 μm).

Appendix B

VIEW FACTORS

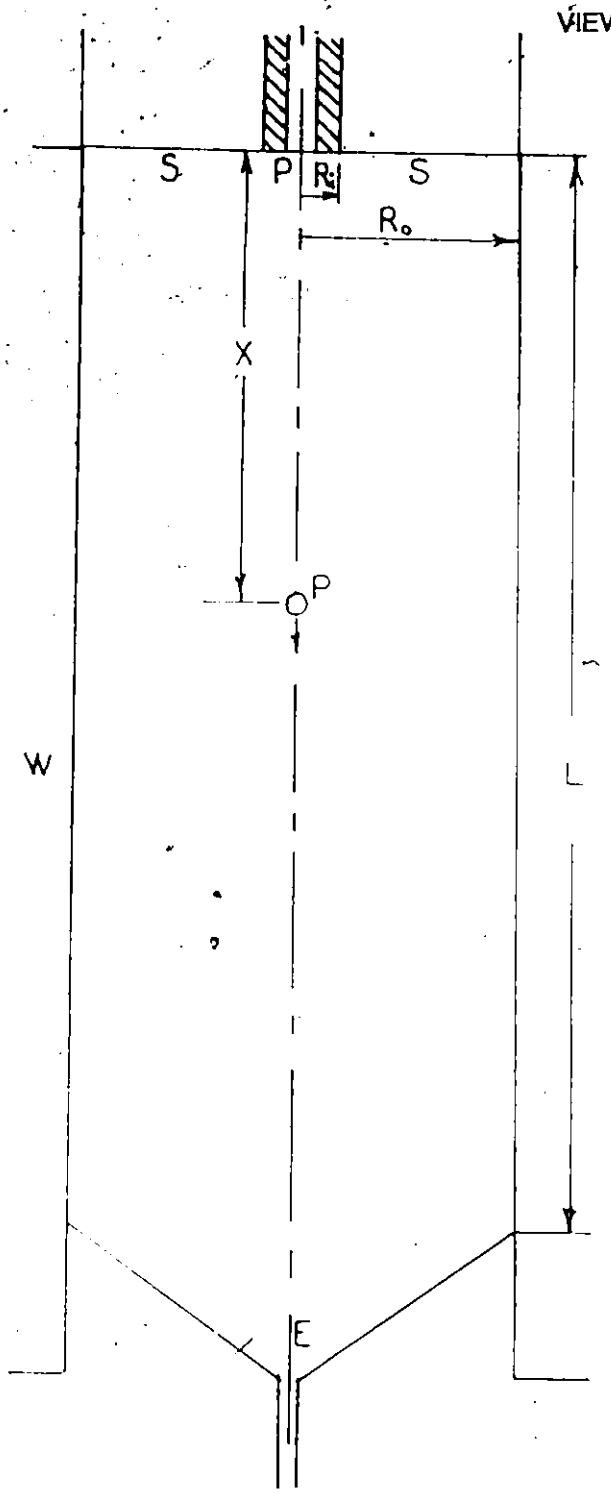

$$F_{PP} \quad \frac{1}{2}\left[1 - \frac{1}{\sqrt{1 + \frac{R_0^2}{x^2}}}\right]$$

$$F_{PE} \quad \frac{1}{2}\left[1 - \frac{1}{\sqrt{1 + \frac{R_0^2}{(L-x)^2}}}\right]$$

$$F_{PS} \quad \frac{1}{2}\left[1 - \frac{1}{\sqrt{1 + \frac{R_0^2}{x^2}}}\right] \quad F_{PP}$$

$$F_{PW} = 1 - F_{PP} - F_{PS} \quad F_{PE}$$

REFERENCES

1. Abarbanel, S., Bennett, S., Brandt, A., Gillis, J., Velocity Profiles of Flow at Low Reynolds Numbers. Journal of Applied Mathematics, Trans. of the ASME, March 1970, pp. 2–4

2. Abdelrehim, Z.E., Heat Transfer in Turbulent Recirculatory Flows Affected by Buoyancy Forces in Rectangular Cavities. University of Ottawa, MASc thesis, 1979, 107pp.

3. Badzioch, S., Hawksley, G.W., Kinetics of Thermal Decomposition of Pulverized Coal Particles. Ind. Eng. Chem. Process Des. Develop., Vol. 9, No. 4, 1970, pp. 521–530

4. Baum, M.M., Street, P.J., Predicting the Combustion Behaviour of Coal Particles. Combustion Science and Technology, Vol. 3, 1971, pp. 231–243

5. Bergman, P.D., Koppel, L.B., Uniform Flux Heat Transfer to a Gas in Laminar Forced Convection in a Circular Tube. A.I.Ch.E. Journal, Vol. 12, No. 4, July 1966, pp. 648–655

6. Biggs, R.C., Stachiewicz, J.W., Combined Free and Forced Convection Heat Transfer of Gases 4th Inter. Ht. Tr. Conf., Paris, Heat Transfer, Vol. 4, 1970, N.C. 3.1

7. Bird, R.B., Stewart, W.E., Lightfoot, E.N., Transport Phenomena., John Wiley and Sons, Inc., 1960, 780 pp.

8. Bolz, R.E., Tuve, G.L., Handbook of Tables for Applied Engineering Science CRC Press, Inc., 1983, 2nd ed., 1166 pp.

9. Brown, C.K., Gauvin, H., Combined Free and Forced Convection I. Heat Transfer in Aiding Flow
   II. Heat Transfer in Oppposing Flow. Can. J. Chem. Eng., Dec. 1965, pp. 306–318

10. Collins, M.W., Combined Convection in Vertical Tubes Heat and Mass Transfer by Combined Forced and Natural Convection, Institute of Mechanical Engineers, Westminster, London, 1971, pp 17–25

11. Eddinger, R.T., Friedman, L.D., Rau, E., Devolatilization of Coal in a Transport Reactor. Fuel, No. 45, 1966, pp. 245–252

12. Eckert, E.R.G., Drake, R.M., Analysis of Heat and Mass Transfer., McGraw-Hill Book Co., Inc., 1972, 806 pp.

13. Fargie,D., Martin, B.W. Developing Laminar Flow in a Pipe of Circular Cross-Section. Proc. Eng. Soc. Lond., A. 321, 1971, pp. 461-476

14. Field, M.A., Rate of Combustion of Size-Graded Fractions of Char from a Low-Rank Coal between 1200 K and 2000 K. Combustion and Flame, Vol. 13, June 1969, pp. 237-252

15. Friedman, M., Gillis, J., Liron, N., Laminar Flow in a Pipe at Low and Moderate Reynolds Numbers Appl. Sci. Res., Vol. 19, Nov. 1968, pp. 426-438

16. Grigull, U., Tratz, H., Thermischer Einlauf in Ausgebildeter Laminarer Rohrstromung Int J. Heat Mass Transfer, Vol. 8, 1965, pp. 669-678

17. Hanratty, T.J., Rosen, E.M., Kabel, R.L., Effect of Heat Transfer on Flow Field at Low Reynolds Numbers in Vertical Tubes Ind. Eng. Chem., Vol. 50, No. 5, May 1958, pp. 815-820

18. Hasan, Q., Natarajan, R., Seshadri, V., Finite Element Analysis of Flow Development in the Entrance Region of a Tube at Moderate Reynolds Numbers with Different Inlet Velocity Profiles. Finite Element Flow Analysis, Proc. 4th Int. Symp. Finite Element Methods in Flow Problems, Tokyo, editor T. Kawai, Univ. Tokyo Press, North-Holland Pub. Co., 1982, pp.145-152

19. Hebert, L.S., Sterns, U.J., Heat Transfer in Vertical Tubes - Interaction of Forced and Free Convection. Chem. Eng. J., No. 4, 1972, pp. 46-52

20. Holman, J.P., Heat Transfer McGraw-Hill Book Co., Inc., 1981, 5th ed., 570 pp.

21. Hottel, H.C., Sarofim, A.F., Radiative Transfer., McGraw-Hill Book Co., 1967, 520 pp.

22. Howard, J.B., Essenhigh, R.H., Pyrolysis of Coal Particles in Pulverized Fuel Flames. Ind. Eng. Chem. Proc. Des. Devel., Vol. 6, No.1, Jan. 1967, pp.74-84

23. Jorgensen, F.R.A., Zuiderwyk, M., Two - Colour Pyrometer Measurement of the Temperature of Individual Combusting Particles. J. Phys. E. Sci. Instrum., Vol. 18, 1985, pp. 486-491

24. Kays, W.M., Numerical Solutions for Laminar Flow Heat Transfer in Circular Tubes. Trans. ASME, Vol. 77, Nov. 1955, pp. 1265-1274

25. Kobayashi, H., Howard, J.B., Sarofim, F., Coal Devolatilization at High Temperatures. 16th Symp. (Int.) Comb., The Combustion Institute, Pittsburgh, PA., 1977, pp. 411-425

26. Lilley, D.G., Rhode, D.L., A Computer Code for Swirling Turbulent Axisymmetric Recirculating Flows in Practical Isothermal Combustor Geometries. NASA Contractor Report 3442, Prepared for Lewis Research Center, 1982, 130 pp.

27. McDonald, J.W., Denny, V.E., Mills, A.F., Numerical Solutions of the Navier-Stokes Equations in Inlet Regions. Journal of Applied Mathematics, Trans. ASME, Dec 1972, pp. 873-878

28. Mitchell, R.E., McLean, W.J., On the Temperature and Reaction Rate of Burning Pulverized Fuels. 19th Symp. (Int.) Comb., The Combustion Institute, 1982, pp. 1113-1122

29. Patankar, S.V., Numerical Heat Transfer and Fluid Flow., Hemisphere Publishing Co., 1980, 197 pp.

30. Scheele, G.F., Hanratty, T.J., Effect of Natural Convection on Stability of Flow in a Vertical Pipe. J. Fluid Mech., Vol. 14, 1962, pp. 244-256

31. Scheele, G.F., Hanratty, T.J., Effect of Natural Convection Instabilities on Rates of Heat Transfer at Low Reynolds Numbers. A.I.Ch.J., Vol. 9, No. 2, Mar. 1963, pp. 183-185

32. Scaroni, A.W., Walker (Jr.), P.L., Essenhigh, R.H., Kinetics of Lignite Pyrolysis in an Entrained-Flow, Isothermal Furnace Fuel, Vol. 60, Jan. 1981, pp. 71-76

33. Schmidt, F.W., Zelder, B., Laminar Flows in Inlet Sections of Tubes and Ducts. A.I.Ch.E. Journal, Vol. 15, No. 4, July 1964, pp. 612-614

34. Siegel, R., Howell, J.R., Thermal Radiation Heat Transfer., Hemisphere Publishing Co., 1981, 2nd ed., 862 pp.

35. Smoot, L.D., Pratt, D.T., Pulverized Coal Combustion and Gasification., Plenum, New York, 1979

36. Solomon, P.R., Hamblen, D.G., Carengelo, R.M., Krause, J.L., Coal Thermal Decomposition in an Entrained Flow Reactor: Experiments and Theory. 19th Symp. (Int.) Comb., The Combustion Institute, 1982, pp. 1139-1149

37. Spalding, D.B., GENMIX - A General Computer Program for Two-Dimensional Parabolic Phenomena The Science and Applications of Heat and Mass Transfer, Pergamon Press, 1977, 380 pp.

38. Sparrow, E.M., Lin, S.H., Lundgren, T.S. Flow Development in the Hydrodynamic Entrance Region of Tubes and Ducts. Phys. Fluids, Vol. 7, No. 3, Mar. 1964, pp.

39. Streeter, V.L., Wylie, E.B., Fluid Mechanics McGraw-Hill Book Co., Inc., 1979, 7th ed., 562 pp.

40. Timothy, L.D., Sarofim, A.F., Beer, J.M., Characteristics of a Single Particle Coal Combustion. 19th Symp. (Int.) Comb., The Combustion Institute, 1982, pp. 1123-1130

41. Wagner, M.H., Developing Flow in Circular Conduits: Transition from Plug Flow to Tube Flow. J. Fluid Mech., Vol. 72, part 2, 1975, pp. 257-268

```
C-----CCRL COAL DROP FURNACE NUMERICAL MODEL-----EMR CONTRACT
C
C-----WRITTEN BY ROBERT J. FLAXMAN ---- MASC MECH. ENG. THESIS
C
C-----THIS PROGRAM PREDICTS THE VELOCITY AND TEMPERATURE PROFILES INSIDE
C     A LAMINAR COAL DROP FURNACE UNDER SPECIFIED FLOW CONDITIONS.
C     THE PROGRAM USES THESE CALCULATED VALUES TO SOLVE TEMPERATURES
C     AND VELOCITIES OF SIZE GRADED PARTICLES AS THEY TRAVEL THROUGH
C     THE FURNACE.
C
C-------------------------------------------------------------------
C
      DIMENSION HEDU(9),HEDV(9),HEDP(9),HEDT(9),HEDM(9),HEDD(9)
      COMMON
     1/UVEL/RESORU,NSWPU,URFU,DXEPU(32),DXPWU(32),SEWU(32)
     1/VVEL/RESORV,NSWPV,URFV,DYNPV(32),DYPSV(32),SNSV(32)
     1/PCOR/RESORM,NSWPP,URFP,DU(30,30),DV(30,30),IPREF,JPREF
     1/VAR/U(30,30),V(30,30),P(30,30),PP(30,30)
     1/ALL/IT,JT,NI,NJ,NIM1,NJM1,GREAT
      COMMON
     1/GEOM/X(32),Y(32),DXEP(32),DXPW(32),DYNP(32),DYPS(32),
     1       SNS(32),SEW(32),XU(32),YV(32),R(32),RV(32),RCV(32)
     1/FLUPR/VISSEC,DENSEC,PRANDL,DEN(30,30),VIS(30,30),CONST,
     1        VISPRM,DENPRM,SECMAS,PRMMAS,SPRAT
      COMMON
     1/PROB1/UINPRM,UINSEC,GRAVTY,FLOWIN,NITER
     1/COEF/AP(30,30),AN(30,30),AS(30,30),AE(30,30),AW(30,30),SU(30,30),
     1       SP(30,30)
      COMMON
     1/TEMP/T(30,30),GAMH(30,30),RESORT,NSWPT,URFT,
     2      TINPRM,TINSEC,TGB(30),HTFLX(30),HFXOLD(30)
      LOGICAL INCALU,INCALV,INCALP,INPRO,INCALT,INCLUP
      READ(5,010) HEDU,HEDV,HEDP,HEDT,HEDM,HEDD
  010 FORMAT(9A4)
C
C------------------------  CCRL   FORTRAN  ------------------------ C
C
CHAPTER  1  1  1  1  1  PARAMETERS AND CONTROL INDICES  1  1  1  1  1  1
C
C-----GRID
C-----THE GRID CONSISTS OF 28 AXIAL POSITIONS AND 20 RADIAL POSITIONS.
C
      GREAT=1.E30
      NITER=0
      IT=30
      JT=30
      IMON=5
      JMON=5
      JPREF=2
      IPREF=2
      NSWPU=3
      NSWPV=3
      NSWPP=5
      NSWPT=3
```

```
      NI=28
      NJ=20
      NIM1=NI-1
      NJM1=NJ-1
C
C-----THE FOLLOWING ARE THE AXIAL POSITIONS OF THE GRID IN METERS.
C
      X(1)=-0.002
      X(2)=0.002
      X(3)=0.007
      X(4)=0.013
      X(5)=0.020
      X(6)=0.028
      X(7)=0.040
      X(8)=0.065
      X(9)=0.105
      X(10)=0.155
      X(11)=0.215
      X(12)=0.285
      X(13)=0.365
      X(14)=0.455
      X(15)=0.545
      X(16)=0.645
      X(17)=0.745
      X(18)=0.845
      X(19)=0.945
      X(20)=1.055
      X(21)=1.175
      X(22)=1.305
      X(23)=1.435
      X(24)=1.565
      X(25)=1.695
      X(26)=1.815
      X(27)=1.935
      X(28)=2.065
C
C-----THE FOLLOWING ARE THE RADIAL POSITIONS OF THE GRID IN METRES
C
      Y(1)=-0.0004
      Y(2)=0.0004
      Y(3)=0.0012
      Y(4)=0.0020
      Y(5)=0.0028
      Y(6)=0.0036
      Y(7)=0.0044
      Y(8)=0.0052
      Y(9)=0.0060
      Y(10)=0.0068
      Y(11)=0.0080
      Y(12)=0.0100
      Y(13)=0.0140
      Y(14)=0.0180
      Y(15)=0.0220
      Y(16)=0.0260
```

```
      Y(17)=0.0278
      Y(18)=0.0294
      Y(19)=0.0310
      Y(20)=0.0326
C
C-----DEPENDENT VARIABLE SELECTION
C-----THIS DETERMINES WHICH SUBROUTINES ARE TO BE USED
C
      INCALU=.TRUE.
      INCALV=.TRUE.
      INCALP=.TRUE.
      INCALT=.TRUE.
      INCLUP=.TRUE.
      INPRO=.TRUE.
C
CC----INITIALIZE GLOW BAR (HEATING ELEMENT) TEMPERATURE
C
      TMPGLB=1400.0
      DO 211 I=2,NIM1
  211 TGB(I)=TMPGLB
C
CC----INLET FLUID PROPERTIES
C
C-----AIR MASS FLOWS IN KG/SEC (1.0 G/MIN COAL FEED RATE)
      PRMMAS=(0.01/60.0)
      SECMAS=9.0*PRMMAS
      SPRAT=SECMAS/PRMMAS
      RATIO=1.0+SPRAT
C
C-----TEMPERATURES IN K
      TINPRM=300.0
      TINSEC=300.0
C
C-----DENSITY IN KG/M**3 AND VISCOSITY IN KG/M*S (DYNAMIC)
      DENSEC=101325.0/(287.0*TINSEC)
      VISSEC=1.5E-6*TINSEC**1.5/(TINSEC+130.0)
      DENPRM=101325.0/(287.0*TINPRM)
      VISPRM=1.5E-6*TINPRM**1.5/(TINPRM+130.0)
C
C-----AVERAGE PRANDTL NUMBER FROM 800-1200 K
      PRANDL=0.700
      PATM=101325.0
      RR=287.0
      CONST=RR/PATM
C
C-----PROGRAM CONTROL AND MONITOR
      MAXIT=300
      URFU=0.5
      URFV=0.5
      URFP=0.2
      URFT=1.0
      SORMAX=0.010
      GRAVTY=9.806
C
```

```
CHAPTER  2  2  2  2  2  2  INITIAL OPERATIONS  2  2  2  2  2  2  2  2  2
C
C-----CALCULATE GEOMETRICAL QUANTITIES AND SET VARIABLES TO ZERO
      CALL INIT
C
C-----CALCULATE AREAS
C-----AREA OF PRIMARY BURNER INLET
      C=1.0
      PI=4.0*ATAN(C)
      APRM=(RV(6)**2)*PI
C-----AREA OF SECONDARY FLOW
      ASEC=(RV(NJ)**2-RV(10)**2)*PI
C
C-----SPECIFY INLET CONDITIONS
      UINPRM=PRMMAS/(APRM*DENPRM)
      UINSEC=SECMAS/(ASEC*DENSEC)
      DO 203 I=1,NI
      DO 200 J=10,NJM1
  200 U(I,J)=UINSEC
      DO 202 J=2,9
      IF(J.LE.5) U(I,J)=2.0*UINPRM*(1.0-(R(J)/RV(6))**2)
      IF(J.GT.5) U(I,J)=0.0
  202 CONTINUE
  203 CONTINUE
C
C-----THIS CALCULATES THE MASS FLOW ENTERING THE FURNACE
      FLOWIN=0.0
      XMONIN=0.0
      DO 111 J=2,NJM1
      ARDEN=DEN(1,J)*RCV(J)*SNS(J)
      XMONIN=XMONIN+ARDEN*U(1,J)*U(1,J)
      FLOWIN=FLOWIN+ARDEN*U(1,J)
  111 CONTINUE
C
C-----INITIAL OUTPUT
      WRITE(6,313) TMPGLB
      WRITE(6,213) RATIO
      WRITE(6,219) UINPRM
      WRITE(6,220) UINSEC
      WRITE(6,221) TINPRM
      WRITE(6,217) TINSEC
C
      REPRM=UINPRM*0.0032*2*DENPRM/VISPRM
C-----HYDRAULIC DIAMETER IS USED BELOW IE HYD DIA = 4*XS-AREA/WET PERMTR
      RESEC=UINSEC*(4.0*ASEC/0.24)*DENSEC/VISSEC
      WRITE(6,223) PRANDL
      WRITE(6,229) REPRM
      WRITE(6,230) RESEC
      WRITE(6,250) VISSEC
      WRITE(6,260) DENSEC
C
      IF(INCALU) CALL PRINT(2,2,NI,NJ,IT,JT,XU,Y,U,HEDU)
C     IF(INCALV) CALL PRINT(2,2,NI,NJ,IT,JT,X,YV,V,HEDV)
C     IF(INCALP) CALL PRINT(2,2,NI,NJ,IT,JT,X,Y,P,HEDP)
```

```
C     IF(INCALT) CALL PRINT(2,2,NI,NJ,IT,JT,X,Y,T,HEDT)
C     IF(INPRO ) CALL PRINT(1,1,NI,NJ,IT,JT,X,Y,VIS,HEDM)
C     IF(INPRO ) CALL PRINT(1,1,NI,NJ,IT,JT,X,Y,DEN,HEDD)
C
C-----------CALCULATE RESIDUAL SOURCE-NORMALIZATION FACTORS----------
C
CHAPTER 3 3 3 3 3 3 3 ITERATION LOOP 3 3 3 3 3 3 3 3 3
C
  300 NITER=NITER+1
C-----UPDATE MAIN DEPENDENT VARIABLES
      IF(INCALU) CALL CALCU
      IF(INCALV) CALL CALCV
      IF(INCALP) CALL CALCP
      IF(INCALT) CALL CALCT
C
C-----THIS CALCULATES THE MASS FLOW LEAVING THE FURNACE
C
      ARDENT=0.0
      FLOW=0.0
      DO 196 J=2,NJM1
      ARDEN=0.5*(DEN(NIM1,J)+DEN(NIM1-1,J))*RCV(J)*SNS(J)
      ARDENT=ARDENT+ARDEN
  196 FLOW=FLOW+ARDEN*U(NIM1,J)
C
C-----THIS ADJUSTS THE FINAL VELOCITY IN ORDER TO CONSERVE MASS
      UINC=(FLOWIN-FLOW)/ARDENT
      DO 197 J=2,NJM1
      U(2,J)=U(1,J)*(T(2,J)+T(1,J))/(2.0*T(1,J))
  197 U(NI,J)=U(NIM1,J)+UINC
C
C-----UPDATE FLUID PROPERITIES
      IF(INPRO) CALL PROPS
C
C-----INTERMEDIATE OUTPUT
C-----THE VALUES ARE NORMALIZED WITH THE INLET CONDITIONS
      RESORM=RESORM/FLOWIN
      RESORU=RESORU/XMONIN
      RESORV=RESORV/XMONIN
      RESORT=RESORT/(FLOWIN*TINPRM)
C
C-----AFTER EACH ITERATION, THE RESIDUAL SOURCE TERMS, A MONITORED
C     GRID POINT (5,5) AND THE HEAT FLUX IS PRINTED
C
      WRITE(6,199)NITER,RESORU,RESORV,RESORM,RESORT,U(5,5),V(5,5),P(5,5)
     *           ,HTFLX(2),HTFLX(NIM1)
  199 FORMAT(I5,7F11.5,2F14.5)
C-----INTERMEDIATE OUTPUT AFTER 40 ITERATIONS
      IF(MOD(NITER,40).NE.0) GO TO 301
C     IF(INCALU) CALL PRINT(2,1,NI,NJ,IT,JT,XU,Y,U,HEDU)
C     IF(INCALV) CALL PRINT(1,2,NI,NJ,IT,JT,X,YV,V,HEDV)
C     IF(INCALP) CALL PRINT(2,2,NI,NJ,IT,JT,X,Y,P,HEDP)
C     IF(INCALT) CALL PRINT(2,2,NI,NJ,IT,JT,X,Y,T,HEDT)
C     IF(INPRO ) CALL PRINT(1,1,NI,NJ,IT,JT,X,Y,VIS,HEDM)
C     IF(INPRO ) CALL PRINT(1,1,NI,NJ,IT,JT,X,Y,DEN,HEDD)
```

```
 301  CONTINUE
C
C-----TERMINATION TEST-----------------------------------------------
      SORCE=AMAX1(RESORM,RESORU,RESORV,RESORT)
      IF(SORCE.LT.SORMAX) GO TO 302
      IF(NITER.EQ.25.AND.SORCE.GT.1.0E4*SORMAX) GO TO 302
      IF(NITER.EQ.MAXIT) GO TO 302
C
      GO TO 300
 302  CONTINUE
C
C-----FINAL OPERATIONS AND OUTPUT
C
      UINC=U(NI,2)-U(NIM1,2)
      WRITE(6,311) NITER,RESORU,RESORV,RESORM,RESORT,UINC
      IF(INCALU) CALL PRINT(2,1,NI,NJ,IT,JT,XU,Y,U,HEDU)
      IF(INCALV) CALL PRINT(1,2,NI,NJ,IT,JT,X,YV,V,HEDV)
C     IF(INCALP) CALL PRINT(2,2,NI,NJ,IT,JT,X,Y,P,HEDP)
      IF(INCALT) CALL PRINT(2,2,NI,NJ,IT,JT,X,Y,T,HEDT)
C     IF(INPRO ) CALL PRINT(1,1,NI,NJ,IT,JT,X,Y,VIS,HEDM)
C     IF(INPRO ) CALL PRINT(1,1,NI,NJ,IT,JT,X,Y,DEN,HEDD)
C
CC----*NOTE - THIS SUBROUTINE IS SPECIFICALLY FOR THE CALCOMP PLOTTER
C
C-----PLOT SUBROUTINE----VELOCITY PROFILES

C
      XAXIS=32.0
      IF(INCLUP) XAXIS=60.0
      CALL PLOTS(XAXIS,27.5)
C
C-----DEVELOPING  VELOCITY PROFILES----RADIAL VS. AXIAL DISTANCE
C
      CALL PLOT(2.0,2.0,-3)
C
C-----THIS DRAWS THE FURNACE WALL
C
      CALL PLOT(22.0,15.95,3)
      CALL PLOT(-1.0,15.95,2)
      DO 166 I=1,46
      TIC=(I-1)*0.5-1.0
      TAC=I*0.5-1.25
      CALL PLOT(TIC,15.95,3)
      CALL PLOT(TAC,16.25,2)
  166 CONTINUE
C     CALL SYMBOL(13.0,16.5,.35,'FURNACE   WALL',0.0,14)
C
C-----THIS DRAWS THE CENTRE LINE
C
      DO 165 I=1,8
      SPC1=3.0*I-4.0
      DASH=SPC1+2.0
      SPC2=DASH+0.45
      DOT=SPC2+0.1
```

```
      CALL PLOT(SPC1,8.0,3)
      CALL PLOT(DASH,8.0,2)
      CALL PLOT(SPC2,8.0,3)
      IF(I.LT.8) CALL PLOT(DOT,8.0,2)
  165 CONTINUE
      DO 177 I=1,3
      PEP=(I-1)*7.5+0.18
      PEP1=(I-1)*1.0
      CALL NUMBER(PEP,7.2,0.35,PEP1,90.0,-1)
  177 CONTINUE
      CALL SYMBOL(2.0,6.2,0.35,'X',90.0,1)
      CALL SYMBOL(7.68,6.2,0.35,'M',90.0,1)
C
C- ---THIS DRAWS THE BURNER MOUTH
C
      CALL PLOT(-1.0,8.80,3)
      CALL PLOT(0.0,8.80,2)
      CALL PLOT(0.0,9.60,2)
      CALL PLOT(-1.0,9.60,2)
C
      DO 701 J=1,3
      TICA=(J*2.5)+8.0
      TICB=TICA-0.25
      RRNUM=J*10.0
      CALL PLOT(0.0,TICA,3)
      CALL PLOT(-0.3,TICA,2)
      CALL NUMBER(-0.4,TICB,0.35,RRNUM,90.0,-1)
  701 CONTINUE
      CALL SYMBOL(-0.4,11.6,0.35,'R',90.0,1)
      CALL SYMBOL(-0.4,14.0,0.35,'MM',90.0,2)
C
      CALL PLOT(0.0,15.95,3)
      CALL PLOT(0.0,7.7,2)
      DO 98 I=4,NI,4
      XX=XU(I)*7.5
      CALL PLOT(XX,15.95,3)
      CALL PLOT(XX,7.7,2)
      NX=XX+0.25
      RR=R(2)*250.0+8.0
      UU=(U(I,2)/UINPRM)*3.75+XX
      CALL PLOT(UU,RR,3)
      DO 99 J=3,NJM1
      RR=R(J)*250.0+8.0
      UU=(U(I,J)/UINPRM)*3.75+XX
      CALL PLOT(UU,RR,2)
   99 CONTINUE
      CALL PLOT(XX,15.95,2)
   98 CONTINUE
      CALL PLOT(6.82,5.0,3)
      CALL PLOT(0.0,5.0,2)
      DO 101 K=1,9
      D=(K-1)*0.8523
      CALL PLOT(D,5.0,3)
      CALL PLOT(D,4.8,2)
```

```
      DD=D+0.18
      DND=(K-1)*1.0
      CALL NUMBER(DD,4.4,0.35,DND,90.0,-1)
  101 CONTINUE
      CALL SYMBOL(2.0,3.35,0.35,'U',90.0,1)
      CALL SYMBOL(4.0,3.0,0.35,'M/S',90.0,3)
      CALL SYMBOL(22.0,9.5,0.35,'M-S/M-P =       ',90.0,16)
      CALL SYMBOL(20.5,9.5,0.35,'   T-GB =      K',90.0,16)
      CALL SYMBOL(21.0,9.5,0.35,'  T-SEC =      K',90.0,16)
      CALL SYMBOL(21.5,9.5,0.35,'  U-SEC =      M/S',90.0,18)
      CALL NUMBER(21.5,13.0,0.35,UINSEC,90.0,2)
      CALL NUMBER(20.5,13.0,0.35,TMPGLB,90.0,-1)
      CALL NUMBER(21.0,13.0,0.35,TINSEC,90.0,-1)
      CALL NUMBER(22.0,13.0,0.35,SPRAT,90.0,1)
      CALL SYMBOL(0.5,23.0,.84,'CCRL FURNACE VELOCITY PROFILES',0.0,30)
      CALL SYMBOL(0.5,21.5,.35,'AVG. PRIMARY INLET VELOCITY       M/S',
     *           ,0.0,37)
      CALL NUMBER(10.3,21.5,.35,UINPRM,0.0,3)
      CALL SYMBOL(0.5,21.0,.35,'AVG. SECONDARY INLET VELOCITY       M/S'
     *           ,0.0,39)
      CALL NUMBER(11.0,21.0,.35,UINSEC,0.0,3)
      CALL SYMBOL(0.5,20.0,.35,'PRIMARY INLET TEMPERATURE      K',.0,32)
      CALL NUMBER(9.9,20.0,.35,TINPRM,0.0,-1)
      CALL SYMBOL(0.5,19.5,.35,'SECONDARY INLET TEMPERATURE      K', .0
     *           ,34)
      CALL NUMBER(10.2,19.5,.35,TINSEC,0.0,-1)
      CALL SYMBOL(0.5,18.5,.35,'PRIMARY INLET REYNOLDS NUMBER',0.0,29)
      CALL NUMBER(11.2,18.5,.35,REPRM,0.0,-1)
      CALL SYMBOL(0.5,18.0,.35,'SECONDARY INLET REYNOLDS NUMBER',0.0,31)
      CALL NUMBER(11.9,18.0,.35,RESEC,0.0,-1)
C
C-----THIS SECTION MUST BE CHANGED MANUALLY FOR CHF OR CWT
C
      CALL SYMBOL(16.5,21.5,.35,'ZONE #1  TEMPERATURE  1400   K',0.0,30)
      CALL SYMBOL(16.5,21.0,.35,'ZONE #2  TEMPERATURE  1400   K',0.0,30)
      CALL SYMBOL(16.5,20.5,.35,'ZONE #3  TEMPERATURE  1400   K',0.0,30)
      CALL SYMBOL(16.5,20.0,.35,'ZONE #4  TEMPERATURE  1400   K',0.0,30)
C
C-----THE FOLLOWING STATEMENT CALLS THE PARTICLE HEATING SUBROUTINE
C
      IF(INCLUP) CALL CALCUP
      CALL PLOT(0.0,0.0,999)
      STOP
C
C-----FORMAT STATEMENTS
  313 FORMAT(1HO,5X,'GLOW BAR TEMPERATURE  ',T50,'=',1PE11.3)
  213 FORMAT(1HO,5X,'LAMBDA                ',T50,'=',1PE11.3)
  221 FORMAT(1H0,5X,'PRM INLET TEMPERATURE ',T50,'=',1PE11.3,2X,'K')
  217 FORMAT(1H0,5X,'SEC INLET TEMPERATURE ',T50,'=',1PE11.3,2X,'K')
  219 FORMAT(1H0,5X,'PRM INLET VELOCITY (PARB)',T50,'=',1PE11.3,2X,
     8      'M/S')
  220 FORMAT(1H0,5X,'SEC INLET VELOCITY (UNFM)',T50,'=',1PE11.3,2X,
     *      'M/S')
  223 FORMAT(1H0,5X,'AVG. PRANDTL NUMBER',T50,'=',1PE11.3)
```

```
  229 FORMAT(1H0,5X,'PRM REYNOLDS NO.',T50,'=',1PE11.3,2X,'(INLET)')
  230 FORMAT(1H0,5X,'SEC REYNOLDS NO.',T50,'=',1PE11.3,2X,'(INLET)')
  250 FORMAT(1H0,5X,'LAMINAR VISCOSITY (VARBL)',T50,'=',1PE11.3,2X,
     •       'KG/M•S (INLET)')
  260 FORMAT(1H0,5X,'FLUID DENSITY (VARBL)',T50,'=',1PE11.3,2X,
     •       'KG/M••3 (INLET)')
  311 FORMAT(//1H0,5X,'NUMBER OF ITERATIONS',T50,'=',I3,/,1H0,5X,
     •       'U VEL RESIDUAL',T50,'=',1PE11.3,/,1H0,5X,'V VEL RESIDUAL',
     •       T50,'=',1PE11.3,/,1H0,5X,'MASS RESIDUAL',T50,'=',1PE11.3,
     •       /,1H0,5X,'TEMP RESIDUAL',T50,'=',1PE11.3,/,1H0,5X,
     •       'FINAL U VELOCITY DIFFERENCE',T50,'=',1PE11.3)
      END
C
C
      SUBROUTINE INIT
C
CHAPTER  0  0  0  0  0  0  0  0  PRELIMINARIES  0  0  0  0  0  0  0  0
C
      COMMON
     1/UVEL/RESORU,NSWPU,URFU,DXEPU(32),DXPWU(32),SEWU(32)
     1/VVEL/RESORV,NSWPV,URFV,DYNPV(32),DYPSV(32),SNSV(32)
     1/PCOR/RESORM,NSWPP,URFP,DU(30,30),DV(30,30),IPREF,JPREF
     1/VAR/U(30,30),V(30,30),P(30,30),PP(30,30)
     1/ALL/IT,JT,NI,NJ,NIM1,NJM1,GREAT
      COMMON
     1/GEOM/X(32),Y(32),DXEP(32),DXPW(32),DYNP(32),DYPS(32),
     1       SNS(32),SEW(32),XU(32),YV(32),R(32),RV(32),RCV(32)
     1/FLUPR/VISSEC,DENSEC,PRANDL,DEN(30,30),VIS(30,30),CONST,
     1       VISPRM,DENPRM,SECMAS,PRMMAS,SPRAT
      COMMON
     1/PROB1/UINPRM,UINSEC,GRAVTY,FLOWIN,NITER
     1/COEF/AP(30,30),AN(30,30),AS(30,30),AE(30,30),AW(30,30),SU(30,30),
     1       SP(30,30)
      COMMON
     1/TEMP/T(30,30),GAMH(30,30),RESORT,NSWPT,URFT,
     2      TINPRM,TINSEC,TGB(30),HTFLX(30),HFXOLD(30)
C
      DO 100 J=1,NJ
  100 R(J)=Y(J)
      DXPW(1)=0.0
      DXEP(NI)=0.0
      DO 101 I=1,NIM1
      DXEP(I)=X(I+1)-X(I)
  101 DXPW(I+1)=DXEP(I)
      DYPS(1)=0.0
      DYNP(NJ)=0.0
      DO 102 J=1,NJM1
      DYNP(J)=Y(J+1)-Y(J)
  102 DYPS(J+1)=DYNP(J)
      SEW(1)=0.0
      SEW(NI)=0.0
      DO 103 I=2,NIM1
  103 SEW(I)=0.5•(DXEP(I)+DXPW(I))
      SNS(1)=0.0
```

```
      SNS(NJ)=0.0
      DO 104 J=2,NJM1
  104 SNS(J)=0.5*(DYNP(J)+DYPS(J))
      XU(1)=0.0
      DO 105 I=2,NI
  105 XU(I)=0.5*(X(I)+X(I-1))
      DXPWU(1)=0.0
      DXPWU(2)=0.0
      DXEPU(1)=0.0
      DXEPU(NI)=0.0
      DO 106 I=2,NIM1
      DXEPU(I)=XU(I+1)-XU(I)
  106 DXPWU(I+1)=DXEPU(I)
      SEWU(1)=0.0
      DO 107 I=2,NI
  107 SEWU(I)=X(I)-X(I-1)
      YV(1)=0.0
      RV(1)=0.0
      DO 108 J=2,NJ
      RV(J)=0.5*(R(J)+R(J-1))
  108 YV(J)=0.5*(Y(J)+Y(J-1))
      RCV(1)=R(1)
      RCV(NJ)=R(NJ)
      DO 113 J=2,NJM1
  113 RCV(J)=0.5*(RV(J+1)+RV(J))
      DYPSV(1)=0.0
      DYPSV(2)=0.0
      DYNPV(NJ)=0.0
      DO 109 J=2,NJM1
      DYNPV(J)=YV(J+1)-YV(J)
  109 DYPSV(J+1)=DYNPV(J)
      SNSV(1)=0.0
      DO 110 J=2,NJ
  110 SNSV(J)=Y(J)-Y(J-1)
C
CHAPTER  2  2  2  2  2  2  SET VARIABLES TO ZERO  2  2  2  2  2  2
C
      DO 201 I=1,NI
      DO 200 J=1,NJ
      U(I,J)=0.0
      V(I,J)=0.0
      P(I,J)=0.0
      IF(J.GE.10) T(I,J)=TINSEC
      IF(J.LT.10) T(I,J)=TINPRM
      PP(I,J)=0.0
      IF(J.GE.10) DEN(I,J)=DENSEC
      IF(J.GE.10) VIS(I,J)=VISSEC
      IF(J.LT.10) DEN(I,J)=DENPRM
      IF(J.LT.10) VIS(I,J)=VISPRM
      IF(J.GE.10) GAMH(I,J)=VISSEC/PRANDL
      IF(J.LT.10) GAMH(I,J)=VISPRM/PRANDL
      DU(I,J)=0.0
      DV(I,J)=0.0
      SU(I,J)=0.0
```

```
      SP(I,J)=0.0
200   CONTINUE
201   CONTINUE
      DO 202 I=1,NI
      HTFLX(I)=0.0
202   HFXOLD(I)=0.0
      RETURN
      END
C
C
      SUBROUTINE PROPS
C
CHAPTER  0  0  0  0  0  0  0  0  PRELIMINARIES  0  0  0  0  0  0  0  0
C
      COMMON
     1/FLUPR/VISSEC,DENSEC,PRANDL,DEN(30,30),VIS(30,30),CONST,
     1       VISPRM,DENPRM,SECMAS,PRMMAS,SPRAT
     1/VAR/U(30,30),V(30,30),P(30,30),PP(30,30)
     1/ALL/IT,JT,NI,NJ,NIM1,NJM1,GREAT
     1/TEMP/T(30,30),GAMH(30,30),RESORT,NSWPT,URFT,
     2      TINPRM,TINSEC,TGB(30),HTFLX(30),HFXOLD(30)
C
C
C---- SUTHERLAND EQUATION; B AND S CONSTANTS
      B=1.5E-6
      S=130.
      DO 100 I=1,NI
      DO 100 J=1,NJM1
      DEN(I,J)=1.0/(T(I,J)*CONST)
      VIS(I,J)=B*(T(I,J)**(1.5))/(S+T(I,J))
      GAMH(I,J)=VIS(I,J)/PRANDL
  100 CONTINUE
      RETURN
      END
C
      SUBROUTINE CALCU
C
CHAPTER  0  0  0  0  0  0  0  0  PRELIMINARIES  0  0  0  0  0  0  0  0
C
      COMMON
     1/UVEL/RESORU,NSWPU,URFU,DXEPU(32),DXPWU(32),SEWU(32)
     1/VVEL/RESORV,NSWPV,URFV,DYNPV(32),DYPSV(32),SNSV(32)
     1/PCOR/RESORM,NSWPP,URFP,DU(30,30),DV(30,30),IPREF,JPREF
     1/VAR/U(30,30),V(30,30),P(30,30),PP(30,30)
     1/ALL/IT,JT,NI,NJ,NIM1,NJM1,GREAT
      COMMON
     1/GEOM/X(32),Y(32),DXEP(32),DXPW(32),DYNP(32),DYPS(32),
     1       SNS(32),SEW(32),XU(32),YV(32),R(32),RV(32),RCV(32)
     1/FLUPR/VISSEC,DENSEC,PRANDL,DEN(30,30),VIS(30,30),CONST,
     1       VISPRM,DENPRM,SECMAS,PRMMAS,SPRAT
      COMMON
     1/COEF/AP(30,30),AN(30,30),AS(30,30),AE(30,30),AW(30,30),SU(30,30),
     1      SP(30,30)
     1/PROB1/UINPRM,UINSEC,GRAVTY,FLOWIN,NITER
```

```
      COMMON
     1/TEMP/T(30,30),GAMH(30,30),RESORT,NSWPT,URFT,
     2      TINPRM,TINSEC,TGB(30),HTFLX(30),HFXOLD(30)
C
CHAPTER 1 1 1 1 1 1 ASSEMBLY OF COEFFICIENTS 1 1 1 1 1 1 1
C
      DO 100 I=3,NIM1
      DO 101 J=2,NJM1
C-----COMPUTE AREAS AND VOLUME
      AREAN=RV(J+1)*SEWU(I)
      AREAS=RV(J)*SEWU(I)
      AREAEW=RCV(J)*SNS(J)
      VOL=RCV(J)*SEWU(I)*SNS(J)
C-----CALCULATE CONVECTION COEFFICIENTS
      GN=0.5*(DEN(I,J+1)+DEN(I,J))*V(I,J+1)
      GS=0.5*(DEN(I,J-1)+DEN(I,J))*V(I,J)
      GNW=0.5*(DEN(I-1,J)+DEN(I-1,J+1))*V(I-1,J+1)
      GSW=0.5*(DEN(I-1,J)+DEN(I-1,J-1))*V(I-1,J)
      GE=0.5*(DEN(I+1,J)+DEN(I,J))*U(I+1,J)
      GP=0.5*(DEN(I,J)+DEN(I-1,J))*U(I,J)
      GW=0.5*(DEN(I-1,J)+DEN(I-2,J))*U(I-1,J)
      CN=0.5*(GN+GNW)*AREAN
      CS=0.5*(GS+GSW)*AREAS
      CE=0.5*(GE+GP)*AREAEW
      CW=0.5*(GP+GW)*AREAEW
C-----CALCULATE DIFFUSION COEFFICIENTS
      VISN=0.25*(VIS(I,J)+VIS(I,J+1)+VIS(I-1,J)+VIS(I-1,J+1))
      VISS=0.25*(VIS(I,J)+VIS(I,J-1)+VIS(I-1,J)+VIS(I-1,J-1))
      DN=VISN*AREAN/DYNP(J)
      DS=VISS*AREAS/DYPS(J)
      DE=VIS(I,J)*AREAEW/DXEPU(I)
      DW=VIS(I-1,J)*AREAEW/DXPWU(I)
C-----CALCULATE COEFFICIENTS OF SOURCE TERMS
      SMP=CN-CS+CE-CW
      CP=AMAX1(0.0,SMP)
      CPO=CP
C-----ASSEMBLE MAIN COEFFICIENTS
C     IF(DS.EQ.0.0) DS=1.0E-25
      AN(I,J)=AMAX1(ABS(0.5*CN),DN)-0.5*CN
      AS(I,J)=AMAX1(ABS(0.5*CS),DS)+0.5*CS
      AW(I,J)=AMAX1(ABS(0.5*CW),DW)+0.5*CW
      AE(I,J)=AMAX1(ABS(0.5*CE),DE)-0.5*CE
C     AN(I,J)=DN*AMAX1(0.0,(1.0-0.1*ABS(CN/DN))**5)+AMAX1(-CN,0.0)
C     AS(I,J)=DS*AMAX1(0.0,(1.0-0.1*ABS(CS/DS))**5)+AMAX1(CS,0.0)
C     AE(I,J)=DE*AMAX1(0.0,(1.0-0.1*ABS(CE/DE))**5)+AMAX1(-CE,0.0)
C     AW(I,J)=DW*AMAX1(0.0,(1.0-0.1*ABS(CW/DW))**5)+AMAX1(CW,0.0)
      DU(I,J)=AREAEW
      DUDXE=(U(I+1,J)-U(I,J))/DXEPU(I)
      DUDXW=(U(I,J)-U(I-1,J))/DXPWU(I)
      SORCE1=(DUDXE*VIS(I,J)-DUDXW*VIS(I-1,J))/SEWU(I)
      DVDXN=(V(I,J+1)-V(I-1,J+1))/SEWU(I)
      DVDXS=(V(I,J)-V(I-1,J))/SEWU(I)
      DYVDYE=(RV(J+1)*V(I,J+1)-RV(J)*V(I,J))/SNS(J)
      DYVDYW=(RV(J+1)*V(I-1,J+1)-RV(J)*V(I-1,J))/SNS(J)
```

```
      SORCE2=(RV(J+1)*VISN*DVDXN-RV(J)*VISS*DVDXS)/(RCV(J)*DYNPV(J))
      SORCE3=-(2.0/3.0)*((VIS(I,J)*(DYVDYE/R(J)+DUDXE)-VIS(I-1,J)*
     *        (DYVDYW/R(J)+DUDXW))/SEWU(I))
      SU(I,J)=CPO*U(I,J)+DU(I,J)*(P(I-1,J)-P(I,J))
      SU(I,J)=SU(I,J)+(SORCE1+SORCE2+SORCE3)*VOL
      SP(I,J)=-CP
      DENU=(DEN(I,J)+DEN(I-1,J))/2.
      DENA=(DEN(I,2)+DEN(I-1,2))/2.
      SU(I,J)=SU(I,J)+GRAVTY*(DENU-DENA)*VOL
  101 CONTINUE
  100 CONTINUE
C
CHAPTER 2 2 2 2 2 2 2 PROBLEM MODIFICATIONS 2 2 2 2 2 2 2
C
      CALL MODU
C
CHAPTER 3 FINAL COEFF. ASSEMBLY AND RESIDUAL SOURCE CALCULATION 3 3
C
      RESORU=0.0
      DO 300 I=3,NIM1
      DO 301 J=2,NJM1
      AP(I,J)=AN(I,J)+AS(I,J)+AE(I,J)+AW(I,J)-SP(I,J)
      DU(I,J)=DU(I,J)/AP(I,J)
      RESOR=AN(I,J)*U(I,J+1)+AS(I,J)*U(I,J-1)+AE(I,J)*U(I+1,J)
     1      +AW(I,J)*U(I-1,J)-AP(I,J)*U(I,J)+SU(I,J)
      VOL=RCV(J)*SEWU(I)*SNS(J)
      SORVOL=GREAT*VOL
      IF(-SP(I,J).GT.0.5*SORVOL)  RESOR=RESOR/SORVOL
      RESORU=RESORU+ABS(RESOR)
C-----UNDER-RELAXATION
      AP(I,J)=AP(I,J)/URFU
      SU(I,J)=SU(I,J)+(1.-URFU)*AP(I,J)*U(I,J)
      DU(I,J)=DU(I,J)*URFU
  301 CONTINUE
  300 CONTINUE
C
CHAPTER 4 4 4 SOLUTION OF DIFFERENCE EQUATION 4 4 4 4 4 4 4
C
      DO 400 N=1,NSWPU
  400 CALL LISOLV(3,2,NI,NJ,IT,JT,U)
      RETURN
      END
C
      SUBROUTINE CALCV
C
CHAPTER 0 0 0 0 0 0 0 0 PRELIMINARIES 0 0 0 0 0 0 0 0
C
      COMMON
     1/UVEL/RESORU,NSWPU,URFU,DXEPU(32),DXPWU(32),SEWU(32)
     1/VVEL/RESORV,NSWPV,URFV,DYNPV(32),DYPSV(32),SNSV(32)
     1/PCOR/RESORM,NSWPP,URFP,DU(30,30),DV(30,30),IPREF,JPREF
     1/VAR/U(30,30),V(30,30),P(30,30),PP(30,30)
      COMMON
     1/GEOM/X(32),Y(32),DXEP(32),DXPW(32),DYNP(32),DYPS(32),
```

```
     1       SNS(32),SEW(32),XU(32),YV(32),R(32),RV(32),RCV(32)
     1/ALL/IT,JT,NI,NJ,NIM1,NJM1,GREAT
     1/FLUPR/VISSEC,DENSEC,PRANDL,DEN(30,30),VIS(30,30),CONST,
     1        VISPRM,DENPRM,SECMAS,PRMMAS,SPRAT
      COMMON
     1/COEF/AP(30,30),AN(30,30),AS(30,30),AE(30,30),AW(30,30),SU(30,30),
     1       SP(30,30)
     1/PROB1/UINPRM,UINSEC,GRAVTY,FLOWIN,NITER
C
CHAPTER 1 1 1 1 1 1 ASSEMBLY OF COEFFICIENTS 1 1 1 1 1 1 1
C
      DO 100 I=2,NIM1
      DO 101 J=3,NJM1
C-----COMPUTE AREAS AND VOLUME
      AREAN=R(J)*SEW(I)
      AREAS=R(J-1)*SEW(I)
      AREAEW=RV(J)*SNSV(J)
      VOL=RV(J)*SEW(I)*SNSV(J)
C-----CALCULATE CONVECTION COEFFICIENTS
      GN=0.5*(DEN(I,J+1)+DEN(I,J))*V(I,J+1)
      GP=0.5*(DEN(I,J)+DEN(I,J-1))*V(I,J)
      GS=0.5*(DEN(I,J-1)+DEN(I,J-2))*V(I,J-1)
      GE=0.5*(DEN(I+1,J)+DEN(I,J))*U(I+1,J)
      GSE=0.5*(DEN(I,J-1)+DEN(I+1,J-1))*U(I+1,J-1)
      GW=0.5*(DEN(I,J)+DEN(I-1,J))*U(I,J)
      GSW=0.5*(DEN(I,J-1)+DEN(I-1,J-1))*U(I,J-1)
      CN=0.5*(GN+GP)*AREAN
      CS=0.5*(GP+GS)*AREAS
      CE=0.5*(GE+GSE)*AREAEW
      CW=0.5*(GW+GSW)*AREAEW
C-----CALCULATE DIFFUSION COEFFICIENTS
      VISE=0.25*(VIS(I,J)+VIS(I+1,J)+VIS(I,J-1)+VIS(I+1,J-1))
      VISW=0.25*(VIS(I,J)+VIS(I-1,J)+VIS(I,J-1)+VIS(I-1,J-1))
      DN=VIS(I,J)*AREAN/DYNPV(J)
      DS=VIS(I,J-1)*AREAS/DYPSV(J)
      DE=VISE*AREAEW/DXEP(I)
      DW=VISW*AREAEW/DXPW(I)
C-----CALCULATE COEFFICIENTS OF SOURCE TERMS
      SMP=CN-CS+CE-CW
      CP=AMAX1(0.0,SMP)
      CPO=CP
C-----ASSEMBLE MAIN COEFFICIENTS
C     IF(DS.EQ.0.0) DS=1.0E-25
      AN(I,J)=AMAX1(ABS(0.5*CN),DN)-0.5*CN
      AS(I,J)=AMAX1(ABS(0.5*CS),DS)+0.5*CS
      AE(I,J)=AMAX1(ABS(0.5*CE),CE)-0.5*CE
      AW(I,J)=AMAX1(ABS(0.5*CW),CW)+0.5*CW
C     AN(I,J)=DN*AMAX1(0.0,(1.0-0.1*ABS(CN/DN))**5)+AMAX1(-CN,0.0)
C     AE(I,J)=DE*AMAX1(0.0,(1.0-0.1*ABS(CE/DE))**5)+AMAX1(-CE,0.0)
C     AS(I,J)=DS*AMAX1(0.0,(1.0-0.1*ABS(CS/DS))**5)+AMAX1(CS,0.0)
C     AW(I,J)=DW*AMAX1(0.0,(1.0-0.1*ABS(CW/DW))**5)+AMAX1(CW,0.0)
      DV(I,J)=0.5*(AREAN+AREAS)
      DUDYE=(U(I+1,J)-U(I+1,J-1))/SNSV(J)
      DUDYW=(U(I,J)-U(I,J-1))/SNSV(J)
```

```
      SORCE1=(DUDYE*VISE-DUDYW*VISW)/DXEPU(I)
      DVDYN=(V(I,J+1)-V(I,J))/DYNPV(J)
      DVDYS=(V(I,J)-V(I,J-1))/DYPSV(J)
      SORCE2=(VIS(I,J)*RCV(J)*DVDYN-VIS(I,J-1)*RCV(J-1)*DVDYS)
     #       /(RV(J)*SNSV(J))
      DYVDYN=(RV(J+1)*V(I,J+1)-RV(J)*V(I,J))/DYNPV(J)
      DYVDYS=(RV(J)*V(I,J)-RV(J-1)*V(I,J-1))/DYPSV(J)
      DUDXN=(U(I+1,J)-U(I,J))/SEW(I)
      DUDXS=(U(I+1,J-1)-U(I,J-1))/SEW(I)
      SORCE3=(2.0/3.0)*(VIS(I,J)*(DYVDYN/RCV(J)+DUDXN)-VIS(I,J-1)*
     #        (DYVDYS/RCV(J-1)+DUDXS))/SNSV(J)
      SU(I,J)=CPO*V(I,J)+DV(I,J)*(P(I,J-1)-P(I,J))
      SU(I,J)=SU(I,J)+(SORCE1+SORCE2+SORCE3)*VOL
      SP(I,J)=-CP
      SP(I,J)=SP(I,J)-(VIS(I,J)+VIS(I,J-1))*VOL/RV(J)**2
  101 CONTINUE
  100 CONTINUE
C
CHAPTER  2  2  2  2  2  2  2  PROBLEM MODIFICATIONS  2  2  2  2  2  2  2
C
      CALL MODV
C
CHAPTER  3  FINAL COEFF. ASSEMBLY AND RESIDUAL SOURCE CALCULATION  3  3
C
      RESORV=0.0
      DO 300 I=2,NIM1
      DO 301 J=3,NJM1
      AP(I,J)=AN(I,J)+AS(I,J)+AE(I,J)+AW(I,J)-SP(I,J)
      RESOR=AN(I,J)*V(I,J+1)+AS(I,J)*V(I,J-1)+AE(I,J)*V(I+1,J)
     1      +AW(I,J)*V(I-1,J)-AP(I,J)*V(I,J)+SU(I,J)
      DV(I,J)=DV(I,J)/AP(I,J)
      VOL=RV(J)*SEW(I)*SNSV(J)
      SORVOL=GREAT*VOL
      IF(-SP(I,J).GT.0.5*SORVOL)  RESOR=RESOR/SORVOL
      RESORV=RESORV+ABS(RESOR)
C-----UNDER-RELAXATION
      AP(I,J)=AP(I,J)/URFV
      SU(I,J)=SU(I,J)+(1.-URFV)*AP(I,J)*V(I,J)
      DV(I,J)=DV(I,J)*URFV
  301 CONTINUE
  300 CONTINUE
C
CHAPTER  4  4  4  SOLUTION OF DIFFERENCE EQUATION  4  4  4  4  4  4  4
C
      DO 400 N=1,NSWPV
  400 CALL LISOLV(2,3,NI,NJ,IT,JT,V)
      RETURN
      END
      SUBROUTINE CALCP
C
CHAPTER  0  0  0  0  0  0  0  0  PRELIMINARIES  0  0  0  0  0  0  0  0
C
      COMMON
     1/PCOR/RESORM,NSWPP,URFP,DU(30,30),DV(30,30),IPREF,JPREF
```

```
      1/VAR/U(30,30),V(30,30),P(30,30),PP(30,30)
      1/ALL/IT,JT,NI,NJ,NIM1,NJM1,GREAT
       COMMON
      1/GEOM/X(32),Y(32),DXEP(32),DXPW(32),DYNP(32),DYPS(32),
      1       SNS(32),SEW(32),XU(32),YV(32),R(32),RV(32),RCV(32)
      1/FLUPR/VISSEC,DENSEC,PRANDL,DEN(30,30),VIS(30,30),CONST,
      1        VISPRM,DENPRM,SECMAS,PRMMAS,SPRAT
      1/COEF/AP(30,30),AN(30,30),AS(30,30),AE(30,30),AW(30,30),SU(30,30),
      1       SP(30,30)
       RESORM=0.0
C
CHAPTER  1  1  1  1  1  1  ASSEMBLY OF COEFFICIENTS  1  1  1  1  1  1  1
C
      DO 100 I=2,NIM1
      DO 101 J=2,NJM1
C-----COMPUTE AREAS AND VOLUME
      AREAN=RV(J+1)*SEW(I)
      AREAS=RV(J)*SEW(I)
      AREAEW=RCV(J)*SNS(J)
      VOL=RCV(J)*SNS(J)*SEW(I)
C-----CALCULATE COEFFICIENTS
      DENN=0.5*(DEN(I,J)+DEN(I,J+1))
      DENS=0.5*(DEN(I,J)+DEN(I,J-1))
      DENE=0.5*(DEN(I,J)+DEN(I+1,J))
      DENW=0.5*(DEN(I,J)+DEN(I-1,J))
      AN(I,J)=DENN*AREAN*DV(I,J+1)
      AS(I,J)=DENS*AREAS*DV(I,J)
      AE(I,J)=DENE*AREAEW*DU(I+1,J)
      AW(I,J)=DENW*AREAEW*DU(I,J)
C-----CALCULATE SOURCE TERMS
      CN=DENN*V(I,J+1)*AREAN
      CS=DENS*V(I,J)*AREAS
      CE=DENE*U(I+1,J)*AREAEW
      CW=DENW*U(I,J)*AREAEW
      SMP=CN-CS+CE-CW
      SP(I,J)=0.0
      SU(I,J)=-SMP
C-----COMPUTE SUM OF ABSOLUTE MASS SOURCES
      RESORM=RESORM+ABS(SMP)
  101 CONTINUE
  100 CONTINUE
C
CHAPTER  2  2  2  2  2  2  2  PROBLEM MODIFICATIONS  2  2  2  2  2  2  2
C
      CALL MODP
C
CHAPTER  3  3  3  3  3  FINAL COEFFICIENT ASSEMBLY  3  3  3  3  3  3  3
C
      DO 300 I=2,NIM1
      DO 301 J=2,NJM1
  301 AP(I,J)=AN(I,J)+AS(I,J)+AE(I,J)+AW(I,J)-SP(I,J)
  300 CONTINUE
C
CHAPTER  4  4  4  4  4  SOLUTION OF DIFFERENCE EQUATIONS  4  4  4  4  4
```

```
C
C
CHAPTER  5  5  5  5  CORRECT VELOCITIES AND PRESSURE  5  5  5  5  5  5
      DO 400 N=1,NSWPP
  400 CALL LISOLV(2,2,NI,NJ,IT,JT,PP)
C
C-----VELOCITIES
      DO 500 I=2,NIM1
      DO 501 J=2,NJM1
      IF(I.NE.2) U(I,J)=U(I,J)+DU(I,J)*(PP(I-1,J)-PP(I,J))
      IF(J.NE.2) V(I,J)=V(I,J)+DV(I,J)*(PP(I,J-1)-PP(I,J))
  501 CONTINUE
  500 CONTINUE
C-----PRESSURES (WITH PROVISION FOR UNDER-RELAXATION)
      PPREF=PP(IPREF,JPREF)
      DO 502 I=2,NIM1
      DO 503 J=2,NJM1
      P(I,J)=P(I,J)+URFP*(PP(I,J)-PPREF)
      PP(I,J)=0.0
  503 CONTINUE
  502 CONTINUE
      RETURN
      END
      SUBROUTINE CALCT
      COMMON
     1/VAR/U(30,30),V(30,30),P(30,30),PP(30,30)
     1/ALL/IT,JT,NI,NJ,NIM1,NJM1,GREAT
      COMMON
     1/GEOM/X(32),Y(32),DXEP(32),DXPW(32),DYNP(32),DYPS(32),
     1       SNS(32),SEW(32),XU(32),YV(32),R(32),RV(32),RCV(32)
     1/FLUPR/VISSEC,DENSEC,PRANDL,DEN(30,30),VIS(30,30),CONST,
     1        VISPRM,DENPRM,SECMAS,PRMMAS,SPRAT
      COMMON
     1/PROB1/UINPRM,UINSEC,GRAVTY,FLOWIN,NITER
     1/COEF/AP(30,30),AN(30,30),AS(30,30),AE(30,30),AW(30,30),SU(30,30),
     1       SP(30,30)
      COMMON
     1/TEMP/T(30,30),GAMH(30,30),RESORT,NSWPT,URFT,
     2      TINPRM,TINSEC,TGB(30),HTFLX(30),HFXOLD(30)
C
CHAPTER  1  1  1  1  1  1  ASSEMBLY OF COEFFICIENTS  1  1  1  1  1  1
C
      DO 100 I=2,NIM1
      DO 101 J=2,NJM1
C-----COMPUTE AREAS VOLUME
      AREAN=RV(J+1)*SEW(I)
      AREAS=RV(J)*SEW(I)
      AREAEW=RCV(J)*SNS(J)
      VOL=RCV(J)*SNS(J)*SEW(I)
C     CALCULATE CONVECTION COEFFICIENTS
      GN=0.5*(DEN(I,J)+DEN(I,J+1))*V(I,J+1)
      GS=0.5*(DEN(I,J)+DEN(I,J-1))*V(I,J)
      GE=0.5*(DEN(I,J)+DEN(I+1,J))*U(I+1,J)
      GW=0.5*(DEN(I,J)+DEN(I-1,J))*U(I,J)
```

```
      CN=GN*AREAN
      CS=GS*AREAS
      CE=GE*AREAEW
      CW=GW*AREAEW
C     CALCULATE DIFFUSION COEFFICIENTS
      GAMN=0.5*(GAMH(I,J)+GAMH(I,J+1))
      GAMS=0.5*(GAMH(I,J)+GAMH(I,J-1))
      GAME=0.5*(GAMH(I,J)+GAMH(I+1,J))
      GAMW=0.5*(GAMH(I,J)+GAMH(I-1,J))
      DN=GAMN*AREAN/DYNP(J)
      DS=GAMS*AREAS/DYPS(J)
      DE=GAME*AREAEW/DXEP(I)
      DW=GAMW*AREAEW/DXPW(I)
C     SOURCE TERMS
      SMP=CN-CS+CE-CW
      CP=AMAX1(0.0,SMP)
      CPO=CP
C     ASSEMBLE MAIN COEFFICIENTS
C     IF(DS.EQ.0.0) DS=1.0E-25
      AN(I,J)=AMAX1(ABS(0.5*CN),DN)-0.5*CN
      AS(I,J)=AMAX1(ABS(0.5*CS),DS)+0.5*CS
      AE(I,J)=AMAX1(ABS(0.5*CE),DE)-0.5*CE
      AW(I,J)=AMAX1(ABS(0.5*CW),DW)+0.5*CW
C     AN(I,J)=DN*AMAX1(0.0,(1.0-0.1*ABS(CN/DN))**5)+AMAX1(-CN,0.0)
C     AS(I,J)=DS*AMAX1(0.0,(1.0-0.1*ABS(CS/DS))**5)+AMAX1(CS,0.0)
C     AE(I,J)=DE*AMAX1(0.0,(1.0-0.1*ABS(CE/DE))**5)+AMAX1(-CE,0.0)
C     AW(I,J)=DW*AMAX1(0.0,(1.0-0.1*ABS(CW/DW))**5)+AMAX1(CW,0.0)
      SU(I,J)=CPO*T(I,J)
      SP(I,J)=-CP
  101 CONTINUE
  100 CONTINUE
C
CHAPTER  2  2  2  2  2  2  PROBLEM MODIFICATIONS  2  2  2  2  2  2
C
      CALL MODT
CHAPTER 3 FINAL COEFFICIENT ASSEMBLY AND RESIDUAL SOURCE CALCULATION 3
C
      RESORT=0.0
      DO 300 I=2,NIM1
      DO 301 J=2,NJM1
      AP(I,J)=AN(I,J)+AS(I,J)+AE(I,J)+AW(I,J)-SP(I,J)
      RESOR=AN(I,J)*T(I,J+1)+AS(I,J)*T(I,J-1)+AE(I,J)*T(I+1,J)
     1       +AW(I,J)*T(I-1,J)-AP(I,J)*T(I,J)+SU(I,J)
      VOL=RCV(J)*SEW(I)*SNS(J)
      SORVOL=GREAT*VOL
      IF(-SP(I,J).GT.0.5*SORVOL) RESOR=RESOR/SORVOL
      RESORT=RESORT+ABS(RESOR)
C     UNDER-RELAXATION
      AP(I,J)=AP(I,J)/URFT
      SU(I,J)=SU(I,J)+(1.0-URFT)*AP(I,J)*T(I,J)
  301 CONTINUE
  300 CONTINUE
C
CHAPTER  4  4  4  4  4  SOLUTION OF DIFFERENCE EQUATIONS  4  4  4  4  4
```

```
C
      DO 400 N=1,NSWPT
  400 CALL LISOLV(2,2,NI,NJ,IT,JT,T)
      RETURN
      END
C
      SUBROUTINE LISOLV(ISTART,JSTART,NI,NJ,IT,JT,PHI)
C
CHAPTER  0  0  0  0  0  0  0  0  PRELIMINARIES  0  0  0  0  0  0  0  0
C
      DIMENSION PHI(IT,JT),A(32),B(32),C(32),D(32)
      COMMON
     1/COEF/AP(30,30),AN(30,30),AS(30,30),AE(30,30),AW(30,30),SU(30,30),
     1     SP(30,30)
      NIM1=NI-1
      NJM1=NJ-1
      JSTM1=JSTART-1
      A(JSTM1)=0.0
C-----COMMENCE W-E SWEEP
      DO 100 I=ISTART,NIM1
      C(JSTM1)=PHI(I,JSTM1)
C-----COMMENCE S-N TRAVERSE
      DO 101 J=JSTART,NJM1
C-----ASSEMBLE TDMA COEFFICIENTS
      A(J)=AN(I,J)
      B(J)=AS(I,J)
      C(J)=AE(I,J)*PHI(I+1,J)+AW(I,J)*PHI(I-1,J)+SU(I,J)
      D(J)=AP(I,J)
C-----CALCULATE COEFFICIENTS OF RECURRENCE FORMULA
      TERM=1./(D(J)-B(J)*A(J-1))
      A(J)=A(J)*TERM
  101 C(J)=(C(J)+B(J)*C(J-1))*TERM
C-----OBTAIN NEW PHI'S
      DO 102 JJ=JSTART,NJM1
      J=NJ+JSTM1-JJ
  102 PHI(I,J)=A(J)*PHI(I,J+1)+C(J)
  100 CONTINUE
      RETURN
      END
C
      SUBROUTINE PRINT(ISTART,JSTART,NI,NJ,IT,JT,X,Y,PHI,HEAD)
      DIMENSION PHI(IT,JT),X(IT),Y(JT),HEAD(9),STORE(50)
      DIMENSION F(7),F4(11)
      DATA F/4H(1H ,4H,A4,,4HI3, ,4H11I ,4H10, ,4H7X, ,
     14HA6) /
      DATA F4/4H 1I ,4H 2I ,4H 3I ,4H 4I ,4H 5I ,4H 6I ,
     1       4H 7I ,4H 8I ,4H 9I ,4H10I ,4H11I /
      DATA HI,HY/4H  I=,4H Y =/
      ISKIP=1
      JSKIP=1
      WRITE(6,110)HEAD
      ISTA=ISTART-12
  100 CONTINUE
      ISTA=ISTA+12
```

```
      IEND=ISTA+11
      IEND=MIN0(NI,IEND)
      F(4)=F4(IEND-ISTA)
      WRITE(6,F) HI, (I,I=ISTA,IEND,ISKIP), HY
      WRITE(6,112)
      DO 101 JJ=JSTART,NJ,JSKIP
      J=JSTART+NJ-JJ
      DO 120 I=ISTA,IEND
      A=PHI(I,J)
      IF(ABS(A).LT.1.E-20) A=0.0
120   STORE(I)=A
      WRITE(6,113)  J,(STORE(I),I=ISTA,IEND,ISKIP),Y(J)
101   CONTINUE
      WRITE(6,114) (X(I),I=ISTA,IEND,ISKIP)
      IF(IEND.LT.NI)GO TO 100
  110 FORMAT(1H0,20(2H*-),7X,9A4,7X,20(2H-*))
  112 FORMAT(3H  J)
  113 FORMAT(1H ,I3,1P12E10.2,0PF7.3)
  114 FORMAT(6H0X=   ,F7.3,11F10.3)
      RETURN
      END
C
      SUBROUTINE PROMOD
C
CHAPTER  0  0  0  0  0  0  0  PRELIMINARIES  0  0  0  0  0  0  0  0  0
C
      COMMON
     1/VVEL/RESORV,NSWPV,URFV,DYNPV(32),DYPSV(32),SNSV(32)
     1/UVEL/RESORU,NSWPU,URFU,DXEPU(32),DXPWU(32),SEWU(32)
     1/PCOR/RESORM,NSWPP,URFP,DU(30,30),DV(30,30),IPREF,JPREF
     1/VAR/U(30,30),V(30,30),P(30,30),PP(30,30)
     1/ALL/IT,JT,NI,NJ,NIM1,NJM1,GREAT
      COMMON
     1/GEOM/X(32),Y(32),DXEP(32),DXPW(32),DYNP(32),DYPS(32),
     1       SNS(32),SEW(32),XU(32),YV(32),R(32),RV(32),RCV(32)
     1/FLUPR/VISSEC,DENSEC,PRANDL,DEN(30,30),VIS(30,30),CONST,
     1        VISPRM,DENPRM,SECMAS,PRMMAS,SPRAT
      COMMON
     1/PROB1/UINPRM,UINSEC,GRAVTY,FLOWIN,NITER
     1/COEF/AP(30,30),AN(30,30),AS(30,30),AE(30,30),AW(30,30),SU(30,30),
     1       SP(30,30)
      COMMON
     1/TEMP/T(30,30),GAMH(30,30),RESORT,NSWPT,URFT,
     2      TINPRM,TINSEC,TGB(30),HTFLX(30),HFXOLD(30)
C
CHAPTER  1  1  1  1  1  1  1  1  PROPERTIES  1  1  1  1  1  1  1  1  1
C
      ENTRY MODPRO
C-----NO MODIFICATIONS FOR THIS PROBLEM
C
      RETURN
CHAPTER  2  2  2  2  2  2  2  2  U MOMENTUM  2  2  2  2  2  2  2  2  2
C
      ENTRY MODU
```

```
C-----TOP WALL
      YP=YV(NJ)-Y(NJM1)
      J=NJM1
      DO 210 I=3,NIM1
      TMULT=(VIS(I-1,J)+VIS(I,J))*0.5/YP
      SP(I,J)=SP(I,J)-TMULT*SEWU(I)*RV(NJ)
  210 AN(I,J)=0.0
C-----SYMMETRY AXIS
      DO 203 I=1,NI
      AS(I,2)=0.0
  203 U(I,1)=U(I,2)
C-----LEFT SIDE WALL
      DO 207 J=2,NJM1
  207 U(2,J)=U(1,J)*(T(2,J)+T(1,J))/(2.0*T(1,J))
      DO 208 J=6,9
  208 AW(2,J)=0.0
C-----RIGHT SIDE WALL
C
      DO 206 J=1,NJ
      AE(NIM1,J)=0.0
 206  CONTINUE
      RETURN
C
CHAPTER  3  3  3  3  3  3  3  3  V MOMENTUM  3  3  3  3  3  3  3  3  3
C
      ENTRY MODV
C-----LEFT SIDE WALL
      DO 303 J=6,10
      XP=X(2)-XU(2)
      TTMULT=(VIS(2,J)+VIS(2,J-1))*0.5/XP
      IF(J.EQ.6)SP(2,J)=SP(2,J)-TTMULT*(R(J)**2-RV(J)**2)/2.0
      IF(J.EQ.10)SP(2,J)=SP(2,J)-TTMULT*(RV(J)**2-R(J-1)**2)/2.0
      IF((J.NE.6).OR.(J.NE.10)) SP(2,J)=SP(2,J)-TTMULT*RV(J)*SNSV(J)
 303  AW(2,J)=0.0
C
C-----RIGHT SIDE WALL
C
      DO 312 J=2,NJM1
  312 AE(NIM1,J)=0.0
      RETURN
C
CHAPTER  4  4  4  4  4  4  PRESSURE CORRECTION  4  4  4  4  4  4  4  4
C
      ENTRY MODP
C
C-----NO MODIFICATION
C
      RETURN
C
C
      ENTRY MODT
C-----TOP WALL (2.0 M VARIABLE WALL TEMP )
      J=NJM1
      YT=YV(NJ)-Y(J)
```

```
      DO 500 I=2,NIM1
C---- SPECIFIC HEAT CORRELATION
      CPP=(T(I,J)-350.0)*0.212+1000.
      TT=VIS(I,J)/(PRANDL*YT)
      RSTG=1.0/(CPP*TT)
      TWLOUT=T(I,J)+HTFLX(I)*(RSTG+RSTW)
C-----C1=RV(NJ)/(ROUT*SIG*EPS1)
C     ROUT=2.75 IN = 0.034925 M
C     EPS1=0.90 EMISSIVITY OF MULLITE ALUMINIUM/SILICON/OXYGEN
      C1=1.7846E7
C-----RSTW=RV(NJ)*ALOG(ROUT/RV(NJ))/KWALL
C     KWALL = 2.076 W/M K  (MULLITE - FROM CRC HANDBOOK)
      RSTW=1.43585E-3
      RSTR=C1/((TGB(I)+TWLOUT)*(TGB(I)**2+TWLOUT**2))
      HTFLX(I)=(TGB(I)-T(I,J))/(RSTR+RSTW+RSTG)
      HTFLX(I)=0.05*HTFLX(I)+0.95*HFXOLD(I)
      HFXOLD(I)=HTFLX(I)
      SU(I,J)=SU(I,J)+RV(NJ)*SEW(I)*HTFLX(I)/CPP
      T(I,NJ)=T(I,J)+HTFLX(I)*RSTG
      AN(I,J)=0.0
  500 CONTINUE
C-----LEFT SIDE WALL
C
      DO 501 J=6,9
      XT=X(2)-XU(2)
      XTT=VIS(2,J)/(PRANDL*XT)
      SP(2,J)=SP(2,J)-XTT*R(J)*SNS(J)
      SU(2,J)=SU(2,J)+XTT*R(J)*SNS(J)*T(1,J)
  501 AW(2,J)=0.0
C-----SYMMETRY AXIS
      DO 502 I=2,NIM1
      T(I,1)=T(I,2)
  502 AS(I,2)=0.0
C-----RIGHT SIDE WALL
C
      DO 503 J=2,NJ
  503 T(NI,J)=T(NIM1,J)
C 503 AE(NIM1,J)=0.0
      RETURN
      END
C
      SUBROUTINE CALCUP
C
      DIMENSION DIST(500),UP(500),TP(500)
      COMMON
     1/GEOM/X(32),Y(32),DXEP(32),DXPW(32),DYNP(32),DYPS(32),
     1      SNS(32),SEW(32),XU(32),YV(32),R(32),RV(32),RCV(32)
     1/FLUPR/VISSEC,DENSEC,PRANDL,DEN(30,30),VIS(30,30),CONST,
     1       VISPRM,DENPRM,SECMAS,PRMMAS,SPRAT
     1/VAR/U(30,30),V(30,30),P(30,30),PP(30,30)
      COMMON
     1/TEMP/T(30,30),GAMH(30,30),RESORT,NSWPT,URFT,
     2      TINPRM,TINSEC,TGB(30),HTFLX(30),HFXOLD(30)
C
```

```
      NI=28
      NJ=20
      NIM1=NI-1
      TMPGLB=TGB(15)
C
C-----*NOTE - THIS IS FOR USE WITH A CALCOMP PLOTTER
C-----THIS PORTION DRAWS THE AXIS FOR THE TEMP VS DIST CURVE
C
      CALL PLOT(32.0,1.0,-3)
      CALL PLOT(0.0,15.0,3)
      CALL PLOT(0.0,0.0,2)
      DO 121 K=1,16
      PR=(K-1)*1.0
      PPRR=PR-0.18
      TMPR=100.0*(K-1)
      IF(AMOD(PR,5.0).EQ.0.)CALL NUMBER(-1.4,PPRR,.35,TMPR,0.0,-1)
      CALL PLOT(0.0,PR,3)
      CALL PLOT(0.25,PR,2)
  121 CONTINUE
      CALL SYMBOL(-1.7,5.0,0.35,'TEMPERATURE  K',90.0,14)
C
      CALL SYMBOL(0.8,12.65,0.35,'M-S/M-P =       ',0.0,16)
      CALL SYMBOL(0.8,14.15,0.35,'   T-GB =      K',0.0,16)
      CALL SYMBOL(0.8,13.65,0.35,'  T-SEC =      K',0.0,16)
      CALL SYMBOL(0.8,13.15,0.35,'  U-SEC =     M/S',0.0,18)
      CALL NUMBER(4.3,13.15,0.35,U(2,10),0.0,2)
      CALL NUMBER(4.3,14.15,0.35,TMPGLB,0.0,-1)
      CALL NUMBER(4.3,13.65,0.35,TINSEC,0.0,-1)
      CALL NUMBER(4.3,12.65,0.35,SPRAT,0.0,1)
C
      CALL SYMBOL(15.0,2.0,0.25,'1 -  10 UM PARTICLE',0.0,19)
      CALL SYMBOL(15.0,1.5,0.25,'2 -  30 UM PARTICLE',0.0,19)
      CALL SYMBOL(15.0,1.0,0.25,'3 - 100 UM PARTICLE',0.0,19)
      CALL SYMBOL(15.0,0.5,0.25,'4 - 300 UM PARTICLE',0.0,19)
      CALL SYMBOL(15.0,2.5,0.25,'  - GAS TEMPERATURE',0.0,19)
      CALL SYMBOL(15.0,2.625,0.10,11,0.0,-1)
C
      CALL PLOT(20.0,0.0,3)
      CALL PLOT(0.0,0.0,2)
      DO 122 I=1,5
      PPR=(I-1)*5.0
      ZZ=PPR/10.0
      ZZP=PPR-0.40
      CALL NUMBER(ZZP,-1.0,.35,ZZ,0.0,1)
      CALL PLOT(PPR,0.25,3)
      CALL PLOT(PPR,0.0,2)
  122 CONTINUE
      CALL SYMBOL(8.0,-2.0,0.35,'DISTANCE  M',0.0,11)
      CALL PLOT(0.0,3.0,3)
      DO 134 I=3,NIM1
      TG=T(I,2)*0.01
      ZG=X(I)*10 0
      CALL SYMBOL(ZG,TG,0.10,11,0.0,-2)
  134 CONTINUE
```

```
C
C------THIS SUBROUTINE USES 4 DIFFERENT PARTICLE DIAMETRES
      DO 191 M=1,4
      IF(M.EQ.1)DIAPAR=0.000010
      IF(M.EQ.2)DIAPAR=0.000030
      IF(M.EQ.3)DIAPAR=0.000100
      IF(M.EQ.4)DIAPAR=0.000300
      WRITE(6,11) DIAPAR
   11 FORMAT(///,'DIA M',E10.2,3X,'TIME  S',3X,'VEL M/S',5X,'DIST M',7X,
     *  'RE',7X,'H W/M2C',2X,'QRAD W/M2',3X,'QCON W/M2',4X,'TEMP K',/)
      GRAVTY=9.806
      DENPAR=1300.0
      CPPAR=1300.0
      EPS=0.8
      SIG=5.669E-8
      UU=U(2,2)
      VSC=VIS(1,2)
      TMP=T(1,2)
      TWL=T(2,NJ)
      TP(1)=T(1,2)
      TEXIT=TINPRM
      DST=DEN(1,2)
      DELTMP=5.0
      DIST(1)=0.0
C
C------THIS GIVES INITIAL DISTANCE TRAVELLED
C
      UP(1)=UU+(SQRT((576.0*VSC**2)/(DIAPAR**4*DENPAR**2)+(32.0*DST*
     *      GRAVTY)/(3.0*DENPAR*DIAPAR))-24.0*VSC/(DIAPAR**2*DENPAR))*
     *      (DENPAR*DIAPAR)/(4.0*DST)
      VFPE=0.5*(1.0-1.0/SQRT(1.0+RV(NJ)**2/XU(NI)**2))
      VFPW=1.0-VFPE-0.5
      QRAD=SIG*EPS*VFPW*(TWL**4-TP(1)**4)
      RELC=0.0
      HTC=0.0
      QCONV=0.0
      TIME=0.0
      K=2
      L=2
C
C
   70 CONTINUE
      DELT=DENPAR*CPPAR*DIAPAR*DELTMP/(6.0*ABS(QRAD-QCONV))
      IF(DELT.GT.0.005) DELT=0.005
      DIST(K)=DIST(K-1)+UP(K-1)*DELT
      WRITE(6,95) TIME,UP(K-1),DIST(K-1),RELC,HTC,QRAD,QCONV,TP(K-1)
   95 FORMAT(17X,F7.5,2X,E10.3,1X,E10.3,2X,E10.3,2X,F8.2,2X,E11.4,2X,
     *       E10.4,2X,F7.1)
      IF(DIST(K).GE.XU(NI)) GO TO 80
      J=L
      DO 90 I=J,NI
      IF((DIST(K).LE.X(I)).AND.(DIST(K).GT.X(I-1))) L=I
   90 CONTINUE
      CST=(DIST(K)-X(L-1))/(X(L)-X(L-1))
```

```
      VSC=VIS(L-1,2)+(VIS(L,2)-VIS(L-1,2))*CST
      DST=DEN(L-1,2)+(DEN(L,2)-DEN(L-1,2))*CST
      TMP=T(L-1,2)+(T(L,2)-T(L-1,2))*CST
      TWL=T(L-1,NJ)+(T(L,NJ)-T(L-1,NJ))*CST
      IF(DIST(K).LT.XU(L)) UU=U(L-1,2)+(U(L,2)-U(L-1,2))*(DIST
     *       (K)-XU(L-1))/(XU(L)-XU(L-1))
      IF(DIST(K).GE.XU(L)) UU=U(L,2)+(U(L+1,2)-U(L,2))*(DIST(K)
     *       -XU(L))/(XU(L+1)-XU(L))
C
C-----THIS CALCULATES FILM TEMPERATURE PROPERTIES
C
      VSCF=(1.5E-6*TP(K-1)**1.5/(TP(K-1)+130.0)+VSC)/2.0
      DSTF=(1.0/(CONST*TP(K-1))+DST)/2.0
C
      RELC=ABS(UP(K-1)-UU)*DIAPAR*DSTF/VSCF
      AUP=18.0*VSCF*(1.0+0.15*RELC**0.687)/(DENPAR*DIAPAR**2)
      UP(K)=UU-((GRAVTY-AUP*(UP(K-1)-UU))*EXP(-AUP*DELT)-GRAVTY)/AUP
C
      CPP=(TMP-350.0)*0.212+1000.0
      VFPP=0.5*(1.0-1.0/SQRT(1.0+RV(10)**2/DIST(K)**2))
      VFPS=0.5*(1.0-1.0/SQRT(1.0+RV(NJ)**2/DIST(K)**2))-VFPP
      VFPE=0.5*(1.0-1.0/SQRT(1.0+RV(NJ)**2/(XU(NI)-DIST(K))**2))
      VFPW=1.0-VFPP-VFPS-VFPE
      VSCP=1.5E-6*TP(K-1)**1.5/(130.0+TP(K-1))
      HTC=(2.0+(0.4*RELC**(1/2)+0.06*RELC**(2/3))*(PRANDL**0.4
     *    )*(VSC/VSCP)**0.25)*VSC*CPP/(PRANDL*DIAPAR)
      HPP=SIG*EPS*VFPP*(TINPRM+TP(K-1))*(TINPRM**2+TP(K-1)**2)
      HPS=SIG*EPS*VFPS*(TINSEC+TP(K-1))*(TINSEC**2+TP(K-1)**2)
      HPE=SIG*EPS*VFPE*(TEXIT+TP(K-1))*(TEXIT**2+TP(K-1)**2)
      HPW=SIG*EPS*VFPW*(TWL+TP(K-1))*(TWL**2+TP(K-1)**2)
      ATP=6.0*(HPP+HPS+HPE+HPW+HTC)/(DENPAR*CPPAR*DIAPAR)
      BTP=6.0*(HPP*TINPRM+HPS*TINSEC+HPE*TEXIT+HPW*TWL+HTC*TMP)/
     *    (DENPAR*CPPAR*DIAPAR)
      TP(K)=(BTP+(ATP*TP(K-1)-BTP)*EXP(-ATP*DELT))/ATP
      QRAD=SIG*EPS*(VFPP*(TINPRM**4-TP(K)**4)+VFPS*(TINSEC**4-TP(K)**4)
     *     +VFPE*(TEXIT**4-TP(K)**4)+VFPW*(TWL**4-TP(K)**4))
      QCONV=HTC*(TP(K)-TMP)
      TIME=TIME+DELT
      K=K+1
      GO TO 70
   80 CONTINUE
C
      TTP=TP(1)*0.01
C     ZP=25.5
      CALL PLOT(0.0,TTP,3)
      KK=K-1
      DO 189 I=2,KK
      ZP=DIST(I)*10.0
      TTP=TP(I)*0.01
      CALL PLOT(ZP,TTP,2)
  189 CONTINUE
  191 CONTINUE
      RETURN
      END
```